Aminolevulinic acid synthase of *Rhodobacter capsulatus*

Von der Fakultät für Lebenswissenschaften
der Technischen Universität Carolo-Wilhelmina
zu Braunschweig
zur Erlangung des Grades einer
Doktorin der Naturwissenschaften
(Dr. rer. nat.)
genehmigte
D i s s e r t a t i o n

von Anna-Lena Hännig

aus Goslar

1. Referent:	Prof. Dr. Dieter Jahn
2. Referentin:	Dr. Gunhild Layer
eingereicht am:	19.01.2011
mündliche Prüfung (Disputation) am:	16.03.2011

Druckjahr 2011

VORVERÖFFENTLICHUNG DER DISSERTATION

Teilergebnisse aus dieser Arbeit wurden mit Genehmigung der Fakultät für Lebenswissenschaften, vertreten durch den Mentor der Arbeit, in folgenden Beiträgen vorab veröffentlicht:

TAGUNGSBEITRÄGE

Hännig, A.L., Hunter, G.A., Ferreira, G.C., Hering, V., Jahn, M. and Jahn, D. N54 - the key amino acid in ALAS determines the transient α-amino-β-ketoadipate-intermediate in *Rhodobacter capsulatus* heme biosynthesis. (Poster) VAAM-Jahrestagung, Hannover, Germany (2010).

Hännig, A.L., Hunter, G.A., Ferreira, G.C., Hering, V., Jahn, M. and Jahn, D. N54 - the key amino acid in ALAS determines the transient α-amino-β-ketoadipate-intermediate in *Rhodobacter capsulatus* heme biosynthesis. (Poster) Tetrapyrrole Discussion Group Meeting (TPDG), Berlin, Germany (2010).

Meiner Familie

und

Torben

“Zwei Dinge sind zu unserer Arbeit nötig:

Unermüdliche Ausdauer und die Bereitschaft,

etwas, in das man viel Zeit und Arbeit gesteckt hat,

wieder wegzuwerfen.“

Albert Einstein, 14.03.1879 - 18.04.1955
deutscher Physiker und Nobelpreisträger

TABLE OF CONTENTS

ABBREVIATIONS ..... **V**

1 INTRODUCTION **1**

1.1 Tetrapyrroles 1
1.1.1 Structure and Relevance of Tetrapyrroles 1
1.1.2 Tetrapyrrole Biosynthesis 4
1.1.3 Aminolevulinic Acid Formation 6
1.1.4 The Common Step of Tetrapyrrole Biosynthesis: From Aminolevulinic Acid to Uroporphyrinogen III 7
1.1.5 From Uroporphyrinogen III to Heme 10

1.2 Aminolevulinic Acid Synthase 13
1.2.1 The Different Aminolevulinic Acid Synthases 14
1.2.2 ALAS Reaction Mechanism 16

1.3 Typical Features of Pyridoxal-5'-phosphate-dependent Enzymes 21

1.4 Succinyl-Coenzyme A Synthetase Synthesizes one ALAS Substrate 23
1.4.1 Cooperativity of Succinyl-Coenzyme A Synthetase and Aminolevulinic Acid Synthase during Heme Biosynthesis 26

1.5 Control of Aminolevulinic Acid Synthase Biosynthesis 26

1.6 Diseases Caused by Tetrapyrrole Deficiency 27
1.6.1 Porphyrias 27
1.6.2 X-linked Sideroblastic Anemia 29

1.7 Aim of this Study 31

2 MATERIALS AND METHODS **32**

2.1 Materials 32
2.1.1 Equipment 32
2.1.2 Chemicals, Enzymes and Kits 33

2.2 Bacterial Strains and Plasmids 34
2.3 Media and Media Additives 36
2.3.1 Media 36
2.3.2 Media Additives 37

2.4 Microbiological Techniques 37
2.4.1 Sterilization 37
2.4.2 Cultivation of Bacteria and Long Term Storage 37
2.4.3 Determination of Cell Density 38

2.5 Molecular Biology Techniques 38
2.5.1 Production and Transformation of Rubidium Chloride Competent *Escherichia coli* Cells 38
2.5.2 Preparation of Plasmid DNA 39
2.5.3 Agarose Gel Electrophoresis 40
2.5.4 Site-Directed Mutagenesis of DNA 41
2.5.5 Amplification of DNA Fragments by PCR 42
2.5.6 Enzymatic Modification of DNA 44
2.5.7 DNA Sequencing 45

2.6 Protein Biochemical Methods 45
2.6.1 Production and Purification of *Rhodobacter capsulatus* Aminolevulinic Acid Synthase 45
2.6.2 Concentrating Protein Solutions 49
2.6.3 Determination of Protein Concentrations 49
2.6.4 Discontinuous SDS Polyacrylamide Gel Electrophoresis 50
2.6.5 Western Blotting 52

2.7 Determination of ALAS Activity 54
2.7.1 Determination of Kinetic Parameters of ALAS 54
2.7.2 Substrate Specificity 58
2.7.3 Quinonoid Formation 59
2.7.4 Reaction of ALAS with Glycine-methylester and *O*-methylglycine 59
2.7.5 Glycine Binding Experiments 60
2.7.6 Dynamic Loop Experiments 60

2.8 Crystallization of *Rhodobacter capsulatus* Aminolevulinic Acid Synthase 60
2.8.1 Crystallization Conditions 61

3 RESULTS AND DISCUSSION 62

3.1 Rationale for Amino Acid Exchanges in $ALAS_{Rc}$ for the Demonstration of the 2-amino-3-ketoadipate Intermediate 62

3.2 Substrate Recognition and Coordination in $ALAS_{Rc}$ 63
3.2.1 Rationale of Amino Acid Exchanges in $ALAS_{Rc}$ for Functional Investigation of Substrate Recognition 63
3.2.2 Rationale of Amino Acid Exchanges in $ALAS_{Rc}$ for the Investigation of Enzyme Dynamics during Substrate Recognition 64

3.3 Rationale of Amino Acid Exchanges in $ALAS_{Rc}$ for the Investigation of ALAS-βSCS Interaction 65

3.4 Production and Purification of Recombinant Wild-type $ALAS_{Rc}$ 66
3.4.1 Construction of an Expression Vector for Wild-type $ALAS_{Rc}$ 66
3.4.2 Production of Recombinant Wild-type $ALAS_{Rc}$ 67
3.4.3 Detection of Recombinantly Produced Wild-type $ALAS_{Rc}$ *via* Western Blotting 67
3.4.4 Purification of Recombinant Wild-type $ALAS_{Rc}$ 68
3.4.5 Oligomerization State of Recombinant Wild-type $ALAS_{Rc}$ 70

3.5 Generation, Production and Purification of Recombinant $ALAS_{Rc}$ Enzyme Variants 71
3.5.1 Purification of $ALAS_{Rc}$ Variants *via* GST Column Chromatography 73

3.6 Experimental Approach 74
3.6.1 Used Test Systems 74
3.6.2 Kinetics of Wild-type $ALAS_{Rc}$ 79
3.6.3 Kinetics of $ALAS_{Rc}$ Variants Involved in Ketoadipate Formation 83
3.6.4 Kinetics of $ALAS_{Rc}$ Variants Involved in Substrate Recognition 91
3.6.5 Kinetics of $ALAS_{Rc}$ Variants Involved in Loop Flexibility 105
3.6.6 Kinetics of $ALAS_{Rc}$ Variants Involved in Protein-protein Interaction with the $βSCS_{Rc}$ 107

4 SUMMARY 112

5 OUTLOOK 114

6 REFERENCES 115

7 DANKSAGUNG 131

ABBREVIATIONS

A	Ampere
Å	Ångstrom
ADP	adenosine diphosphate
5-ALA, δ-ALA, ALA	5-aminolevulinic acid
ALAS	aminolevulinic acid synthase
ALAS1	housekeeping aminolevulinic acid synthase in mitochondria of humans
ALAS2	erythroid aminolevulinic acid synthase in mitochondria of humans
$ALAS_{Rc}$	aminolevulinic acid synthase of *Rhodobacter capsulatus*
amp	ampicillin
APS	ammonium peroxodisulfate
AONS	8-amino-7-oxononanoate synthase
ATP	adenosine triphosphate
βSCS	β-subunit of the succinyl-Coenzyme A synthetase
$βSCS_{Rc}$	β-subunit of the succinyl-Coenzyme A synthetase of *Rhodobacter capsulatus*
BCIP	5-bromo-4-chloro-3-indolylphosphate
bp	base pair
BSA	bovine serum albumin
℃	degree Celsius
cm	chloramphenicol
CoA, CoASH	Coenzyme A
coprogen	coproporphyrinogen III
CPDH	coproporphyrinogen III dehydrogenase, HemN
CPO	coproporphyrinogen III oxidase
Cyd	cytochrome *bd* oxidase
Cyo	ubiquinone cytochrome bo_3 oxidase
Da	Dalton
dNTP	deoxyribonucleotide triphosphate
ddNTP	dideoxyribonucleotide triphosphate
DNA	deoxyribonucleic acid
DSMZ	‘Deutsche Sammlung von Mikroorganismen und Zellkulturen GmbH’
DTT	1,4-dithio-D,L-threitol
E. coli	*Escherichia coli*

et al.	*et alteri* (and others)
e.g.	*exempli gratia* (for example)
FC	ferrochelatase
Fig.	Figure
FMN	flavin mononucleotide
forw	forward
FPLC	fast performance liquid chromatography
Frd	fumarate reductase
g	centrifugation: earth gravity (x *g*)
	weight: gram
GDP	guanosine diphosphate
GluTR	glutamyl-tRNA-reductase
gly	glycine
GPC	gel permeation chromatography
GSA	glutamate-1-semialdehyde
GSAM	glutamate-1-semialdehyde-2,1-aminomutase
GST	glutathione-S-transferase
GTP	guanosine triphosphate
H_2O_{dest}	distilled water
h	hour
HemA	5-aminolevulinic acid synthase
HEPES	4-(2-hydroxyethyl)-piperazine-1-ethane sulfonic acid
HMBS	hydroxymethylbilane synthase
HZI	'Helmholtzzentrum für Infektionsforschung'
i.e.	*id est* (that is to say)
IPTG	Isopropyl-β-D-thiogalactopyranoside
IRE	iron responsive element
k_{cat}	catalytic constant
kDa	kilo Dalton
α-KGD	α-ketoglutarate dehydrogenase
K_M	Michaelis Menten constant
L	litre
ʎ	wavelength
LB	Luria Bertani
m	milli
M	molar (mol/L)
µ	micro
M	mol/L
min	minute

mM	millimolar
MPOS	3-(N-morpholino)propanesulfonic acid
M_r	relative molecular mass
MW	molecular weight
n	nano
n/a	*non-available*
NaCl	sodium chloride
NAD^+	nicotinamide adenine dinucleotide
NADH	nicotinamide adenine dinucleotide hydrate
Nar	nitrate reductase
O_2	oxygen
OD_λ	optical density at a wavelength λ in nm
PBG	porphobilinogen
PBGD	porphobilinogen deaminase
PBGS	porphobilinogen synthase
PBS	phosphate buffered saline
PCR	polymerase chain reaction
PLP	pyridoxal-5'-phosphate
PPO	protoporphyrinogen IX oxidase
proto	protoporphyrin
PVDF	polyvinylidene fluoride
Q_{d1}	first step of quinonoid decay in ALAS reaction mechanism
Q_{d2}	second step of quinonoid decay in ALAS reaction mechanism
Q_f	quinonoid formation in ALAS reaction mechanism
R. capsulatus	*Rhodobacter capsulatus*
rev	reverse
RT	room temperature
rpm	rotation per minute
s.	see
succinyl-CoA	succinyl-Coenzyme A
SCS	succinyl-Coenzyme A synthetase
sec, s^{-1}	second, per second
SDS	sodium dodecyl sulfate
SDS-PAGE	sodium dodecyl sulfate polyacrylamide gel electrophoresis
Tab.	table
TEMED	tetramethylen diamine
T_m	melting temperature
Tris	tris-(hydroxymethyl)-aminomethane
tRNA	transfer ribonucleic acid

TPP	thyamine pyrophosphate
U	unit
UROD	uroporphyrinogen III decarboxylase
UROS	uroporphyrinogen III synthase
UV	ultraviolet
V	volt
v_{max}	maximal velocity
v/v	volume per volume
WT	wild-type
w/v	weight per volume
XLDPP	X-linked dominant protoporphyria
XLSA	X-linked sideroblastic anemia

1 INTRODUCTION

1.1 Tetrapyrroles

1.1.1 Structure and Relevance of Tetrapyrroles

The family of tetrapyrroles comprises a group of biosynthetically related pigment molecules which are present in most organisms on earth. There, they are integral part of essential processes of life. They fullfill important functions as prosthetic groups in various enzymes, as redox active molecules in electron transport chains of energy generation or as photoreceptors during photosynthesis (Jahn *et al.*, 1996; Frankenberg *et al.*, 2003). Tetrapyrroles consist of four covalent attached pyrrole rings which are interconnected *via* methyine bridges in a linear or cyclic form (Fig. 1). The corrinoides are an exception because the fourth carbon bridge is lacking between the fourth and the first ring (C_{20}, Fig. 1). The pyrrole rings of a cyclic macrocycle are linked to each other clockwise in the following order: first ring A, then rings B, C and D. The carbon atoms in α-position are directly adjacent to one nitrogen atom (*e.g.* C_1, Fig. 1). The carbon atoms which form the methine bridges are located in *meso*-position (*e.g.* C_5, Fig. 1), the rest of them are situated in β-position (*e.g.* C_2, Fig. 1).

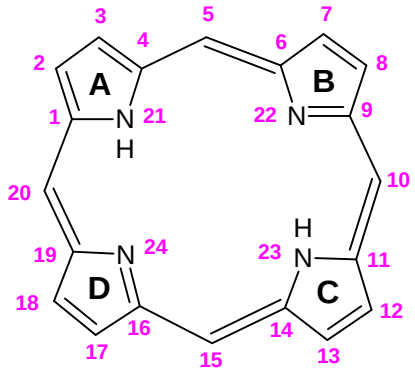

Fig. 1: The porphyrin ring, the general basic structure of cyclic tetrapyrroles.
Pyrrole rings are denoted A - D, nitrogen and carbon atoms are termed as N21 - N24 and C1 - C20.

A characteristic property of the tetrapyrroles is their variegation due to the expanded π-electron system. Tetrapyrroles are named the ‘colors of life’ due to obviously visible quantities of chlorophylls and bacteriochlorophylls (green) in nature and of heme in hemoglobin of blood (red). Tetrapyrroles differ in the rate of saturation of their ring systems, the structure of the side chains as well as in the chelated metal ion in the center of the porphyrin ring (Frankenberg *et al.*, 2003; Heinemann *et al.*, 2008; Layer *et al.*, 2010). They can be divided into eight categories: hemes, chlorophylls, bacteriochlorophylls, siroheme, heme d_1, corrinoides, coenzyme F_{430} and linear tetrapyrroles with uroprophyrinogen III as a common precursor, respectively (Fig. 2). An important feature of cyclic tetrapyrroles is their ability to chelate diverse divalent metal ions such as Fe^{2+}, Mg^{2+}, Ni^{2+} and Co^{2+}. Iron-containing heme constitutes the active centers in cytochromes, peroxidases and reductases. Heme-containing cytochromes are important in respiration and photosynthetic electron transport chains (Panek and O’Brien, 2002). Heme is involved in the oxygen transport in blood and tissue as a cofactor of hemoglobin and myoglobin. It also serves as a prosthetic group in catalases, peroxidases and oxygenases including cytochromes P450 and in sensor proteins for diatomic gases like O_2, CO and NO as well as for CO_2 in signal transduction pathways (Heinemann *et al.*, 2008; Munro *et al.*, 2009). Siroheme has a greenish color and acts as a cofactor in reactions during assimilatory nitrite or sulfite reduction (Murphy *et al.*, 1974; Raux *et al.*, 2003). The yellow coenzyme F_{430} with a chelated nickel ion is the cofactor of methyl Coenzyme M reductase and involved in methane formation in methanogenic archaea (Thauer and Bonacker, 1994). Cobalt is found in vitamin B_{12} and structural related compounds. Derivatives of the cobalt-containing vitamin B_{12} are the cofactors of a number of enzymes that catalyze radical-dependent reactions such as methyl transfer reactions or nucleotide reduction (Banerjee and Ragsdale, 2003).

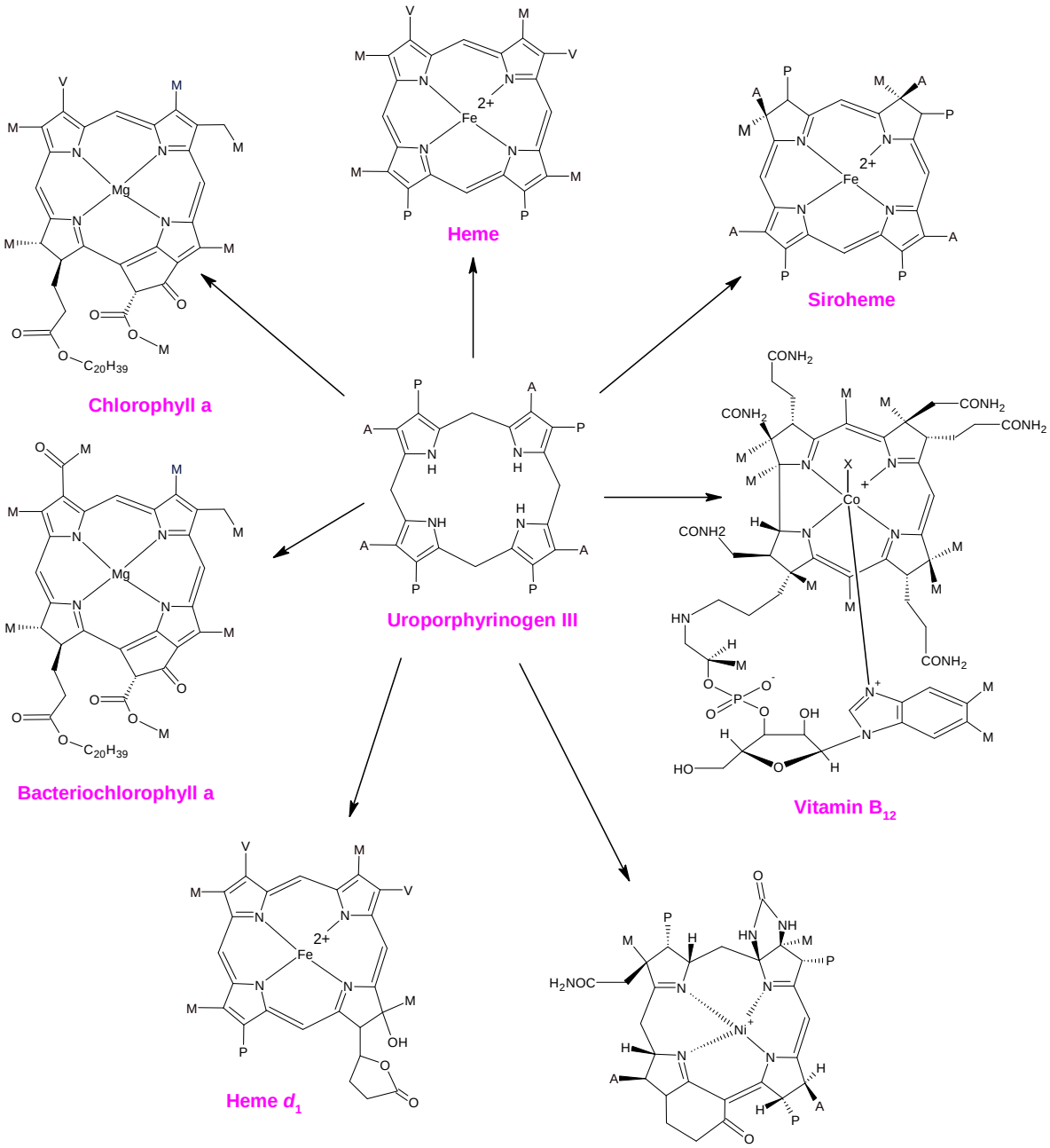

Fig. 2: Structures of important types of the eight tetrapyrrole categories and their common precursor uroporphyrinogen III.
The cyclic as well as the non-cyclic tetrapyrroles derive from the common precursor uroporphyrinogen III.
A = acetate side chain; P = propionate side chain; M = methyl group; V = vinyl group.

Magnesium-complexes of chlorophylls and bacteriochlorophylls are the active components in the reaction centers of the light accumulating complexes of photosynthesis. They generate the conversion of sunlight energy into chemical energy (Jahn *et al.*, 1996; Beale, 1999; Vavilin and Vermaas, 2002; Frankenberg *et al.*, 2003; Layer *et al.*, 2010). In contrast, bilins are linear

tetrapyrroles with only three bridged carbons. They are the result from the cleavage of previously cyclic tetrapyrroles. Furthermore, there is no tightly bound metal ion in linear tetrapyrroles. They serve as chromophoric photoreceptors in cyanobacterial and higher-plant light-harvesting systems (Frankenberg and Lagarias, 2003).

1.1.2 Tetrapyrrole Biosynthesis

The pathway for the tetrapyrrole biosynthesis is save from a few exceptions highly conserved and the first branching point occurs after formation of the first cyclic tetrapyrrole, uroporphyrinogen III. This intermediate is converted into protoporphyrin XI or precorrin-2. The former is required to synthesize hemes, chlorophylls and bacteriochlorophylls while the latter is utilized for the synthesis of siroheme, heme d_1, coenzyme F_{430} and corrinoids (Warren and Smith, 2008). Eukaryotes are only able to synthesize hemes, siroheme, chlorophyll and bilins while prokaryotes also synthesize additional tetrapyrroles like corrinoids, coenzyme F_{430} and heme d_1 (Jahn *et al.*, 1996). Tetrapyrrole biosynthesis starts in all organisms with the synthesis of 5-aminolevulinic acid (ALA).

Fig. 3 shows the tetrapyrrole biosynthesis and its different pathways.

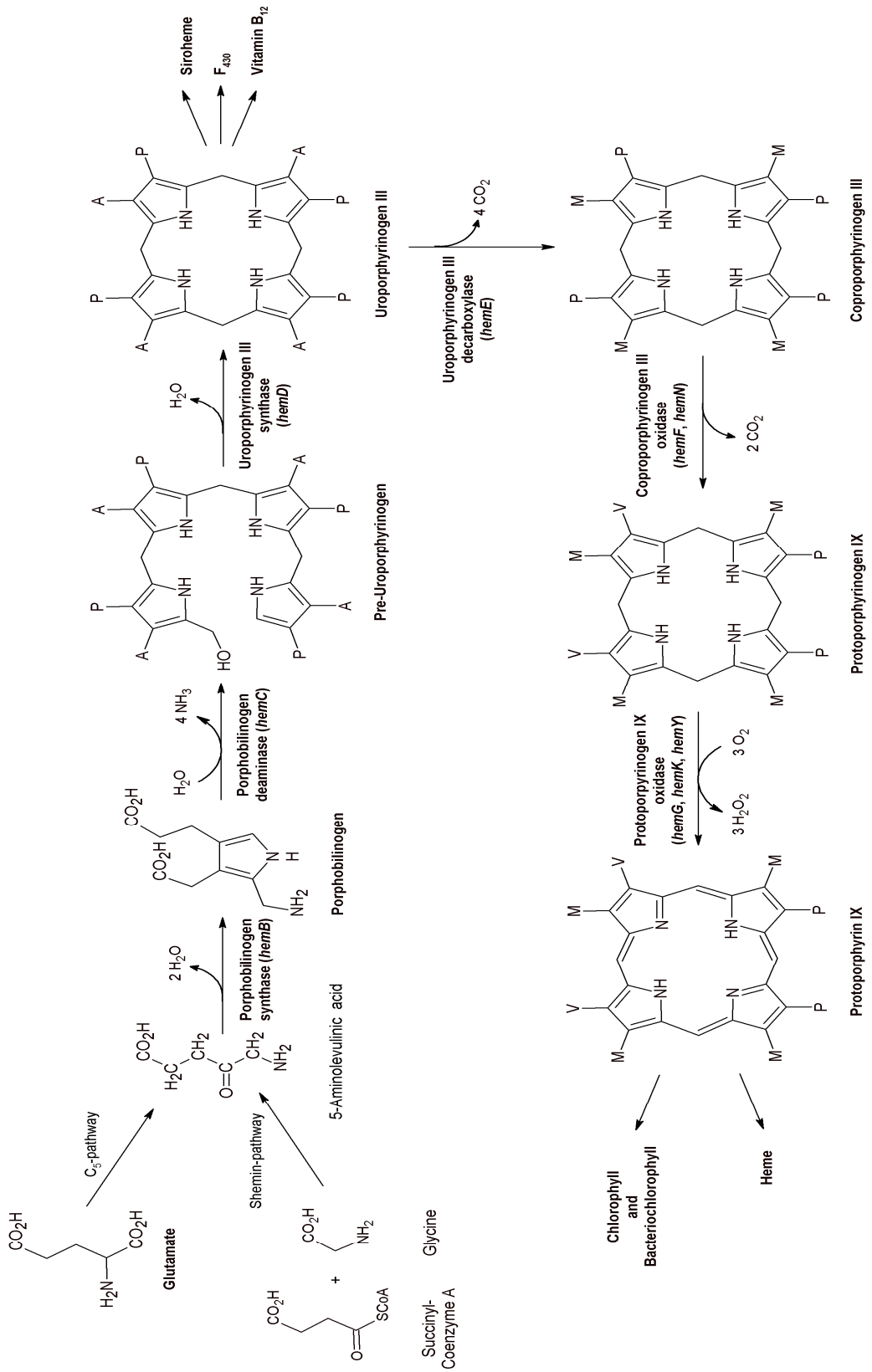

Fig. 3: Tetrapyrrole biosynthesis.
Enzyme names and corresponding bacterial genes are given above the arrows.
A = acetate side chain; P = propionate side chain; M = methyl group; V = vinyl group.

1.1.3 Aminolevulinic Acid Formation

Tetrapyrrole biosynthesis starts in all organisms with the synthesis of ALA (Fig. 3) representing the sole source of carbon and nitrogen atoms required for heme formation. There are two different, unrelated biosynthetic pathways to form ALA. In α-proteobacteria, yeast and animal mitochondria ALA is formed *via* the 'Shemin (C_4-)-pathway'. Here, the pyridoxal-5'-phosphate (PLP-) dependent enzyme, 5-aminolevulinic acid synthase (ALAS, encoded by *hemA,* EC 2.3.1.37), catalyzes the condensation of glycine and succinyl-Coenzyme A (succinyl-CoA) that gives CO_2, Coenzyme A (CoA) and ALA (Shemin and Russel, 1953; Kikuchi *et al.*, 1958; O'Brian and Thöny-Meyer, 2002). In chloroplasts from green algae and plants, cyanobacteria, archaea and in most other bacteria, ALA is synthesized from the C_5-skeleton of glutamic acid (Beale and Castelfranco, 1973; Jahn *et al.*, 1992). This pathway is called 'C_5-pathway' and the reaction is catalyzed by two different enzymes: glutamyl-tRNA-reductase (GluTR; encoded by *hemA*, EC 6.1.1.17) and glutamate-1-semialdehyde-2,1-aminomutase (GSAM; encoded by *hemL*, EC 5.4.3.8). The first step is a reduction from tRNA-bound glutamate in a nicotinamide adenine dinucleotide hydrate (NADPH)-dependent reaction into the unstable glutamate-1-semialdehyde (GSA) by the GluTR, in which the $tRNA^{Glu}$ is released (Jahn *et al.*, 1991; Moser *et al.,* 1999; Jahn and Heinz, 2009). The initial substrate, glutamyl-tRNA, is used for heme formation as well as for protein synthesis. The final step is a PLP-dependent transamination reaction of the semialdehyde to ALA by the action of GSAM (Ilag and Jahn*,* 1992). Thereby the C_5-skeleton of glutamate is incorporated into ALA which is the eponym for this pathway. The aldehyde GSA is highly reactive in free solution. Therefore, a proposal of a GluTR/GSAM complex existed which was in accordance with the structural complementarity of GluTR and GSAM (Moser *et al.*, 2001). This complex was verified *in vivo* and thus explained the direct channeling of the instable intermediates by obviation of solvent exposure (Luer *et al.*, 2005). *Euglena gracilis*, a photosynthetic phytoflagellate, is the only organism known that uses both pathways, the 'Shemin-' and the 'C_5-pathway' for heme biosynthesis (Iida *et al.*, 2002). Here, ALA for mitochondrial tetrapyrroles

derived from ALAS while ALA for plastidic pigments is formed by the 'C_5-pathway' (Weinstein and Beale, 1983). Another interesting route of heme biosynthesis occurs in the malarian parasite *Plasmodium falciparum*. This organism has, besides its mitochondrion, a second unique organelle known as apicoplast which represents a relict plastid with 'plant-like' characteristics, yet devoid of photosynthesis. The apicoplast is believed to have once contained a complete set of heme biosynthesis proteins with ALA synthesis occurring *via* the 'C_5-pathway'. However, the 'C_5-pathway' components seem to have been lost in the course of evolution. Thus, in *P. falciparum* ALA is exclusively synthesized by ALAS in the mitochondrion and then shuttled to the apicoplast for further conversion into porphobilinogen (PBG, Lim and McFadden, 2010).

1.1.4 The Common Step of Tetrapyrrole Biosynthesis: From Aminolevulinic Acid to Uroporphyrinogen III

The next three steps after ALA formation are common for all tetrapyrroles with uroporphyrinogen III as central intermediate product. Following ALA formation is the synthesis of PBG through an asymmetrical condensation of two ALA molecules. This is catalyzed by the porphobilinogen synthase (PBGS, encoded by *hemB*, EC 4.2.1.24, also known as ALA dehydratase; Frankenberg *et al.*, 1999b). This enzyme usually functions as a homooctameric protein with the exception of the *Rhodobacter capsulatus* enzyme which was shown to be a hexamer (Bollivar *et al.*, 2004). PBGS enzymes from different organisms can be divided into subgroups according to their dependency on different metal ions. Human and yeast PBGS contain two zinc ions, one of them playing a role in catalysis which are coordinated by highly conserved cysteine residues (Gibbs *et al.*, 1985; Senior *et al.*, 1996; Senior *et al.*, 1997; Shoolingin-Jordan *et al.*, 2002). *Escherichia coli* PBGS contains zinc in the active site and an additional magnesium ion. *Pseudomonas aeruginosa* PBGS harbors magnesium ions at an allosteric site and monovalent cations in the active site (Frankenberg *et al.*, 1999a; Frankenberg *et al.*, 1999b; Mitchel and Jaffe, 1993). Furthermore, it was reported that some PBGS enzymes are metal-independent (Bollivar *et al.*, 2004). The PBGS enzymes possess two different ALA binding sites, called

‘P-site’ and ‘A-site’. The first ALA molecule which contributes the propionate group of PBG forms a Schiff’base to a conserved lysine residue within the ‘P-site’. In addition, a second ALA molecule also forms a Schiff’base to a second strictly conserved active site lysine residue to produce the acetate group carrying half of PBG. The Schiff’base at the ‘A-site’ is then transformed into an enamine. In an aldole addition reaction the C-3 atom of the ‘A-site’-ALA attacks the C-4 of the ‘P-site’-ALA with the result of the C-C bond between the two ALA molecules. Subsequently, the amino group of the ‘P-site’-ALA attacks the Schiff’base at the C-4 atom of the ‘A-site’-ALA leading to a C-N bond formation and release of the ‘A-site’-lysine. Liberation of the ‘P-site‘-lysine and the reaction intermediate is triggered by protonation and possibly by conformational changes of the enzyme. A final proton abstraction leads to the aromatization and PBG release. (Erskine *et al.*, 2001; Frere *et al.*, 2002; Erskine *et al.*, 2003; Jaffe, 2004; Frere *et al.*, 2006).

In most investigated bacteria the genes for the next two enzymes of heme biosynthesis, porphobilinogen deaminase or hydroxymethylbilane synthase (PBGD, HMBS) and uroporphyrinogen III synthase (UROS), are located in one operon. A reason for the coordinated expression of these two genes could be the formation of an enzyme complex to channel the pre-uroporphyrinogen intermediate to prevent formation of the toxic uroporphyrinogen I (Fig. 4A), *via* spontaneous cyclisation of pre-uroporphyrinogen (Jordan, 1991).

The PBGD (encoded by *hemC*, EC 4.3.1.8; Burton *et al.*, 1979; Battersby *et al.,* 1979*;* Battersby *et al.*, 1982) catalyzes the stepwise condensation of four PBG molecules under eliminiation of an amino group at each step to form the linear and unstable tetrapyrrole intermediate pre-uroporphyrinogen (1-hydroxy-methylbilane). In mammalian cells and yeast the enzyme is located as a soluble protein in the cytosol. In higher plants and algae it is located in the stroma of the chloroplasts (Elder, 1976; Labbe-Bois and Labbe, 1990; Smith, 1988; Spano and Timko, 1991). The PBGD occurs in all so far determined organisms as a monomer with a size range from 33’000 Da to 45’000 Da and is composed in three domains. The dipyrromethane cofactor is a PBG dimer and covalently attached to domain three through its free amino group (Jordan and Warren, 1987; Warren and Jordan, 1988). The cofactor serves as a primer for the

oligomerization of another four PBG molecules with the result of a protein bound linear hexapyrrole. Furthermore, the cofactor is anchored inside the cleft between domain one and two over expanded salt bridges and hydrogen bonds (Louie *et al.*, 1992). The active site is located between these both domains (Louie *et al.*, 1996). A highly conserved aspartate residue plays an important role during the deamination process of PBG after it is linked to the growing oligopyrrole chain (Louie *et al.*, 1992; Woodcock and Jordan 1994).

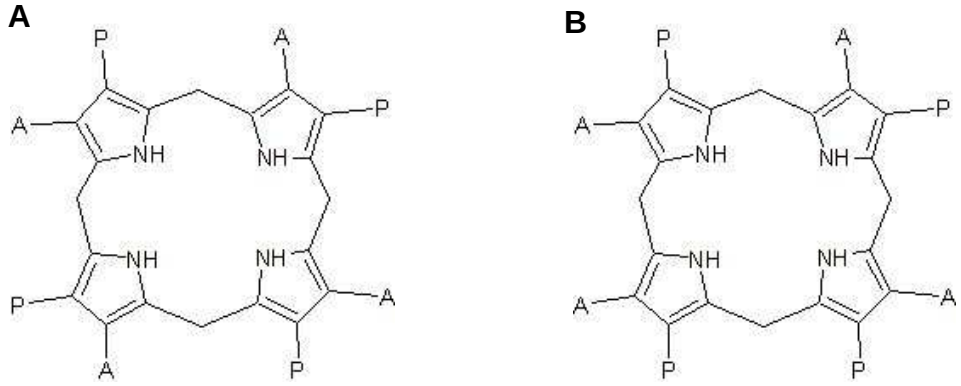

Fig. 4: Uroporphyrinogen I and uroporphyrinogen III.
A. Uroporphyrinogen I. **B.** Uroporphyrinogen III.

Pre-uroporphyrinogen is converted into the cyclic, asymmetric uroporphyrinogen III by the UROS (encoded by *hemD*, EC 4.2.1.75). UROS is a monomeric protein consisting of two α/β-domains which are connected by a flexible, two-stranded linker. Domain I belongs to the flavodoxin-like fold family while domain II shows a DNA glycosylase-like fold (Mathews *et al.*, 2001). The asymmetry of the tetrapyrrole intermediate provided by UROS is caused by the inversion of ring-D *via* a spiro-mechanism with spiro-pyrrolenine as an intermediate (Chadwick, 1994; Shoolingin-Jordan and Cheung, 1999). In the first step of UROS catalysis the hydroxyl group on ring A of pre-uroporphyrinogen is lost as a water molecule with the result of the first azafulvene intermediate. Subsequently, the spirocyclic pyrrolenine intermediate is formed by reaction of the azafulvene with the substituted α-position of ring D. The second azafulvene intermediate at the C-ring is formed by bond breakage between rings C and D. In the final steps of catalysis the enzyme has to orientate the ring-D-pyrrole in such a way that the C-ring azafulvene can react with its free α-position. Finally, uroporphyrinogen III is formed by deprotonation

and bond rearrangements (Stark *et al.*, 1986; Cassidy *et al.*, 1996; Pichon *et al.*, 1994; Shoolingin-Jordan, 1995; Silva and Ramos, 2008). The product of this reaction, uroporphyrinogen III (Fig. 4B), is the last common product of the biosynthesis of all tetrapyrroles (Fig. 3).

1.1.5 From Uroporphyrinogen III to Heme

The biosynthetic pathways of the porphonoides like siroheme and the cofactor F_{430} as well as the corrinoids get already separated after five steps from the pathway of porphyrine formation. The fifth enzyme in the heme and chlorophyll biosynthesis, uroporphyrinogen III decarboxylase (UROD*,* encoded by *hemE*, EC 4.1.1.37), catalyzes the formation of coproporphyrinogen III (coprogen) by the sequential displacement of carboxyl groups from the four acetate side chains of the uroporphyrinogen III into methyl groups (Luo *et al.*, 1993), starting on ring D, then A, B and finally C (Akhtar, 1991; Luo and Lim, 1993). UROD is an unusual decarboxylase in that it is not dependent on any prosthetic goup or cofactor. Furthermore, it is a dimeric protein in which the two single-domain subunits are orientated head-to-head with the active site clefts facing each other at the dimer interface resulting in one large active site (Martins *et al.*, 2001). One proposal for the UROD reaction mechanism suggests a reorientation of the substrate by 90° for each decarboxylation step. A highly conserved aspartate residue seems to be involved in substrate binding and catalysis. The first step in the proposed reaction mechanism is the protonation of the substrate pyrrole ring at the α-position close to the C-atom bearing the acetate side chain. An aspartate residue stabilizes the formed positively charged reaction intermediate. Decarboxylation of the acetate side chain results in another intermediate which has to be protonated at the methylene carbon and deprotonated at the α-C-atom to yield the reaction product. A highly conserved arginine residue within the active site was proposed to be involved in the final protonation step. The subsequent decarboxylation takes place after substrate rotation by 90° at the same active site and in the same manner as the first one (Phillips *et al.*, 2003; Lewis and Wolfenden, 2008). The two protonation steps are supported by two arginine residues (Arginine 37 and Arginine 41) lying in the active site and

serving as acid catalysts. It was proposed that the flexibility of Arginine 37 allows this residue to donate protons to each of the four pyrrole rings without substrate rotation (Silva *et al.*, 2010).

The next enzyme, coproporphyrinogen III oxidase (CPO, encoded by *hemF, hemN*, EC 1.3.3.3) catalyzes the sequential oxidative decarboxylation of the propionate groups in position three and eight (ring A and B) of coproporphyrinogen III to vinyl groups yielding protoporphyrinogen IX. The decarboxylation of the propionate side chain of ring A occurs *prior* to that on ring B *via* the reaction intermediate harderoporphyrinogen (Cavaleiro *et al.*, 1974; Elder *et al.*, 1978; Rand *et al.*, 2010). This reaction is catalyzed under aerobic and anaerobic conditions by two different, structural unrelated enzymes. HemF performs this task under aerobic conditions. HemN, a 'Radical-SAM' enzyme catalyzes this reaction under anaerobic conditions and should rather be named coproporphyrinogen III dehydrogenase (CPDH, EC 1.3.99.22; Breckau *et al.*, 2003; Layer *et al.*, 2002). Bacterial and plant CPOs are soluble proteins while yeast and animal enzymes are loosely associated with mitochondrial membranes (Smith *et al.*, 1993; O'Brian and Thöny-Meyer, 2002). The oxygen-dependent CPO is a dimeric enzyme with molecular oxygen as terminal electron acceptor. Each monomer consists of a single domain adopting an exceptional fold in which a large seven-stranded antiparallel β-sheet is covered on both sides by α-helices. Both β-sheets face each other and the subunits are rotated by approximately 40° relative to another. T he oxygen-independent CPO (CPDH) needs another terminal electron acceptor than oxygen for the oxidative decarboxylation reaction. The reaction sequence and its stereochemistry is the same as for the oxygen-dependent CPO (Seehra *et al.*, 1983). CPDH is a monomeric protein with a C- and an N-terminal domain with the N-terminal domain being the larger one (Layer *et al.*, 2003). As a member of the 'Radical-SAM' protein family it harbors an oxygen-labile [4Fe-4S] cluster. Three of the four iron atoms are coordinated by three highly conserved cysteine residues of the characteristic CX_3CX_2C motif (Layer *et al.*, 2002). The fourth iron atom is ligated by an *S*-adenosyl-L-methionine (SAM) molecule serving as cofactor by initiating the radical based catalysis (Layer *et al.*, 2003).

The penultimate enzyme of heme formation, protoporphyrinogen IX oxidase (PPO, encoded by *hemG, hemY*, EC 1.3.3.4) is the last common enzyme of the heme and chlorophyll biosynthesis. The relative molecular masses of PPO monomers range from M_r = 36'000 to M_r = 65'000. In contrast, the HemG enzyme of *E. coli* only has a molecular mass of approximately M_r = 21'000. PPO converts protoporphyrinogen IX to protoporphyrin IX (proto) which requires the elimination of six electrons and results in the formation of a planar system of completely conjugated double bonds. In eukaryotes and some bacteria HemY, the oxygen-dependent flavin-containing enzyme form, catalyzes this reaction and requires molecular oxygen as final electron acceptor (Hansson and Hederstedt, 1994a; Koch *et al.*, 2004). PPOs which require oxygen are usually homodimeric, membrane-associated proteins with the exception of monomeric PPO from *Bacillus subtilis* and *Aquifex aeolicus* (Hansson and Hederstedt, 1994a; Hansson *et al.*, 1997). *B. subtilis* PPO was found to be soluble in the cytoplasm (Corrigall *et al.*, 1998). Each monomer of dimeric PPOs as well as the monomeric *B. subtilis* enzyme consists of three domains, an FAD-binding, a substrate-binding and a dimerization domain. The dimerization domain is responsible for membrane association (Hansson and Hederstedt, 1994a; Dailey and Dailey, 1997). In contrast to oxygen-dependent PPOs, oxygen-independent PPOs are one of the first examples for the direct coupling of anabolic heme biosynthesis with catabolic ATP generating electron transport chains. Under aerobic conditions HemG abstracts six electrons from its substrate and transfers them *via* ubiquinone, cytochrome bo_3 (Cyo) and cytochrome *bd* (Cyd) oxidase to oxygen. Under anaerobic conditions electrons are transferred *via* menaquinone, fumarate (Frd) and nitrate reductase (Nar) to fumarate and nitrate, respectively. Cyo, Cyd and Nar contribute to the proton motive force that drives ATP formation (Jacobs and Jacobs, 1976; Dailey and Dailey, 1996; Möbius *et al.*, 2010).

In the ultimate step of heme biosynthesis, chelatases catalyze the insertion of metals into the centers of the generated tetrapyrroles. The ferrochelatase (FC, encoded by *hemH*, EC 4.99.1.1; Dailey, 2002) forms heme b by insertion of iron into protoporphyrin IX. In eukaryotes FC is a membrane-associated homodimer while it is monomeric in bacteria (Wu *et al.*, 2001; Wang *et al.*,

2001; Grzybowska *et al.*, 2002). In Gram-positive bacteria, *e.g. B. subtilis*, FC is a soluble protein located in the bacterial cytoplasm (Hansson and Hederstedt, 1994b). Compared to the eukaryotic FCs which contain one [2Fe-2S] cluster per subunit, the bacterial counterparts have been described with and without FeS clusters (Dailey *et al.*, 1994; Day *et al.*, 1998; Dailey and Dailey, 2002; Shepherd *et al.*, 2006). Furthermore, it was shown that the position of the propionate side chains on rings C and D are critical for catalysis in contrast to the substituents on rings A and B which are variable. FCs are also able to insert divalent metal ions like Ni^{2+} and Zn^{2+} into porphyrins whereas others like Mn^{2+} or Pb^{2+} have inhibitory effects (Hunter *et al.*, 2008; Medlock *et al.*, 2009). The eukaryotic enzyme consists of two similar domains with a C-terminal extension forming a helix-turn-helix structure and which is involved in coordination of the FeS cluster. In the FC homodimer this C-terminal extension is responsible for the interaction between the monomers of the dimer. Moreover, the C-terminal extension is lacking in bacteria explaining their monomeric structure. Both active site pockets of dimeric human FC are located on the same hydrophobic surface which is believed to be integrated within the membrane (Medlock *et al.*, 2007). In *Thermosynechococcus elongatus* the metabolic channeling between PPO and FC has been shown *in vivo* that prevent solvent exposure of the photoreactive protoporphyrin IX (Masoumi *et al.*, 2008).

1.2 Aminolevulinic Acid Synthase

Aminolevulinic acid synthase (ALAS, EC 2.3.1.37) is the first enzyme in tetrapyrrole biosynthesis in humans, animals and the α-proteobacteria. It catalyzes the condensation of the amino acid glycine and succinyl-CoA to the products ALA, carbon dioxide and CoA (Fig. 5).

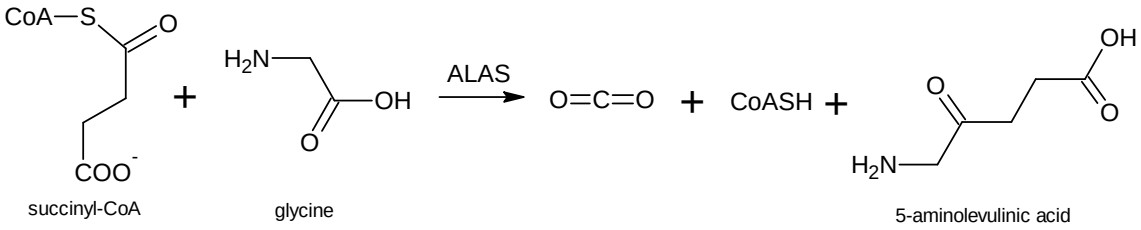

Fig. 5: ALAS catalyzed reaction.
The ALAS catalyzes the condensation of glycine and succinyl-CoA that gives carbon dioxide, CoA and ALA.

1.2.1 The Different Aminolevulinic Acid Synthases

The ALAS is a homodimer with an active site at the subunit interface. Within the α-family of PLP-dependent enzymes ALAS belongs to the aminotransferase fold-type II subfamily which catalyzes the condensation of a carboxylic acid CoA thioester and small amino acids (Nandi, 1978b; Fanica-Gaigner and Clement-Metral, 1973a; Alexander *et al.*, 1994; Astner *et al.*, 2005; Schulze *et al.*, 2006). The relative molecular masses of the monomers range from M_r = 43'000 to M_r = 66'000. It catalyzes the PLP-dependent condensation of two substrates, succinyl-CoA (produced in the citric acid cycle) and glycine in non-plant eukaryotes as well as the α-subclass of purple bacteria (Christen and Mehta, 2001; Ferreira and Zhang, 2002; Schulze *et al.*, 2006). This step is the rate-limiting one and leads to the product ALA, the first common precursor of all tetrapyrroles. Some bacteria, *e.g. Rhodobacter sphaeroides,* and humans encode two different ALAS genes. In humans there are an erythroid-specific (ALAS2), and a housekeeping ALAS (ALAS1; Riddle *et al.*, 1989; Bishop *et al.*, 1990). The erythroid ALAS is difficult to purify because of a short biological half-life (Furuyama and Sassa, 2002). In *R. sphaeroides* there are HemA and HemT (encoded by *hemA* or *hemT*, respectively; Neidle and Kaplan, 1993). In contrast to humans, *R. sphaeroides* can survive with only one intact ALAS gene, in humans the two different isoforms cannot replace the function of each other.

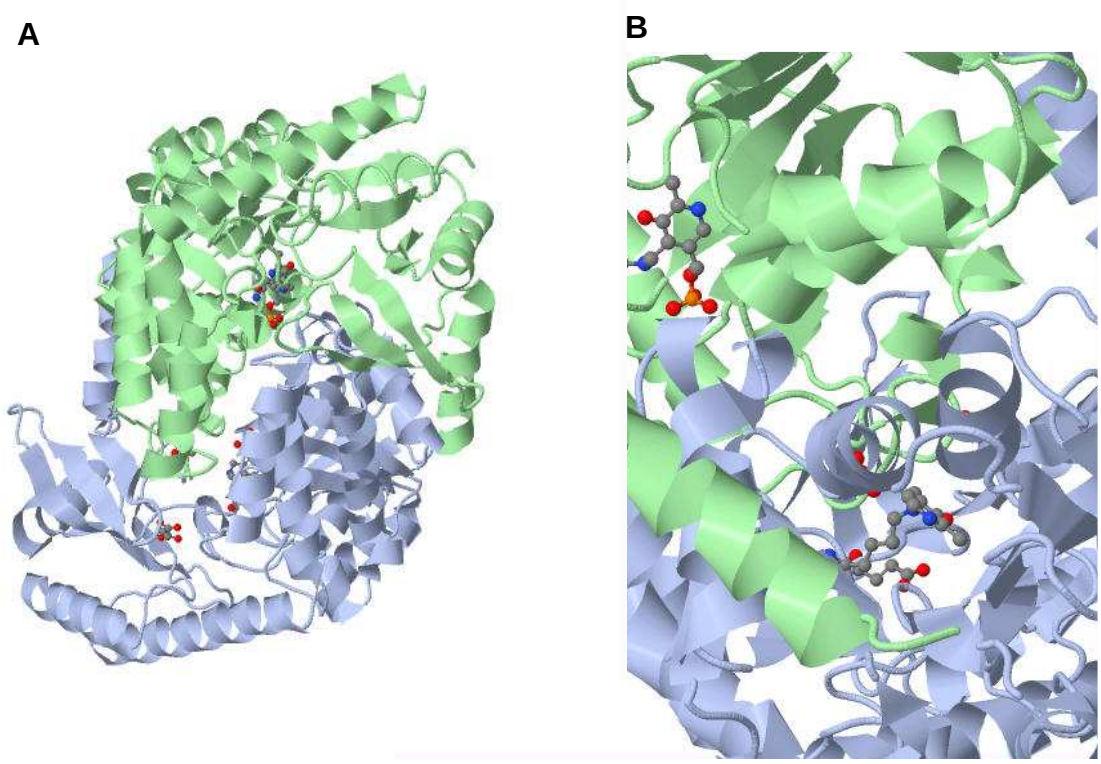

Fig. 6: Crystal structure of *Rhodobacter capsulatus* ALAS.
A. The ALAS of *R. capsulatus* is a homodimer. Each monomer consists of one chain, chain A is depicted in blue and chain B in green. The α-helices are displayed as spirals and β-sheets as arrows. **B.** Magnification of the active site with two bound PLP-molecules, displayed as grey-blue-red-orange stick-and-ball molecules (Astner, 2007).

ALAS is highly conserved from α-proteobacteria to humans with amino acid sequence identities ranging from 40 to 80 %. The cofactor is bound to an active site lysine residue (*e.g.* in mouse: Lysine 313) *via* a Schiff'base linkage (Ferreira *et al.*, 1993a). Its ε-amino group undergoes changes in absorptive properties during substrate binding and catalysis. Moreover, substrate binding triggers closure of an extended loop over the active site (Astner *et al.*, 2005). Kinetic and crystallographic studies propose the availability of such an active site loop that affects the rate of ALA production coincident with product release (Hunter and Ferreira, 1999; Astner *et al.*, 2005; Hunter *et al.*, 2007).

1.2.2 ALAS Reaction Mechanism

The ALAS-catalyzed reaction involves the mechanistically cleavage of two amino acid α-carbon bonds. This reaction mechanism is highly unusual for PLP-dependent enzymes. Contrary to ALAS that cleaves two α-carbon bonds, most commonly known PLP enzymes (Percudani and Peracchi, 2003) catalyze only the cleavage of a single α-carbon substrate bond. There are only three other enzymes known that also catalyze the cleavage of two α-carbon bonds *i.e.* 8-amino-7-oxononanoate synthase (AONS; Alexeev *et al.*, 1998), serine palmitoyltransferase and dialkylglycine decarboxylase (Mehta and Christen, 1994). In contrast to the first two of them which catalyze a reaction similar to the ALAS reaction, dialkylglycine decarboxylase (Toney, 2005) uses a ping-pong reaction mechanism involving transamination and decarboxylation half-reactions.

Dunathan proposed that for efficient electron delocalization into the conjugated ring system, the bond to be cleaved must be oriented perpendicular to the plane of the PLP ring (Dunathan, 1966). The ALAS reaction with cleavage of two α-carbon bonds is difficult to align with Dunathan's hypothesis. Granted that the sequential cleavage of two of the glycine α-carbon bonds in the ALAS reaction is in agreement with Dunathan's hypothesis, the stereochemistry in the ALAS mechanism would assume torsion about the aldimine linkage of approximately 60° at some point during the time interval between formation of the two quinonoid intermediates. Another possibility to explain the unusual ALAS reaction is that the decarboxylation of the 2-amino-3-ketoadipate intermediate occurs through the β-keto-group rather than into the cofactor ring, as was suggested for AONS (Alexeev *et al.*, 2006). The third possibility is that ALAS is an exception to Dunathan's hypothesis. Recently, it could be shown that decarboxylation occurs through the carbonyl group with Histidine 207 of murine ALAS acting as a general acid catalyst. Furthermore, it is the enol intermediate (VI, Fig. 7) in which the alkene bond is aligned orthogonal to the plane of the cofactor that gives rise to the resonance stabilized quinonoid (VII, Fig. 7).

Fig. 7 shows the postulated reaction mechanism for ALAS using the example of the mouse enzyme.

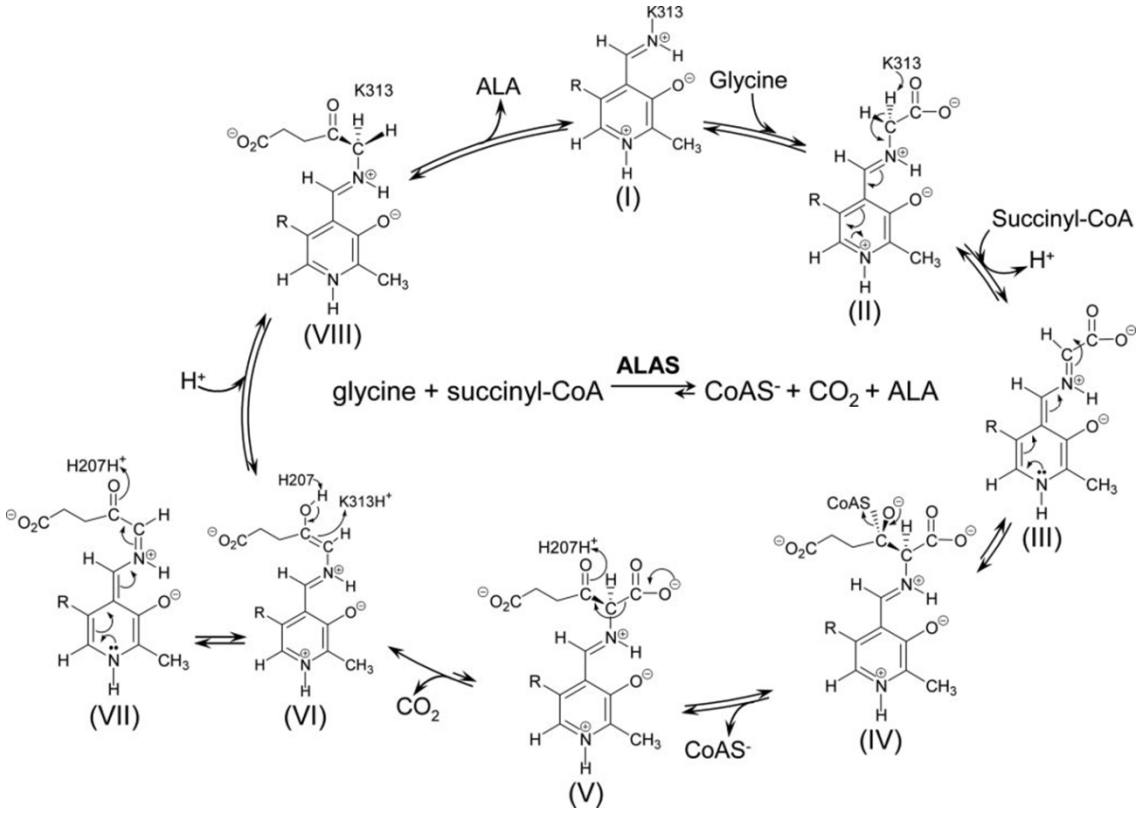

Fig. 7: Postulated ALAS reaction mechanism (Hunter *et al.*, 2007).
Postulated ALAS reaction mechanism for the mouse enzyme.
I = internal aldimine; II = external aldimine; III = first quinonoid; IV = condensation with succinyl-CoA; V = 2-amino-3-ketoadipate intermediate; VI = enol acts as electron sink; VII = second quinonoid; VIII = ALA-bound external aldimine. ALA will be released and the holoenzyme is regenerated.

The ALAS reaction mechanism is an ordered *bi-bi*-kinetic mechanism with glycine binding prior to succinyl-CoA, and ALA release after carbon dioxid and CoA (Fig. 7; Fanica-Gaigner and Clement-Metral, 1973b; Nandi, 1978a; Astner *et al.*, 2005). The internal aldimine consists of the covalently bound PLP-cofactor at an active site lysine residue and the enzyme (I, Fig. 7; Ferreira *et al.*, 1993a). It was shown that a conserved tyrosine residue (murine ALAS2 Tyrosine 121) is essential for cofactor binding while a conserved lysine residue (murine ALAS2 Lysine 313) is essential for catalysis (Ferreira *et al.*, 1995a; Tan *et al.*, 1998). The first step in the reaction is the formation of the external aldimine, *i.e.* association of glycine with the enzyme (II, Fig. 7). The first quinonoid (III, Fig. 7) will be formed by stereo-specific murine ALAS2 K313-catalyzed abstraction of the pro-*R*-proton from the PLP-glycine external aldimine. The next step is the attachment of the electrophilic carbonyl group of

succinyl-CoA to the glycine α-carbon (IV, Fig. 7) that provides the second proposed intermediate, 2-amino-3-ketoadipate (V, Fig. 7). The existence of this intermediate has as of yet not been definitively confirmed. However, the occurrence of the corresponding intermediate in AONS (Kerbarh *et al.*, 2006) and 2-amino-3-ketobutyrate ligase (Schmidt *et al.*, 2001), enzymes that are structurally and mechanistically related, points to the ALAS reaction pathway. The release of CoA from this tetrahedral intermediate, 2-amino-3-ketoadipate, and decarboxylation of the carboxyl carbon of glycine leads to the formation of an enol (VI, Fig. 7). This species is the third intermediate in this reaction pathway and serves as electron sink. Additionally, it is in equilibrium with the second quinonoid (VII, Fig. 7; Hunter and Ferreira, 2009) as well as with the ALA-bound external aldimine upon protonation of the C-5 position. The last steps are protonation (VIII, Fig. 7) of the quinonoid intermediate (formation of the ALAS-ALA-aldimine) and ALA release. An active site histidine residue acts as a general acid, and finally regeneration of the internal aldimine in a transaldimination reaction occurs (Hunter and Ferreira, 1999; Zhang and Ferreira, 2002). ALA release represents the rate-limiting step of the reaction and is kinetically influenced by a conformational change of the enzyme (Hunter and Ferreira, 2009).

The holoform of the *R. capsulatus* ALAS ($ALAS_{Rc}$) was crystallized and the X-ray crystal structure was solved at 2.1 Å resolution (Astner *et al.,* 2005) as well as enzyme-substrate complexes with glycine and succinyl-CoA, respectively. With the $ALAS_{Rc}$ crystal structure it was possible to create a structural model of the human erythroid ALAS dimer for the first time. Both monomers of the $ALAS_{Rc}$ homodimer are closely connected with each other. The ALAS consists of three domains, an N-terminal domain (amino acids in $ALAS_{Rc}$ 1 - 53), a central catalytic domain (amino acids in $ALAS_{Rc}$ 54 - 296) and a C-terminal domain (amino acids in $ALAS_{Rc}$ 297 - 401). The C- and N-termini are located at the protein surface and they are easily accessible. Each of the three domains of one monomer is connected to two domains of the second monomer (Astner, 2007).

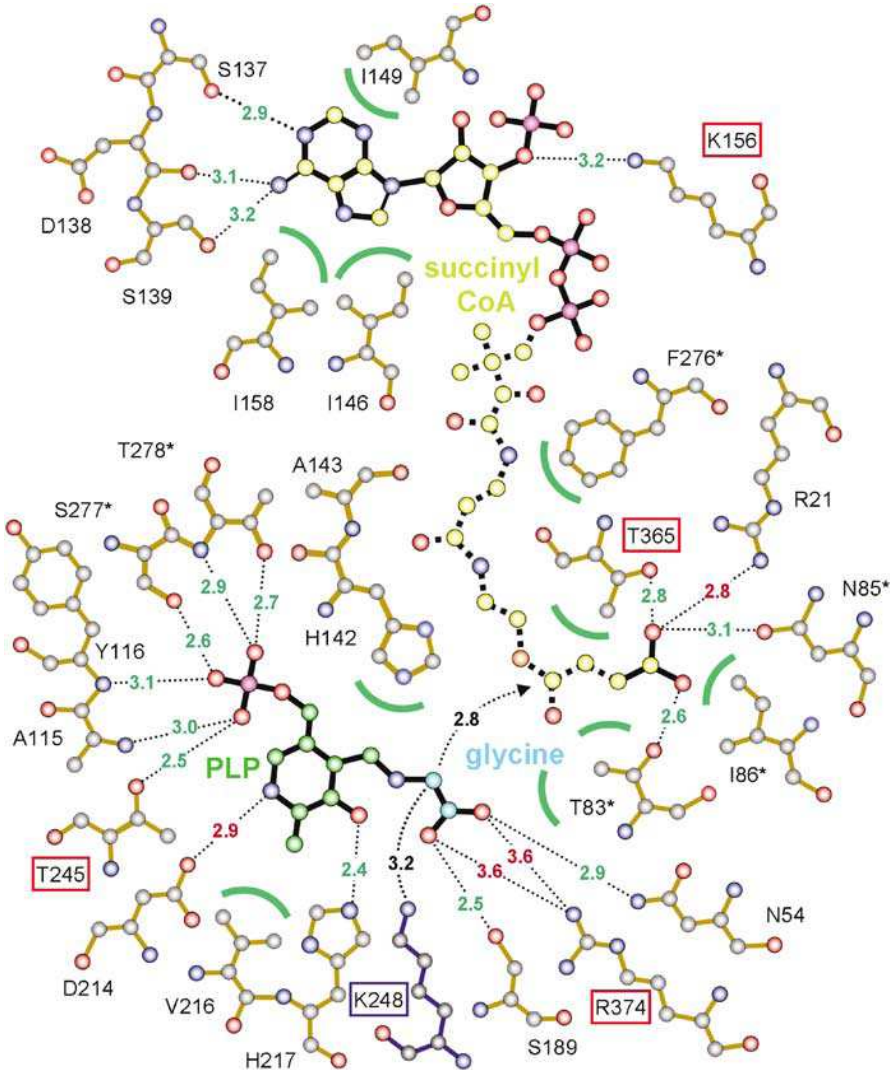

Fig. 8: Schematic representation of the active site of the *R. capsulatus* ALAS (Astner *et al.*, 2005).
Glycine-bound PLP and succinyl-CoA are highlighted by black bonds while surrounding residues show a dark orange color. Hydrogen bonds are displayed by dotted lines (green numbers) and salt bridges (red numbers) between substrates or cofactor and ALAS. Van der Waals interactions are denoted by green semicircles. Residues from the second monomer are marked with an asterisk. K248, the lysine residue involved in PLP binding and catalysis, is marked by a blue box while residues affected by mutations in human ALASe are marked by a red box.

In *R. capsulatus* the PLP-cofactor is tightly bound *via* interactions like hydrogen bonds from the oxygen atoms of the phosphate residue to the main chain amides from Alanine 115, Tyrosine 116 and Threonine 278* from the catalytic domain and to the side chains from Serine 277*, Threonine 278* and Threonine 245* (* residues from the second monomer; Fig. 8). The plane of the PLP-pyridine ring is sterically focused *via* hydrophobic stacking with Valine 216 and Histidine 142. A hydrogen bond between the PLP-hydroxyl group and

Histidine 217 stabilizes the cofactor, too (Astner *et al.*, 2005; Turbeville *et al.*, 2007). In mouse erythroid ALAS Asparagine 279 was identified as an important residue in this enzyme-catalyzed reaction by enhancing the electron withdrawing capacity of the PLP-cofactor and stabilizing the protonated form of the PLP-pyridinium ring nitrogen (Gong *et al.*, 1998). Additionally, Arginine 439 seems to play a role in recognition and binding of glycine by forming an ionic bond between its guanidinium side chain and the carboxylate of the substrate glycine (Tan *et al.*, 1998). The ALAS dimer forms a hole close to the PLP-cofactor, called the active site, located at the subunit interface. In the absence of the two substrates the PLP-cofactor is covalently attached to the active site lysine as a Schiff'base in the active site pocket. There are two channels leading to the active site. The first one is built from the catalytic domain, the C-terminal domain from the PLP-giving monomer and part of a strand of the N-terminal domain. The second one is smaller and here the N-terminal domain is the main component that builds this channel, C-terminus and catalytic domain are also involved (Astner *et al.*, 2005). Glycine and succinyl-CoA can enter the active site pocket *via* these channels. Glycine is covalently linked to PLP as an external aldimine. Thereby, Arginine 374 of *R. capsulatus* is highly conserved and essential for binding of the glycine carboxyl group. Furthermore, the position of the carboxyl residue is stabilized by hydrogen bonds to Asparagine 54 and Serine 189 (Astner *et al.*, 2005). There are two different conformations in the ALAS enzyme, an open and a closed one. In the open conformation the substrates are bound; the closed conformation is formed, induced by the binding of the second substrate, succinyl-CoA (Zhang and Ferreira, 2002). The existence of the 2-amino-3-ketoadipate intermediate has not be confirmed yet, but it is known that the corresponding intermediates occur in AONS (Kerbarh *et al.*, 2006) as well as in ketobutyrate ligase (Schmidt *et al.*, 2001).

1.3 Typical Features of Pyridoxal-5'-phosphate-dependent Enzymes

Several enzymes like ALAS utilize PLP, the active form of vitamin B_6 (Pyridoxin; Heyl *et al.*, 1951), as coenzyme for their catalytic reactions. PLP-dependent enzymes catalyze a variety of different reactions, *e.g.* racemizations, decarboxylations or transaminations (Eliot and Kirsch, 2004). Almost all PLP enzymes follow a similar reaction mechanism: The aldehyde group of PLP is covalently linked to an active site lysine residue whereby the so called internal aldimine is formed. In a first common step a Schiff'base is generated after condensation of the amino acid substrate and the PLP-cofactor, also known as external aldimine. In a following step one of the bonds to the α-carbon atom is broken with PLP serving as an electron sink and stabilizing the negative charge at the α-carbon atom by delocalization through its *pi*-system. The subsequently formed and stabilized carbanion is called quinonoid (Schneider *et al.*, 2000; Eliot and Kirsch, 2004). For bond breaking and efficient electron delocalization into the conjugated ring system the cofactor weakens the sigma bonds around a carbon atom which is oriented perpendicular to the pyridine ring of the cofactor in the transition state of the reaction (Corey and Sneen, 1956; Dunathan, 1966). The exceptions to this mechanism are the PLP-dependent phosphorylases. Their reaction chemistry is different in that they use the phosphate group of the cofactor for catalysis (Schneider *et al.*, 2000). PLP-catalyzed reaction types can be divided into several groups depending on the position at which the net reaction occurs. Fig. 9 shows the quinonoid formation after deprotonation of the external aldimine (Eliot and Kirsch, 2004).

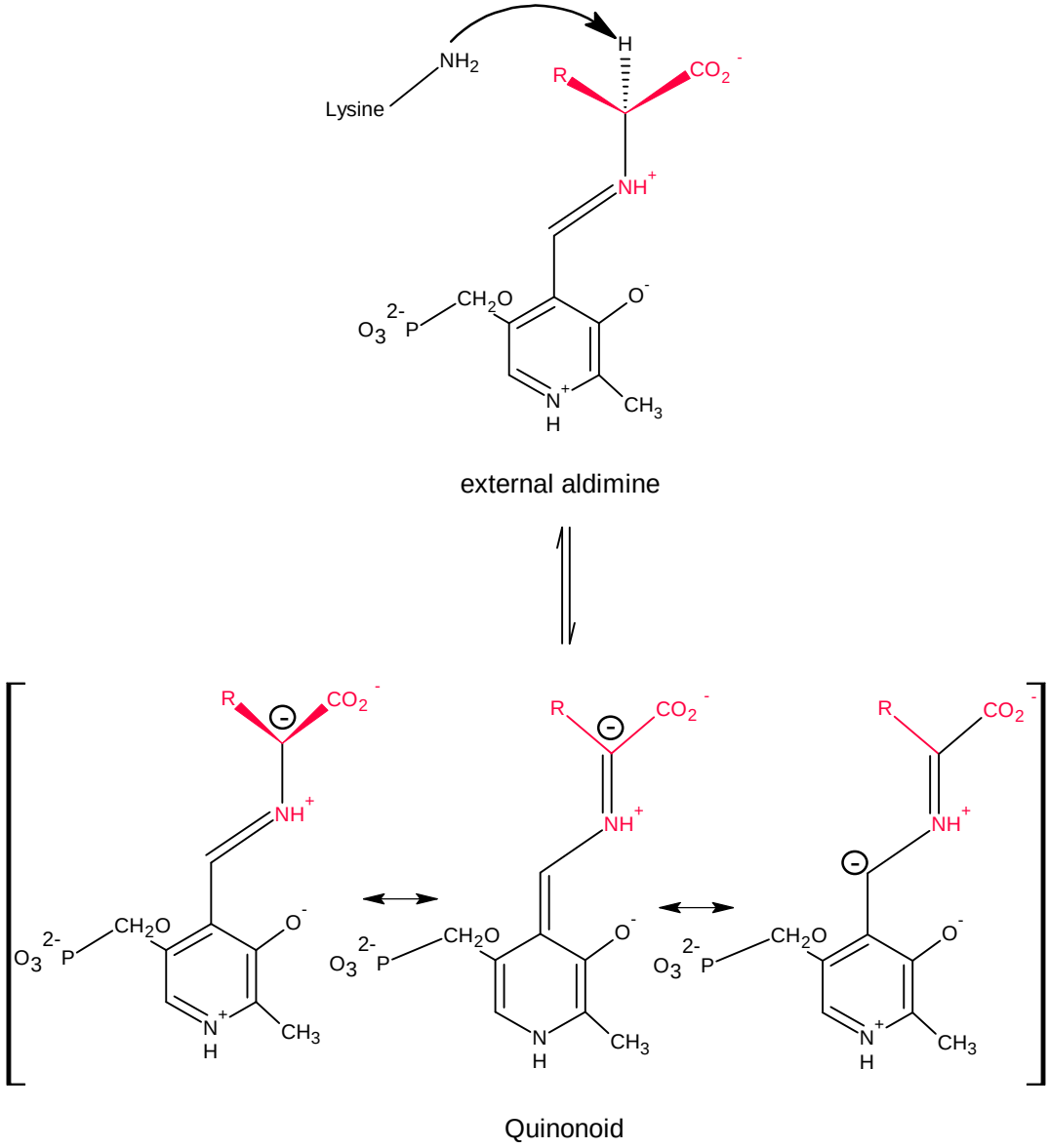

Fig. 9: Quinonoid formation in PLP-catalyzed reaction (Eliot and Kirsch, 2004).
After loss of a proton from the external aldimine the negative charge is delocalized in the *pi*-system of the cofactor whereby the quinonoid is formed. Residues deriving from the amino acid are marked in red.
R = residue.

1.4 Succinyl-Coenzyme A Synthetase Synthesizes one ALAS Substrate

One of the substrates of ALAS is succinyl-CoA which is formed by an enzyme called succinyl-Coenzyme A synthetase (SCS; EC 6.2.1.4 for the adenosine diphosphate (ADP) forming enzyme and EC 6.2.1.5 for the guanosine diphosphate (GDP) forming enzyme). The SCS's catalyze the solely substrate-level phosphorylation step of the tricarboxylic acid cycle. It uses the energy of succinyl-CoA to form nucleotide triphosphate from inorganic phosphate and nucleotide diphosphate (Equation (1) with N denotes guanosine or adenosine):

$$\text{succinyl-CoA} + \text{NDP} + P_i \underset{-\,O_2}{\overset{+\,O_2}{\rightleftharpoons}} \text{succinate} + \text{CoASH} + \text{NTP} \qquad (1)$$

Equation 1: SCS catalyzed reaction.
Under aerobic conditions SCS couples succinyl-CoA hydrolysis to the synthesis of nucleotide triphosphate. In the anaerobic metabolism it provides succinyl-CoA.

During aerobic metabolism the enzyme couples the hydrolysis of succinyl-CoA to the synthesis of adenosine triphosphate (ATP). In the anaerobic metabolism it provides succinyl-CoA when the oxidative route from 2-ketoglutarate is severely repressed (Buck *et al.*, 1985) or when succinyl-CoA is necessary for heme biosynthesis (Miles and Guest, 1987). Succinyl-CoA for the ALAS reaction is formed exclusively within mitochondria by SCS. Furthermore, the SCS is composed of two dissimilar subunits, an α- and a β-subunit. The α-subunit has a relative molecular mass of around M_r = 30'000 while the β-subunit is a little larger (M_r = 40'000). The binding sites for CoA and the nucleotide substrate are located in the α-subunit and there exists a histidine residue that is phosphorylated during catalysis (Histidine 246 in the *E. coli* enzyme; Wang *et al.*, 1972; Buck and Guest, 1989). The succinate binding site is located in the β-subunit (Bailey *et al.*, 1993; Fraser *et al.*, 1999). The complete catalytic sites are formed by regions of contact between the α- and β-subunits (Wolodko *et al.*, 1994).

The SCS found in mammalian mitochondria, Gram-positive bacteria and yeast are α-β-dimers while the enzyme of *E. coli* and other Gram-negative bacteria are $(\alpha\beta)_2$-tetramers with two active sites, one in each dimer (Wolodko *et al.*,

1986; Bailey *et al.*, 1993). Mammalian cells contain two distinct isoforms of the enzyme that are either guanosine triphosphate (GTP)- or adenosine triphosphate (ATP)-specific, while the bacterial enzymes have a degenerated nucleotide specificity but prefer adenosine (Bailey *et al.*, 1993; Wolodko *et al.*, 1994). Enzymes preferring ADP/ATP are referred to as 'A'-form (A-SCS) and enzymes with a favor for GDP/GTP are referred to as 'G'-form (G-SCS; Birney, 1997). The mammalian α-subunit shows 70 % sequence identity to its bacterial counterpart and 45 % to the β-subunit (Henning *et al.*, 1988; Bailey *et al.*, 1993). The two isoforms, A-SCS and G-SCS, contain an identical α-subunit, but they differ in their β-subunit indicating that in this subunit the specificity for one of the two nucleotides is determined (Johnson *et al.*, 1998a; Johnson *et al.*, 1998b). The *E. coli* SCS was crystallized and its structure solved with 2.5 Å resolution (Wolodko *et al.*, 1984; Fraser *et al.*, 1999). The α-subunit is composed of 10 α-helices and 14 β-strands forming two predominantly parallel β-sheets of seven strands each where one strand is antiparallel to the other resulting in an N- and a C-terminal β-sheet. The nucleotide-binding motif is the result of a doubly wound parallel β-sheet formed by the N- and the C-terminal β-sheet, sandwiched by α-helices (Fraser *et al.*, 1999). At the nucleotide-binding motif of the N-terminal sheet CoA is bound. The loop containing the phosphorylated histidine residue is found at the carboxy termini of the strands that are part of the nucleotide-binding motif in the C-terminal domain.

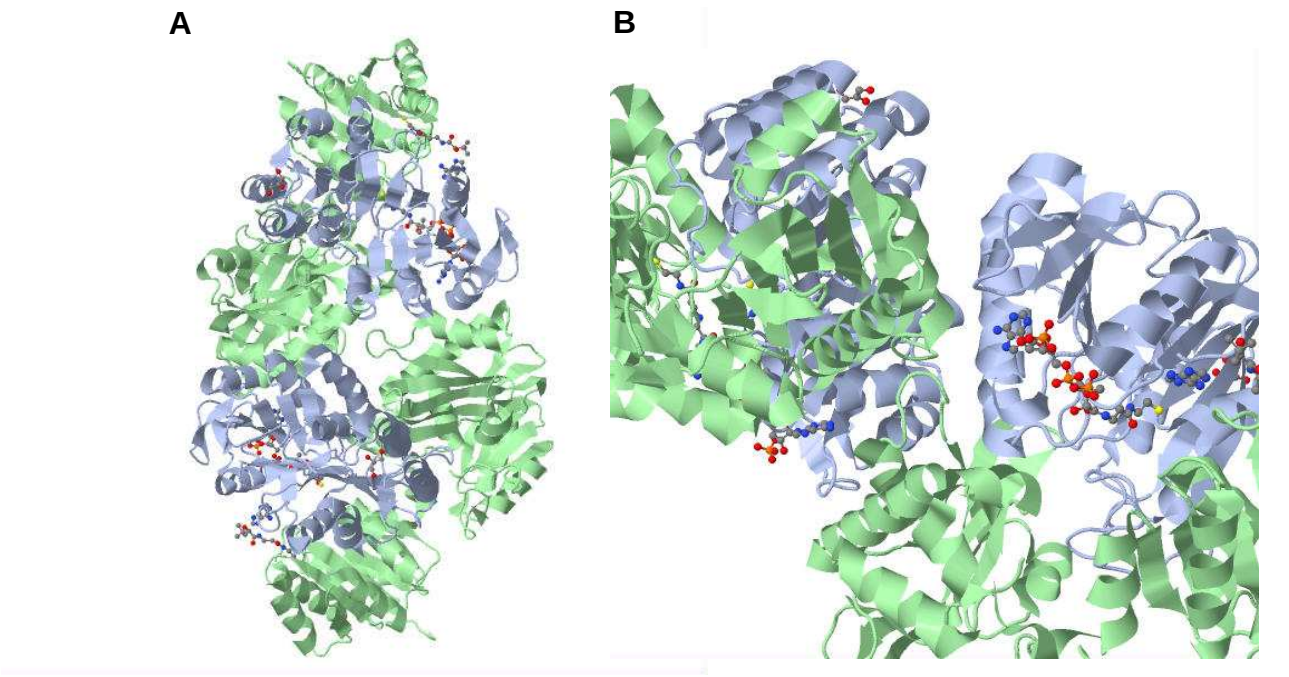

Fig. 10: Crystal structure of *E. coli* SCS.
A. The SCS is a $(\alpha\text{-}\beta)_2$-tetramer. Each dimer consists of two subunits, the α-subunit is depicted in blue and the β-subunit in light green. The α-helices are displayed as spirals and the β-sheets as arrows. **B.** Magnification of the active site with bound Coenzyme A in each α-subunit, displayed as grey-blue-red-orange stick-and-ball molecules (Wolodko *et al.,* 1984; Fraser *et al.*, 1999).

Similar to each domain of the α-subunit, the C-terminal domain of the β-subunit also has a nucleotide-binding motif. Here, the β-sheets consist of five parallel and one antiparallel β-strand and six α-helices (Fraser *et al.*, 1999). Within the N-terminal domain of the β-subunit are two subdomains of unequal size. The SCS subunits are connected *via* the C-terminal domain of the β-subunit with the C-terminal domain of the α-subunit. Through a second major interface between residues of the larger N-terminal subdomain of the β-subunit and residues in both domains of the α-subunit, the subunits in the α-β-dimer are also connected. (Fraser *et al.*, 1999). The fold of the N-terminal domain of the β-subunit also was observed in other nucleotide-binding enzymes including glutathione synthetase (Yamaguchi *et al.*, 1993; Murzin, 1996), pyruvate phosphate dikinase (Herzberg *et al.*, 1996) or biotin carboxylase (Waldrop *et al.*, 1994). Both subunits of the *E. coli* SCS are encoded by the genes *sucC* (β-subunit) and *sucD* (α-subunit), at the distal end of the *sucABCD* operon, which also encodes the specific 2-oxoglutarate dehydrogenase (E1o, encoded by *sucA*, EC 1.2.4.21) and dihydrolipoamide succinyltransferase (E2o, encoded

by *sucB*, EC 2.3.1.61). These enzymes are components of the 2-oxoglutarate dehydrogenase complex employed in the citric acid cycle (Darlison *et al.,* 1984; Spencer *et al*., 1984; Buck *et al*., 1985; Buck and Guest, 1989).

1.4.1 Cooperativity of Succinyl-Coenzyme A Synthetase and Aminolevulinic Acid Synthase during Heme Biosynthesis

The ALAS is responsible for the production of ALA, the first common precursor of all tetrapyrroles. It needs succinyl-CoA and glycine for ALA formation. One of these two substrates, succinyl-CoA, is formed by SCS. A specific association of human ALAS2 with the β-subunit of A-SCS was demonstrated (Furuyama and Sassa, 2000). This interaction seems to be an important process and its failure is responsible for some forms of X-linked sideroblastic anemia (XLSA). Today it is known that the expression of ALAS2 is well controlled at several levels during transcription (Fujita *et al.*, 1991b), translation (Melefors, 1993) and import into mitochondria (Lathrop and Timko, 1993), but also by interaction with other proteins. Mutation of ALAS2 (*e.g.* D190V) resulted in an unstable protein (Furuyama *et al.*, 1997). *In vitro* expression lead to a pre-ALAS2 of normal size, but after translocation into mitochondria the D190V protein was processed in a product with higher molecular weight than the normal mature ALAS form. The D190V ALAS2 variant showed drastically decreased protein-protein interaction with the β-subunit of A-SCS. This leads to the suggestion that the β-A-SCS plays a major role in protecting ALAS2 from degradation (Furuyama and Sassa, 2000).

1.5 Control of Aminolevulinic Acid Synthase Biosynthesis

Usually, heme biosynthesis is a tightly controlled mechanism and the amount of formed heme is equal to the amount needed by the body. ALAS seems to be a perfect target for regulation because of its low endogenous activity and its short half-life. At the level of ALA formation a negative ‘feedback’ control mechanism was found, which means ALA controls its own production (Meissner *et al.*, 2001). Nevertheless, the heme concentration needed for inhibition of enzyme

production is around 10^{-7} M, but for inhibition of enzyme activity a larger amount is required (10^{-5}). The conclusion is that ALAS availability and activity depend on the intracellular heme concentration and the heme requirement in metabolic processes (James and Hift, 2000).

In humans heme acts as a regulator by controlling the amount of ALAS1 mRNA, in avian even the mRNA stability (Srivasata *et al.*, 1988; Yamamoto *et al.*, 1988; Drew and Ades, 1989; Hamilton *et al.*, 1991). Furthermore, the translocation of ALAS1 from cytosol to mitochondria is also controlled by heme (Yamauchi *et al.*, 1980). The control mechanisms of ALAS2 is different. Erythroid-specific transcription factors interact with the promoter and regulate transcription of the ALAS2 gene (Drew and Ades, 1989; May *et al.*, 1995). Posttranscriptional regulation occurs *via* a *cis*-acting regulatory iron responsive element (IRE) in the 5'-untranslated region of the ALAS2 mRNA (Cox *et al.*, 1991). This element is analogous to the stem-loop structure that could be found in the 5'-untranslated region of ferritin mRNAs (Klausner *et al.*, 1993). If iron is absent the mRNA translation is inhibited by an IRE binding protein. Once iron is available the protein dissociates, so that the mRNA binds to ribosomes where its translation is initiated (Melefors *et al.*, 1993).

In bacteria the *hemA* gene is subject to oxygen tension and heme-dependent regulation (Zeilstra-Ryalls and Kaplan, 1996). In *R. capsulatus* the expression of the ALAS encoding *hemA* gene seems to be one of the key regulatory points of tetrapyrrole biosynthesis. The h*emA* transcription was found to be up-regulated under conditions of low oxygen tension mediated by the transcriptional regulator RegA while a down-regulation takes place in the presence of excess heme (Zappa *et al.*, 2010).

1.6 Diseases Caused by Tetrapyrrole Deficiency

1.6.1 Porphyrias

Genetic defects in any of the seven enzymes involved in heme biosynthesis or gain of function mutations in the ALAS gene (Whatley *et al.*, 2008) result in several genetic disorders, known as porphyrias (Sarkany, 1999; Ajikoa *et al.*,

2006; Poblete-Gutierrez *et al.*, 2006; Sassa, 2006). The different porphyrias are consequently the result of heme biosynthetic enzyme deficiencies and result in the accumulation of heme precursors. Usually, porphyrias are the result of inherited genetic diseases, but they can also be acquired by chemical inactivation of the involved enzymes. Porphyrias are classified as hepatic porphyrias (acute porphyrias) and erythropoetic (cutaneous) porphyrias, dependent on the site of the overproduction and accumulation of the porphyrins or their biosynthetic intermediates. The two major clinical manifestations are rather the effect of heme intermediate accumulation than the lack of heme itself. In case of acute porphyrias the porphyrin level in blood is elevated and leads to skin rashes and blistering (Roehl *et al.*, 1988), but also to neurovisceral symptoms like nausea or confusion which can be life-threatening. The characteristical feature of cutaneous porphyrias is photosensitivity (Lecha *et al.*, 2009; Puy *et al.*, 2010).

Fig. 11 shows a schematic representation of tetrapyrrole biosynthesis and the location of known porphyria constitutions in humans (adapted from Puy *et al.*, 2010).

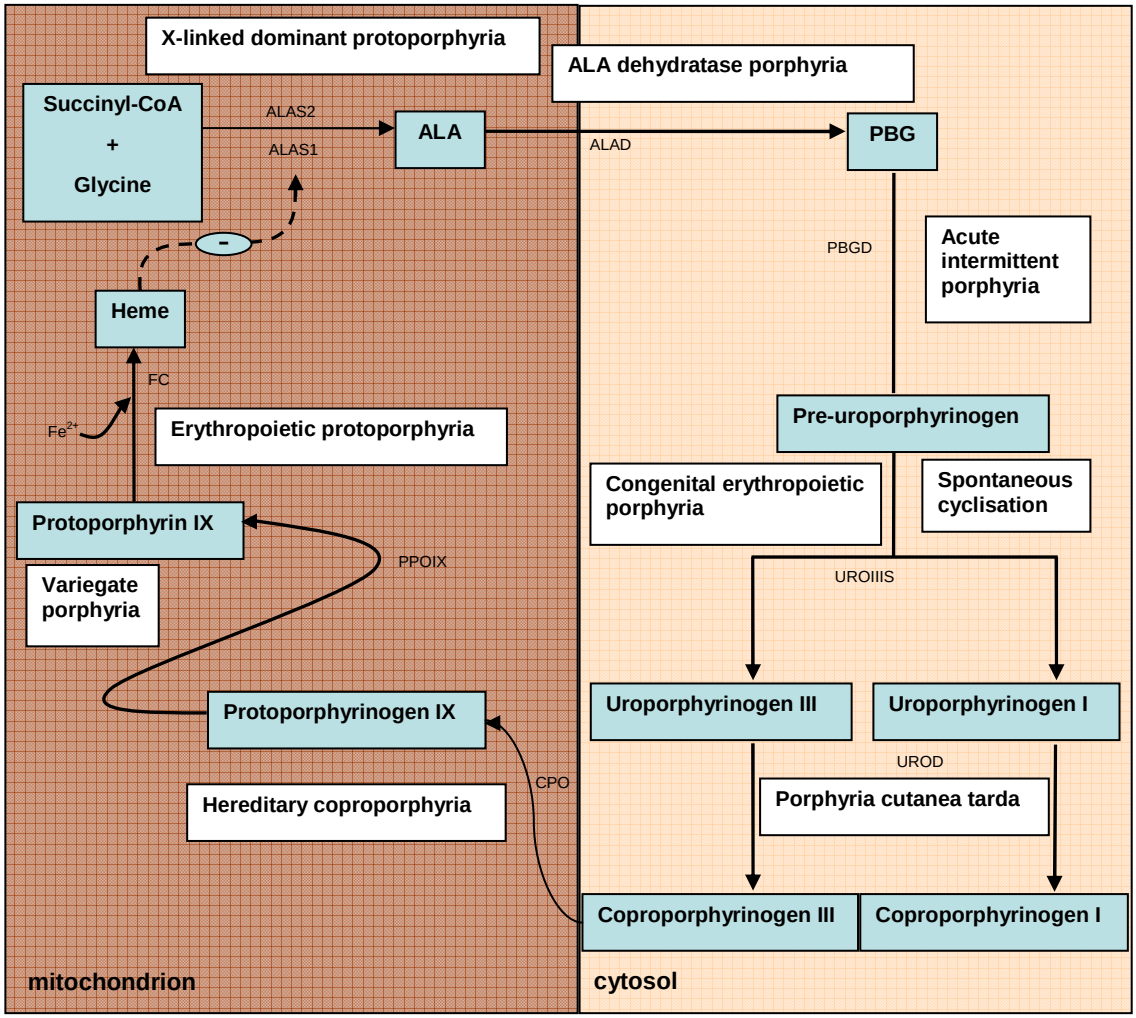

Fig. 11: Schematic representation of tetrapyrrole biosynthesis and the location of porphyria constitution in humans (adapted from Puy *et al.*, 2010).
The mitochondrion is marked in brown and the cytosol in beige. Intermediates in tetrapyrrole biosynthesis are highlighted in blue and porphyrias in white. Catalyzing enzymes are found next to the arrows. ALAS1 = housekeeping ALAS; ALAS2 = erythroid ALAS; ALA = 5-Aminolevulinic acid; PBGS = Porphobilinogen synthase (also known as ALAD = Aminolevulinic acid dehydratase); PBG = Porphobilinogen; PBGD = Porphobilinogen deaminase; UROS = Uroporphyrinogen III synthase; UROD = Uroporphyrinogen III decarboxylase; CPO = Coproporphyrinogen III oxidase; PPOIX = Protoporphyrinogen IX oxidase; FC = Ferrochelatase.

1.6.2 X-linked Sideroblastic Anemia

Humans and other mammals have two different ALAS isoforms, the housekeeping (ALAS1) and the erythroid-specific (ALAS2) enzyme. Both isoforms show 50 % amino acid identity. While the ALAS1 gene is located on chromosome 3p.21, the ALAS2 gene could be found on chromosome Xp11.21 (Cox *et al.*, 1994). Mutations in the ALAS2 lead to an interruption in interaction with the β-subunit of human ATP-specific SCS and this causes a disease called

X-linked sideroblastic anemia (XLSA; Furuyama and Sassa, 2000). In this case red cell mitochondria are iron-overloaded and heme-deficient (May and Bishop, 1998; Bottomley, 2004). Generally, the iron concentration is tightly controlled so that non-specific iron binding cannot occur (Andrews, 1999). If the iron concentration is too high, the cellular reduction-oxidation state is interrupted and cellular lifetime is reduced (Harigae *et al.*, 2003). One example for an XLSA causing mutation is the replacement of the Arginine 517 of human ALAS2 by a cysteine. Usually this Arginine 517 is crucial for glycine recognition and discrimination. Furthermore, in $ALAS_{Rc}$ Threonine 245 (Threonine 388 in human ALAS2) is involved in hydrogen bonding of the PLP-phosphate group. The replacement by serine leads to an XLSA form where patients can be treated by supplemental pyridoxine (Astner *et al.*, 2005).

1.7 Aim of This Study

Aminolevulinic acid synthases are studied since the fifties of the last century. However, only recently a solved crystal structure for a bacterial ALAS became available and opened the door to structure-function-analyses at the atomic level. In this thesis the following three major questions were to be answered:

1. Is 2-amino-3-ketoadipate the second elusive intermediate of ALAS catalysis? What is the role of N54 of $ALAS_{Rc}$ in its formation and stabilization?

2. How are the both substrates succinyl-CoA and glycine functionally recognized, bound and metabolized?

3. What is the detailed molecular basis of ALAS-β-SCS interaction, latter enzyme synthesizing the succinyl-CoA ALAS substrate?

To answer these questions a variety of mutant $ALAS_{Rc}$ variants should be designed, constructed, purified and their steady state kinetics be determined. Single turnover experiments and substrate analog studies should help to complete the picture. The crystal structure of selected variants was of interest. A close cooperation with Prof. Dr. Gloria C. Ferreira for the advanced kinetic characterizations with a 6 months stay at the corresponding laboratory in Tampa, Florida, USA was envisaged.

2 MATERIALS AND METHODS

2.1 Materials

In the following tables (Tab. 1 and Tab. 2) the equipment as well as the chemicals, enzymes and kits used in this work are listed.

2.1.1 Equipment

In Tab. 1 all used equipments are listed.

Tab. 1: Equipment

Equipment	Model	Source
Agarose gel electrophoresis	Agagel	Biometra
Agarose gel documentation	GelDoc	Bio-Rad
Anaerobic chamber	MACS-MG-1000 anaerobic workstation	DW Scientific
Autoclave	LVSA 50/70	Zirbus
Blotting equipment	Semidry-Blot Trans-Blot®SD	Bio-Rad
Centrifuges	5804	Eppendorf
	Avanti®J-26XP	Beckmann Coulter
	Biofuge primoR	Heraeus
	L8-70M ultracentrifuge	Beckmann
	Minispin	Eppendorf
	Qik Spin QS 7000	Edwards instruments
	RC 5B Plus	Sorvall
	Speed Vac SPD 110B	Savant
96 Well CrystalQuick™ plates	96 well plates for sitting drop applications	Greiner Bio One
	Crystal Clear tape	tesa
Dialysis visking	type 27/32 exclusion 14000	Roth
DNA sequencing	Genetic Analyzer ABI Prism™ 310	Applied Biosystems
Electrophoresis power supply	PowerPac 300	Bio-Rad
FPLC	ÄKTApurifier™ 900 series	Amersham Bioscience
Homogenizer	FastPrep®24 Instruments	MP Biomedicals
Stopped-flow spectrophotometer	OLIS model RSM-1000	On-line Instrument Systems Incorporation
pH-determination	pH meter C 6840 B	Schott
Photometer	Ultrospec 2000	Amersham Bioscience

Tab. 1 (continued): Equipment

Equipment	Model	Source
Pipettes	Reference	Eppendorf
Protein concentration cells	VIVASPIN 4 concentrator	Sartorius stedim biotech
	VIVASPIN 15 concentrator	Sartorius stedim biotech
Prepacked columns	Superdex®200 FPLC® HR 10/30	Pharmacia Biotech
	MonoQ™ HR 10/10	Pharmacia Biotech
Scales	BL 1500	Sartorius
	BL 61S	Sartorius
	SBA 52	Scaltec
SDS-PAGE system	Mini Protean II	Bio-Rad
Thermocycler	Tpersonal	Biometra
Thermomixer	Thermomixer compact	Eppendorf
Ultrasonic bath		Merck eurolab
UV/visible Spectrophotometer	Ultrospec 2000	Amersham Bioscience
	Jasco V-550 with ETC-505T	Jasco®
	Temp controller	
Vortex	Vortex Genie 2	Scientific Industries
Water purification	Milli-Q-System	Millipore

2.1.2 Chemicals, Enzymes and Kits

Tab. 2: Used chemicals and enzymes

	Product	Source
Antibodies	Anti-Glutathione-S-Transferase (rabbit-anti-GST)	Sigma
	Anti-Rabbit IgG, Alkaline Phosphatase Conjugated	Pierce
Blotting material	Gel blotting paper	Roth
	Roti-PVDF-membrane	Roth
Chemicals	5-aminolevulinic acid hydrochloride	Sigma
	Pyridoxal-5'-phosphate monohydrate	Fluka
	α-ketoglutaric acid sodium salt	Sigma
	Bradford reagent	Sigma
	Succinyl-Coenzyme A sodium salt	Sigma
	Complete Mini, protease inhibitor cocktail tablets	Roche
Crystal Screens	Classics Lite Suite	Qiagen
	Classics II Suite	Qiagen
	PEGs II Suite	Qiagen
	Cryos Suite	Qiagen
Enzymes	Benzonase®Nuclease	Merck
	Phusion DNA polymerase	Finnzymes

Tab. 2 (continued): Used chemicals and enzymes

	Product	Source
	PreScission™ Protease	GE Healthcare
	T4 DNA Ligase	New England Biolabs
	Restriction enzymes	New England Biolabs, Qiagen, Fermentas
	α-ketoglutarate dehydrogenase from porcine heart	Sigma
Kits	BigDye Terminator v1.1 Cycle	Applied Biosystems
	QIAquick Gel Extraction Kit	Qiagen
	QIAquick PCR Purification Kit	Qiagen
	QuikChange®II Site-Directed Mutagenesis Kit	Stratagene
Molecular weight standards	GeneRuler™ DNA Ladder Mix	MBI Fermentas
	MassRuler™ DNA Ladder Mix	MBI Fermentas
	PageRuler™Prestained Protein Ladder	MBI Fermentas
	Unstained Protein Molecular Weight Marker	MBI Fermentas
PCR materials	Oligonucleotides	Metabion, Biomers
	Nucleotides (dNTPs)	Fermentas
Other materials	Econo-Pac Chromatography Columns	Bio-Rad
	Glutathione Sepharose™ 4 Fast Flow	GE Healthcare
	Protino® Glutathione Agarose 4B	Macherey-Nagel
	Instant*Blue*™	Expedeon
	Lysing Matrix B Bulk	MP Biomedicals
	Steril filter (0.2 µm)	Millipore
	Dialysis visking, type 27/32 exclusion 14‘000	Roth

Non-listed chemicals, materials and enzymes were purchased from following companies:
Fluka (Munich, Germany), Merck (Darmstadt, Germany), Roth (Karlsruhe, Germany), Sigma (Munich, Germany), MP Biomedicals (Illkirch, France), GE Healthcare (Munich, Germany).

2.2 Bacterial Strains and Plasmids

All bacterial strains and plasmids used in this work are listed in Tab. 3 and Tab. 4.

Tab. 3: Bacterial Strains

Strain	Genotype	Reference
***Escherichia coli* DH10β**	F$^-$ *mcr*A Δ(*mrr-hsd*RMS-*mcr*BC) ϕ80*lac*ZΔM15Δ*lac*X74 *rec*A1 *end*A1 *ara*D139 Δ(*ara, leu)*7697 *gal*U *gal*K λ$^-$ *rps*L (Str^R) *nup*G	GibcoBRL (Invitrogen)
***Escherichia coli* BL21(DE3)pLysS**	F$^-$ *omp*T *hsd*S($r_B^-m_B$) *dcm*$^+$ *gal* λ(DE3) [pLysS *cm*^{R}]	Stratagene
***Escherichia coli* BL21(DE3)RIL**	F$^-$ *omp*T *hsdS*($r_B^-m_B$-) *dcm*$^+$ *tet*^{R} galλ(DE3) *end*A Hte[*arg*U *ile*Y *leu*W *cm*^{R}]	Novagen

Tab. 4: Plasmids

Conservative amino acid exchanges in the *R. capsulatus hemA* gene were highlighted in light pink

Plasmid	Description	Reference
pGEX-6P-1	Expression vector carrying N-terminal sequence for GST from *Schistosoma japonicum* and recognition sequence from PreScission™Protease, *lac* promotor, *amp*^{R}	Amersham Bioscience
p*Rc*-A	pGEX-6P-1 derivative encoding *R. capsulatus* aminolevulinc acid synthase. Resulting protein is referred to as wild-type.	This work
p*Rc*A-N54Q	p*Rc*A derivative with exchange of triplet AAC to CAG, protein carries glutamine instead of asparagine in position 54.	This work
p*Rc*A-N54D	p*Rc*A derivative with exchange of triplet AAC to GAC, protein carries aspartic acid instead of asparagine in position 54.	This work
pRcA-R21K	p*Rc*A derivative with exchange of triplet CGC to AAG, protein carries lysine instead of arginine in position 21.	This work
p*Rc*A-R21E	p*Rc*A derivative with exchange of triplet CGC to GAG, protein carries glutamic acid instead of arginine in position 21.	This work
p*Rc*A-D47E	p*Rc*A derivative with exchange of triplet GAC to GAG, protein carries glutamic acid acid instead of aspartic acid in position 47.	This work
p*Rc*A-D47S	p*Rc*A derivative with exchange of triplet GAC to AGC, protein carries serine acid instead of aspartic acid in position 47.	This work
p*Rc*A-T83S	p*Rc*A derivative with exchange of triplet ACC to AGC, protein carries serine instead of threonine in position 83.	This work
p*Rc*A-T83L	p*Rc*A derivative with exchange of triplet ACC to CTC, protein carries leucine instead of threonine in position 83.	This work
p*Rc*A-N85Q	p*Rc*A derivative with exchange of triplet AAC to CAG, protein carries glutamine instead of asparagine in position 85.	This work
p*Rc*A-N85F	p*Rc*A derivative with exchange of triplet AAC to TTC, protein carries phenylalanine instead of asparagine in position 85.	This work

Tab. 4 (continued):

Plasmid	Description	Reference
p*Rc*A-I86L	p*Rc*A derivative with exchange of triplet ATC to CTC, protein carries leucine instead of isoleucine in position 86.	This work
p*Rc*A-I86H	p*Rc*A derivative with exchange of triplet ATC to CAC, protein carries histidine instead of isoleucine in position 86.	This work
p*Rc*A-M309L	p*Rc*A derivative with exchange of triplet ATG to CTG, protein carries leucine instead of methionine in position 309.	This work
p*Rc*A-M309W	p*Rc*A derivative with exchange of triplet ATG to TGG, protein carries tryptophan instead of methionine in position 309.	This work
p*Rc*A-C52S-C201S-C400S	p*Rc*A derivative with exchange of triplets TGC and TGT to AGC, TCT or TCC, protein carries serine instead of cysteine in positions 52, 201 and 400.	This work
p*Rc*A-N54Q-C52S-C201S-C400S	p*Rc*A derivative with exchange of triplets AAC, TGC and TGT to CAG, AGC, TCT or TCC, protein carries glutamine instead of asparagine and serine instead of cysteine in positions 52, 201 and 400.	This work
p*Rc*A-N54D-C52S-C201S-C400S	p*Rc*A derivative with exchange of triplets AAC, TGC and TGT to GAC, AGC, TCT or TCC, protein carries aspartic acid instead of asparagine and serine instead of cysteine in positions 52, 54, 201 and 400.	This work
p*Rc*A-T365C-C52S-C201S-C400S	p*Rc*A derivative with exchange of triplets ACG, TGC and TGT to TGC, AGC, TCT or TCC, protein carries cysteine instead of threonine and serine instead of cysteine in positions 52, 54, 201 and 400.	This work
p*Rc*A-T365S-C52S-C201S-C400S	p*Rc*A derivative with exchange of triplets ACG, TGC and TGT to TCG, AGC, TCT or TCC, protein carries serine instead of threonine and serine instead of cysteine in positions 52, 201, 365 and 400.	This work
p*Rc*-βSCS	pGEX-6P-1 derivative encoding the *R. capsulatus* β-subunit of the succinyl-Coenzyme A synthetase (*sucC*). Resulting protein is referred to as wild-type.	This work

2.3 Media and Media Additives

2.3.1 Media

The rich medium Luria Bertani (LB) was used for the cultivation of the *E. coli* cells (Sambrook *et al.*, 1989).

LB-medium

tryptone	10	g/L
NaCl	10	g/L
yeast extract	5	g/L

For solid media 15 g/L agar was added before sterilization.

2.3.2 Media Additives

The additives for the media were prepared as concentrated stock solutions. They were sterile filtrated and added to the chilled medium. Stock solutions were frozen with the exception of ALA (4 °C) at -20 °C.
Tab. 5 shows the stock solutions which were used in this work.

Tab. 5: Medium additives

Medium additive	Stock solution	End concentration
Chloramphenicol (Cm)	34 mg/mL in 70 % ethanol (v/v)	34 µg/mL
Ampicillin (Amp)	100 mg/mL in H_2O_{dest}	100 µl/mL
Isopropyl-1-thio-β-D-galactoside (IPTG)	1 Molar in H_2O_{dest}	50 µM
5-Aminolevulinic acid hydrochloride (ALA)	0.1 Molar in H_2O_{dest}	5 mM

2.4 Microbiological Techniques

2.4.1 Sterilization

If there is no other information solutions were sterilized for 20 min at 120 °C and 1 bar overpressure.
In case of sterile filtration a sterile filter with a pore size of 0.2 µm was used.

2.4.2 Cultivation of Bacteria and Long-Term Storage

Cells for recombinant protein production were cultivated under vigorous aeration. For the preparatory culture *E.* coli cells containing appropriate plasmids were grown in LB medium (100 mL) containing the required additives in Erlenmeyer flasks. The incubation was carried out over night at 37 °C and 200 rpm. From these preparatory cultures the main cultures (500 mL) were inoculated with a dilution of 1:100 in Erlenmeyer flasks with fresh medium. The bacterial suspension was cultivated to an OD_{600} of 0.6 - 0.8 at 37 °C and 200 rpm and the induction of protein production was initiated by the addition of 200 µM isopropyl-1-thio-β-D-galactoside (IPTG). Further growth occurred at 25 °C or 17 °C, respectively.
For cultivation on agar plates the required antibiotics were added to LB-agar-medium. After plates were congealed a bacteria suspension (50 - 250 µL) was

plated with a Drigalski spatula. The dried plates were incubated at 37 °C over night. Storage of the agar plates occurred at 4 °C for no more than four weeks. For long-term storage at -80 °C glycerol stocks were prepared by mixing 800 µL of a bacterial culture with 300 µL of a sterile 80 % (v/v) glycerol stock solution. Stocks were immediately frozen and stored at -80 °C.

2.4.3 Determination of Cell Density

For the determination of cell density the optical density (OD) was measured at a wavelength of 600 nm. For cell densities with an OD_{600} ≥1 dilutions were prepared (1:10). An OD_{600} of 1 corresponds to a cell count of 1 x 10^9 *E. coli* cells per mL.

2.5. Molecular Biology Techniques

2.5.1 Production and Transformation of Rubidium Chloride Competent *Escherichia coli* Cells

Competent cells are cells which are able to take up external DNA from the environment after a chemical treatment. For the production of competent cells 100 mL LB-medium with required additives was inoculated with a corresponding overnight-culture (1:100) and incubated at 37 °C and 200 rpm up to an OD_{600} 0.6 - 0.8 (logarithmic growth phase). The bacterial suspension was then centrifuged for 5 min at 4 °C and 4'500 x *g*. The supernatant was discarded and the sediment was washed with 0.4 volume ice-cold TBF-1 and incubated for 5 min on ice. After a new centrifugation step for 5 min at 4 °C and 4'500 x *g* the supernatant was discarded again and the cell sediment was dissolved in 1/25 volume ice-cold TBF-2. After an incubation time of 15 - 60 min on ice the cells were aliquotated in 50 µL aliquots into precooled reaction tubes and stored at -80 °C.
For the transformation of $RbCl_2$ cells, 50 µL of these cells were mixed with 1 - 3 µL (50 µg/mL) of the desired plasmid DNA and incubated for 30 min on ice. The mixture was subjected to a heat shock at 42 °C for 60 sec and afterwards cooled on ice for 2 min. Finally, 500 µL preheated LB-medium was added and cells were incubated at 37 °C for 15 - 45 min and 200 rpm. Depending on the expected colony density, different volumes were streaked on agar plates containing the appropriate antibiotics and plates were incubated overnight at 37 °C.

TBF-1

potassium acetate	30	mM
$CaCl_2$	10	mM
$MnCl_2$	50	mM
$RbCl_2$	100	mM
glycerol	15	% (v/v)

in H_2O_{dest}; adjust to pH 5.8 with 1 M HCl

TBF-2

3-(N-morpholino)propane-sulfonic acid (MOPS)	10	mM
$CaCl_2$	75	mM
$RbCl_2$	10	mM
glycerol	5	% (v/v)

in H_2O_{dest}; adjust to pH 6.5 with 1 M KOH

2.5.2 Preparation of Plasmid DNA

The isolation of plasmid DNA was based on the principle of the alkaline lysis of the cell wall and a concomitant denaturation step. In the following decrease of pH resulted in the renaturation of DNA whereas the genomic DNA and the proteins precipitated.
LB-medium (5 mL) with required antibiotics was incubated with a colony of an agar plate in a test tube overnight at 37 °C. Three mL from this overnight culture were centrifuged at the beginning of the preparation in two centrifugation steps for 3 min and 11'000 x *g* at 4 °C. The cell sediment was dissolved in 300 µL buffer-P1 and subsequently mixed with buffer-P2. The mixture was carefully inverted and incubated at RT for 5 min. Next, 300 µL of neutralization buffer-P3 were added, carefully inverted and further incubated on ice for 5 min. The precipitated cell debris and proteins were separated by centrifugation from the supernatant (15 min at 4 °C and 11'500 x *g*). Six hundred µL of the supernatant were transferred into a fresh reaction tube and 420 µL (0.7 volume) isopropanol were added, mixed and incubated for 10 min at RT. In this step plasmid DNA was precipitated and harvested in a following centrifugation step (15 min at RT and 11'000 x *g*). The supernatant was discarded and plasmid DNA was washed twice with 500 µL 70 % ethanol. Each washing step went along with a centrifugation step (15 min at 4 °C and 13'400 x *g*). After all traces of ethanol had evaporated, the DNA was solubilized in 60 µL of H_2O_{dest}.

Buffer-P1

Tris-HCl	50	mM
ethylene diamine tetraacetic acid (EDTA)	10	mM
RNAse A	100	µg/mL

in H_2O_{dest}; pH 8.0

Buffer-P2

NaOH	200	mM
sodium dodecyl sulfate (SDS)	1	% (w/v)
in H_2O_{dest}; pH 8.0		

Buffer-P3

potassium acetate	3	M
in H_2O_{dest}; pH 5.5		

2.5.3 Agarose Gel Electrophoresis

Charged DNA molecules with a different charge/mass proporption were separated by agarose gel electrophoresis. Gels consisted of 1 % (w/v) agarose in TAE buffer. Depending on gel size, a voltage of 80 - 100 V was applied. The negative charged DNA molecules migrate towards the anode with a different velocity depending on their size. Prior to loading, DNA samples were mixed with loading dye to facilitate loading and indicate the progress of the samples in the gel. GeneRuler™ DNA Ladder Mix or MassRuler™ DNA Ladder Mix (MBI Fermentas, St. Leon-Rot, Germany) were used as size standards according to manufacturer's instructions. After electrophoresis gels were stained with ethidium bromide for 15 - 40 min. This dye is incorporated into DNA helices and under UV light it shows fluorescence at a wavelength of 312 nm. After staining the gels were rinsed with H_2O and DNA was detected *via* its fluorescence due to incorporated ethidium bromide. If DNA fragments were to be extracted from the gel, extraction was carried out using the QIAquick Gel Extraction Kit (Qiagen, Hamburg, Germany) according to manufacturer's instructions.

TAE-buffer

Tris-acetate	40	mM
EDTA	1	mM
in H_2O_{dest}; pH 8.0		

5 x DNA loading dye

bromphenol blue	0.35	mM
xylen cyanol FF	0.45	mM
orange G	0.25	mM
sucrose	115	mM
in TAE-buffer		

Ethidium bromid

ethidium bromide	0.1	% (v/v)
in H_2O_{dest}		

2.5.4 Site-Directed Mutagenesis of DNA

Site-specific mutations can be inserted into the DNA sequence of a gene of interest whereby single amino acids in the corresponding protein are exchanged. In this work the QuikChange Site-directed Mutagenesis Kit (Qiagen, Hamburg, Germany) served for the development of several $ALAS_{Rc}$ variants. This method (Fig. 12) utilizes a dsDNA plasmid carrying the gene of interest and two synthetic oligonucleotide primers which contain the desired mutation (Tab. 6) and are complementary to opposite strands of the vector. In a polymerase chain reaction (PCR) with *PfuTurbo* DNA polymerase (Fermentas, St. Leon-Rot, Germany) or *Phusion* DNA polymerase (Finnzymes, Frankfurt am Main, Germany) a mutated plasmid is generated. The PCR reactions with the QuikChange Site-Directed Mutagenesis Kit were carried out according to manufacturer's instruction.

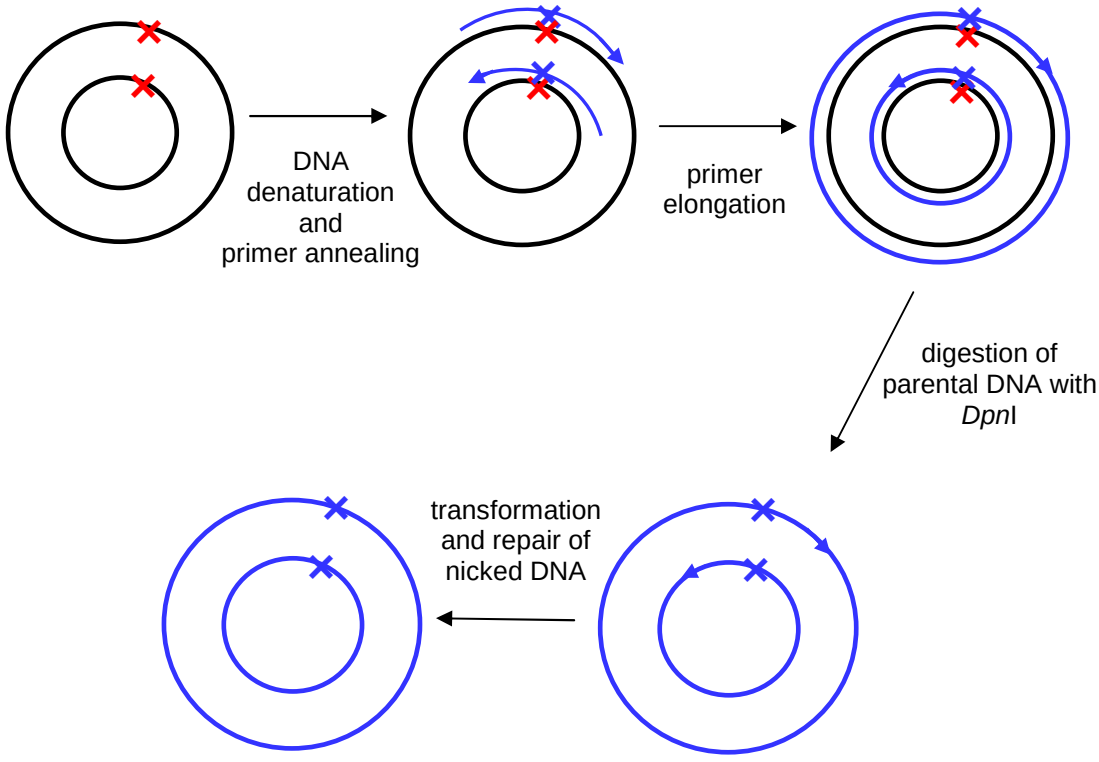

Fig. 12: Site-Directed Mutagenesis.
Overview of the QuikChange Site-Directed Mutagenesis method (modified from Stratagene Instruction Manual, 1998). Black line: parental DNA; blue line: mutated DNA; red cross: position of the desired mutation; blue cross: introduced mutation; blue arrow: mutagenic primer. A detailed description is given in the text.

In a following step with the endonuclease *Dpn*I which digests specifically partially methylated DNA, the parental template DNA is digested. After isolation of the newly synthesized unmethylated and mutated DNA plasmid, the DNA was transformed into the *E. coli* strains XL1Blue or DH10B. Here, a DNA ligase

closes the nicked DNA circles. DNA sequencing was used for the determination of all mutated genes.

Tab. 6: Oligonucleotide primers used for site-directed mutagenesis of $ALAS_{Rc}$.
Only oligonucleotide primers in forward orientation are listed. The second oligonucleotide primer (reverse) always corresponds to the reverse complementary sequence. Conservative amino acid exchanges were highlighted in light pink.

Mutant designation in $ALAS_{Rc}$	Sequence of oligonucleotide primer (forward) (5'→3')
R21K	CGAGGGACGTTAC**AAG**ACGTTCATCG
R21E	CGAGGGACGTTAC**GAG**ACGTTCATCG
D47E	GCGGCAAGCAG**GAG**ATCACCGTCTG
D47S	GCGGCAAGCAG**AGC**ATCACCGTCTG
N54Q	CTGGTGCGGC**CAG**GACTATCTGGGC
N54D	CTGGTGCGGC**GAC**GACTATCTGGGC
T83S	GGTTCGGGCGGC**AGC**CGCAACATCTC
T83L	GGTTCGGGCGGC**CTC**CGCAACATCTC
N85Q	GCGGCACCCGC**CAG**ATCTCGGGCAC
N85F	GCGGCACCCGC**TTC**ATCTCGGGCAC
I86L	GCACCCGCAAC**CTC**TCGGGCACCAC
I86H	GCACCCGCAAC**CAC**TCGGGCACCAC
M309L	CGCGCAACAG**CTG**CACGCGAAGG
M309W	CGCGCAACAG**TGG**CACGCGAAGG
C52S	ATCACCGTCTGG**AGC**GGCAACGACTAT
C201S	ATCAAGGAAATC**TCC**GACATCGCCGAT
C400S	CTCTGGGCGCGC**TCT**GCGTGATCGAGC
T365C	ATCAACTTCCCG**TCG**GTGCCGCGCGGC
T365S	ATCAACTTCCCG**TGC**GTGCCGCGCGGC

2.5.5 Amplification of DNA Fragments by PCR

2.5.5.1 Design and Synthesis of Oligonucleotide Primers

Oligodeoxynucleotides are short single stranded DNA fragments which are also used as primers in PCR. There, they serve as a starting point for the polymerase by binding at complementary sequences of melted DNA.
For amplification of the *hemA* and *sucC* genes of *R. capsulatus* oligonucleotide primers were designed with the aim of subsequent cloning into the pGEX-6P-1 vector. Recognition sequences for restriction endonucleases were inserted *via* these primers at both ends of the gene. The orientation of the primer is given by the abbreviation 'forw' for forward, 'rev' for revers and recognition sequences were underlined. Oligonucleotide primers are outlined in Tab. 7 with recognition sequences of restriction underlined.

Tab. 7: Oligonucleotide primers used for the amplification of DNA fragments.
The restriction sites for the amplification of *hemA* and *sucC* from the genomic DNA of *R. capsulatus* are marked thick and underlined in the respective primers. 'Forw' refers to forward primer and 'rev' to reverse primer.

Primer	Sequence of oligonucleotide primer (5'→3')	Restriction site
*Rc*WTHemAforw	CGC**GGATCC**GCGATGGACTACAATCTCGCG	*Bam*HI
*Rc*WTHemArev	CCG**CTCGAG**CGGTCACGCACAGCGCGCCCA	*Xho*I
*Rc*Sucforw	CGGCCC**GTCGAC**AAATGAACATCCACGAAT	*Sal*I
*Rc*Sucrev	CTC**GCGGCCGC**TTATCCCTTCACCGCTTTGAC	*Not*I

2.5.5.2 Polymerase Chain Reaction

PCR serves as an *in vitro* amplification of a DNA molecule which is defined with two specific primers. The first step of PCR was an initial DNA denaturation step which was followed by a cycle of three steps: denaturation, primer annealing and primer elongation for 30 times. By continuous repetition of these three cycles the amount of the desired DNA fragment will be increased exponentially. The final step then was a terminating elongation. Denaturation and elongation temperatures of 95 °C and 72 °C, respectively, rema ined unchanged. In contrast, the annealing temperature depended on oligonucleotide length and the G+C content and was also influenced by the insertion of mismatches. The melting temperature (T_m) was calculated as following:

$$T_m\,[°C] = 69.3 + 0.41\ (\%\ G+C) - 650/n$$

The G+C content of the primer is denoted by G+C in % while *n* represented the number of nucleotides.

Phusion DNA polymerase (Finnzymes, Frankfurt am Main, Germany) was used for all reactions. According to manufacturer's instructions the duration of elongation was chosen according to the length of the amplifying DNA fragment.

Standard thermocycler program

First denaturation	95 °C	5	min	
Denaturation	95 °C	1	min	30 x
Primer hybridization	50 - 60 °C	30	s	
Elongation	71 °C	1 - 4	min	
Final elongation	71 °C	5 - 10	min	
	4 °C		∞	

2.5.5.3 Purification of PCR Products

Agarose gel electrophoresis was used for quality control of the amplified DNA. By using this method an aliquot of the PCR reaction was loaded onto an 1 % agarose gel and after chromatography it could be detected under UV light (s. 2.5.3). If only one PCR product could be detected, the whole sample was purified with the QIAquick PCR Purification Kit (Qiagen, Hamburg, Germany). If more than one PCR product were detected, the DNA fragment of interest was excised from the gel and purified with the QIAquick Gel Extraction Kit (Qiagen, Hamburg, Germany). All kits were used according to manufacturer's instructions. With this purification step polymerases, buffers and unbound nucleotides also can removed from the sample.

2.5.6 Enzymatic Modification of DNA

2.5.6.1 DNA Cleavage with Restriction Endonucleases

Bacteria can accumulate the so called restriction endonucleases to protect themselves against external DNA. The class II endonucleases are the most occurring restriction enzymes. They recognize a palindromic arranged DNA sequence with four or eight nucleotides. The restriction reaction catalyzes the hydrolysis of two phosphordiester bonds inside the recognition sequence that leads to 'blunt' or 'sticky' ends.
Restriction of DNA, vectors and PCR products, was carried out using restriction endonucleases purchased from New England BioLabs (Frankfurt am Main, Germany). According to manufacturer's instruction reaction buffers, concentrations of enzymes, DNA and incubation temperature were selected as prescribed. The digestion was proceeded for 1 - 4 h and if it was possible enzymes were heat inactivated.

2.5.6.2 Ligation

The ligation reaction is the covalent connection between the free 5'-phosphate group of one DNA fragment with the free 3'-hydroxyl group of a second DNA fragment. Such a reaction is catalyzed by ligases (T4 DNA ligase; New England Biolabs, Frankfurt am Main, Germany).
Before a ligation reaction could be performed the two DNA fragments (vector and insert) had to have compatible ends. Additionally, the 5'-phosphate groups of linearized vectors were removed to avoid re-circularization of digested vector DNA by adding 1 U/µg DNA of antarctic alkaline phosphatase (New England BioLabs, Frankfurt am Main, Germany). The mixture with digested vector and phosphatase was incubated at 37 °C for 30 min, followed by heat inactivation (15 min at 65 °C). After this step the two fragments can covalently attach to

each other. The ligation reaction was performed for 2 h at 25 ℃ with 25 - 50 ng vector DNA and insert DNA in excess (insert to vector ratio with regard to molar concentrations was 10:1 or 5:1, respectively). After the incubation time it followed a transformation into the *E. coli* strain DH10β.
Conditions and buffers were used according to manufacturer's instructions.

2.5.7 DNA Sequencing

DNA sequences were obtained with an Abi Prism™ 310 Genetic Analyzer (Applied Biosystems, Darmstadt, Germany) in our laboratory. The required preparatory PCR with fluorescence-labeled ddNTPs (dideoxyribonucleotide triphosphates) and purification of the PCR product were carried out as described by manufacturer's instruction.

Standard PCR program

96 ℃	1	min
96 ℃	30	sec
50 ℃	15	sec
60 ℃	4	min
4 ℃	∞	

30 x

Tab. 8: Oligonucleotide primers.
Oligonucleotide primers used for sequencing.
'Forw' refers to forward primer and 'rev' to reverse primer.

primer	Sequence of oligonucleotide primer (5'→3')	application
T7 Promoter	TAATACGACTCACTATAGGG	DNA sequencing of several vectors
T7 Terminator	CTAGTTATTGCTCAGCGGT	DNA sequencing of several vectors

2.6 Protein Biochemical Methods

2.6.1 Production and Purification of *Rhodobacter capsulatus* Aminolevulinic Acid Synthase

2.6.1.1 Cell Growth and Cell Disruption

A total of 10 liters (20 x 500 mL) vapor sterilized LB medium containing 100 µg/mL ampicillin and 34 µg/mL chloramphenicol in 1 L Erlenmeyer flasks were each inoculated with 5 mL of an overnight culture of *E. coli* BL21(DE3)RIL or BL21(DE3)pLysS, respectively, carrying pGEX-6P-1-*Rc*-A (pGEX-6P-1

vector with the *R. capsulatus* wild-type *hemA* gene) and incubated under vigorous aeration at 37 ℃. After cells reached an OD_{600} of 0.6 the expression of *hemA* was initiated by addition of IPTG (end concentration: 200 µM). The optimal growth temperature was 25 ℃ or 17 ℃, resp ectively, for 22 h and 180 rpm. Cells were harvested by centrifugation for 20 min at 3'000 x *g* and 4 ℃. The cell sediment was suspended in 15 - 40 mL lysis buffer. Cells were disrupted using FastPrep®24 (MP Biomedicals, Illkirch, France) at 4 ℃ (three times for 45 sec). For this method 125 mg/mL Lysing Matrix B Bulk (MP Biomedicals, Illkirch, France) were added into a 2 mL reaction tube and filled up with suspended cell sediment. FastPrep®24 conditions were used according to manufacturer's instructions. Cell debris and insoluble protein fractions were removed by centrifugation for 30 - 45 min at 4 ℃ and 14'000 x *g*. The resulting supernatant was loaded onto a glutathione sepharose column.

Lysis buffer

Hepes, pH 7.5	20	mM
sodium chloride	200	mM
dithiothreitol (DTT)	10	mM
PLP	20	µM
Benzonase	20	µL
complete protease Inhibitor	1	tablet
in H_2O_{dest}		

2.6.1.2 Affinity Chromatography Using Glutathione Sepharose

After harvesting cells were suspended in lysis buffer and subsequently broken by FastPrep®24 (s. 2.6.1.1). The cell-free extract was cleared by centrifugation at 14'000 *x g* for 30 min. An empty Econo-Pac Chromatography column (Bio-Rad, Hercules, USA) was packed with 5 - 10 mL Glutathione Sepharose™ 4 Fast Flow (GE Healthcare, Munich, Germany) and equilibrated with 25 - 50 mL of elution buffer. The cell-free extract was mixed with the column resin and incubated for 1 h under mild rotation conditions. The flow through was collected and the column was washed 6 times with 10 mL of elution buffer to remove unbound proteins and other cell debris. The next step was incubation with PreScision™ Protease (GE Healthcare, Munich, Germany) for 48 hours to clip the GST-tag. Protein elution with 10 mL of elution buffer and regeneration of the columns with 60 - 100 mL of regeneration buffer were the last steps for protein purification. Proteins were analyzed by SDS-PAGE as described previously (Laemmli, 1970) with modifications by Righetti (Righetti, 1990). Protein concentrations were determined with the Bradford assay (Bradford, 1976) with BSA (bovine serum albumin) as standard. All concentrations are reported on the basis of a subunit molecular weight of 43'575 Da. If it was necessary protein containing fractions were pooled and concentrated by ultrafiltration.

Elution buffer

Hepes, pH 7.5	20	mM
sodium chloride	200	mM
DTT	10	mM
PLP	20	µM

in H_2O_{dest}; sterile filtrated and degased

Regeneration buffer

Hepes, pH 7.5	20	mM
sodium chloride	200	mM
DTT	10	mM
PLP	20	µM
glutathione	10	mM

in H_2O_{dest}; sterile filtrated and degased

2.6.1.3 Dialysis of Protein Solutions

For removal of salt in protein solutions or for buffer alterations, samples were dialyzed. The dialysis tubes were boiled up for 5 min in H_2O_{dest}, chilled and washed with H_2O_{dest} prior to use. Subsequently, the sample was filled inside, the tube sealed and the dialysis was started under slight shaking at 4 ℃ overnight. After 24 h the buffer was changed against fresh buffer for 3 - 4 h. Before loading of the sample onto a chromatography column it was sterile filtrated and centrifuged at 5'000 *x g* for 15 - 30 min to remove precipitated protein.

Dialysis buffer for $ALAS_{Rc}$
For MonoQ

Hepes, pH 7.5	20	mM
DTT	10	mM
PLP	20	µM
Mini Complete Protease Inhibitor	1	tablet

in H_2O_{dest}

For gel permeation chromatography

Hepes, pH 7.5	20	mM
sodium chloride	200	mM
DTT	10	mM
PLP	20	µM

in H_2O_{dest}

2.6.1.4 Ion Exchange Column Chromatography (MonoQ)

Anion exchange chromatography using MonoQ was performed as second purification step at RT. Pooled protein containing fractions were sterile filtrated and applied at a flow rate of 1 mL/min to a 1 mL MonoQ column equilibrated with buffer-A. To remove unbound proteins the column was washed with

7 column volumes of buffer-A. Bound proteins including recombinant $ALAS_{Rc}$ were eluted with 1 M NaCl in buffer-B. Fractions containing recombinant $ALAS_{Rc}$ were identified *via* SDS-PAGE-analysis, pooled and concentrated by ultrafiltration.

Buffer-A

Hepes, pH 7.5	20	mM
DTT	10	mM
in H_2O_{dest}		

Buffer-B

Hepes, pH 7.5	20	mM
DTT	10	mM
sodium chloride	1	M
in H_2O_{dest}		

2.6.1.5 Gel Permeation Column Chromatography (Superdex-200)

The matrices of a gel permeation chromatography (GPC) column consist of a porous material. Proteins with a higher size or hydronamic volume than the pores of the material cannot remain on the column and are eluted first, while smaller proteins can permeate the material and remain longer on the column. The GPC was used for the determination of the oligomerization state of $ALAS_{Rc}$ as well as for further protein purification. Before ALAS was loaded onto the GPC it was concentrated with a VIVASPIN 4 mL or 15 mL concentrator membrane. A 30 mL Superdex-200 HR 10/30 was equilibrated with GPC buffer. The column was calibrated using carbonic anhydrase (M_r = 29'000), bovine serum albumin (M_r = 66'000) and yeast alcohol dehydrogenase (M_r = 150'000) as marker proteins. One mg of these substances was dissolved in 1 mL of the GPC buffer and 100 µL of these suspensions were loaded onto the column. All proteins were chromatographed under identical conditions at a flow rate of 0.5 mL/min. With the elution profiles the elution volume (V_e) of the proteins from the column could be determined. The natural logarithm of the molecular weight of the proteins (ln (MW)) was plotted against V_e divided with the 'dead volume' (V_0) of the column.
For purification of the protein elution was carried out in 100 - 500 µL fractions which were subsequently analyzed *via* SDS-PAGE, pooled and concentrated if necessary. For long-term storage 100 % glycerol were added with a final concentration of 10 % and samples were frozen at -80 ℃.

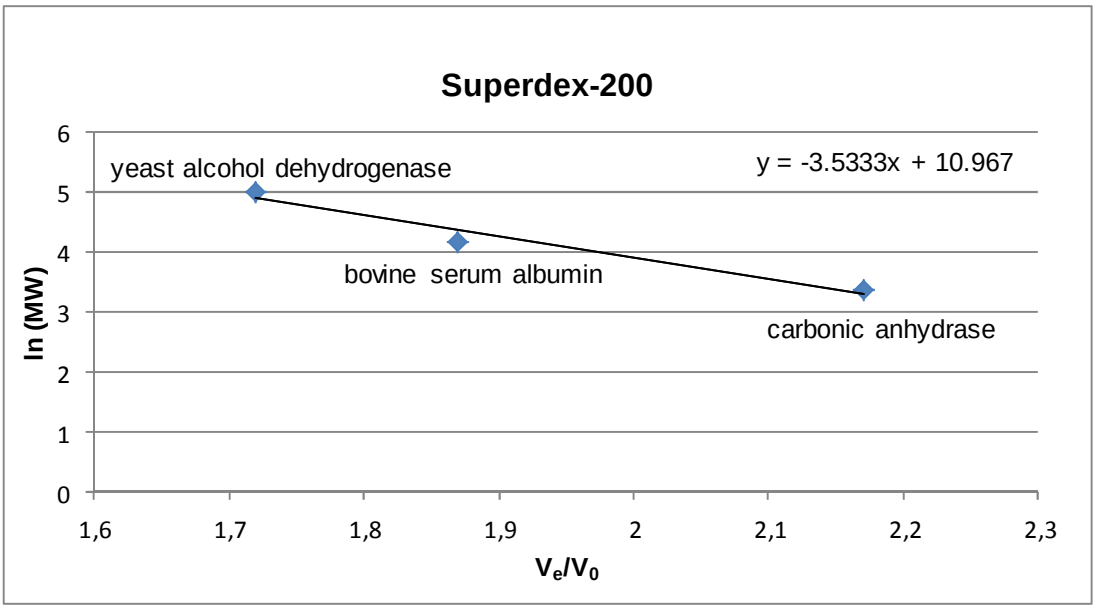

Fig. 13 Calibration curve for GPC Superdex-200 for the determination of the oligomerization state of $ALAS_{Rc}$.
The natural logarithm of the molecular weight (ln (MW)) of the marker proteins is plotted against their elution volume (V_e) divided with the 'dead volume' (V_0) of the column.

GPC buffer

Hepes, pH 7.5	20	mM
NaCl	200	mM
DTT	10	mM
PLP	20	µM

in H_2O_{dest}; sterile filtrated and degased

2.6.2 Concentrating Protein Solutions

The concentration of protein solutions was performed with the ultrafiltration membrane system VIVASPIN concentrator (Sartorius stedim biotech, Göttingen, Germany) with a start volume of 4 - 15 mL. All proteins with a molecular mass less than M_r = 10'000 could pass the membrane. Initially the membrane was equilibrated four times with the buffer in which the protein was dissolved. Finally, it was centrifuged at 4 ℃ and 2'500 - 3'000 rpm.

2.6.3 Determination of Protein Concentrations

In this work the Bradford Protein Assay Method (Bio-Rad, Munich, Germany) was used for the determination of protein concentrations. This is a photometric method that based on the formation of complexes of proteins and the dye Coomassie Brilliant Blue G-250. These complexes were formed in acidic solutions from the dye with the cationic as well as with the non-polar, hydrophobic side chains of the proteins. Due to the complex formation the

absorption maximum was shifted from 470 nm to 595 nm because the dye was stabilized here in its blue, non-protonated, anionic sulfate form. Furthermore, the extinction coefficient from the protein-dye-complex is higher than the coefficient from the free dye. An increase in absorption at 595 nm due to the complex formation could be measured with a high sensitivity against the free dye. Thus, the complex represented a mass for the protein concentration.
BSA with a known concentration was used for the calibration curve. The resulting curve is shown in Fig. 14. The assays contained 1.5 mL Bradford reagent (Sigma-Aldrich, Munich, Germany) and 1 µL, 10 µL or 100 µL of the protein solution. After mixing and incubation for 25 min at RT the absorption at 595 nm was measured against the reference (Bradford reagent only). The data were compared with the calibration curve and the protein concentration could be determined.

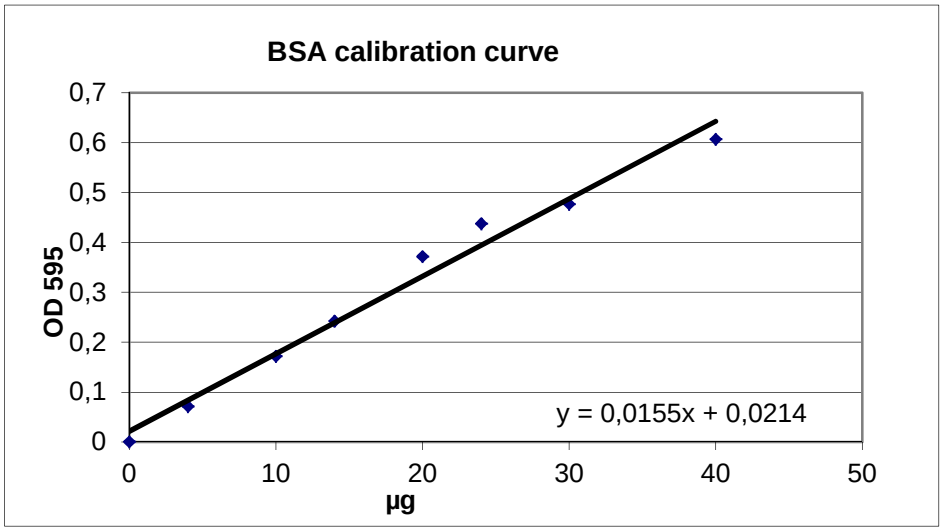

Fig. 14: BSA calibration curve for the determination of protein concentrations.
The used amount of BSA was plotted against the absorption at 595 nm after incubation with the Bradford reagent.

2.6.4 Discontinuous SDS Polyacrylamide Gel Electrophoresis

The cell sediment of a 1 mL cell culture was dissolved in H_2O_{dest} and in a corresponding amount of 2 x SDS-loading buffer (~ 20 - 240 µL) to mask the charge at the surface of the proteins which leads to a separation according to their size. To denature the proteins in the analytes they were heated for 5 min at 95 ℃ in a thermomixer and then electrophoretically separated in a 12 % SDS polyacrylamide gel electrophoresis (SDS-PAGE) at 45 mA *per* gel. In the stacking gel (pH 6.8) a potential difference between the slow glycine ions (because they are predominantly uncharged) and the fast chloride ions is generated. When the proteins arrive at the resolving gel (pH 8.8) they are decelerated because of the little size of the pores. At this point the glycine ions pass the proteins. Due to the pH-shift in the resolving gel the glycine ions are

now completely charged and the field force in the gel is constant. Due to the change of the migration speed of the glycine ions, the proteins are concentrated in the gel matrix according to their denaturell molecular weight. Subsequently, the gel was stained with Instant *Blue*™ solution (Expedeon, Eching, Germany) in order to visualize the location of the analytes in the gel matrix. After an incubation time of 15 - 30 min on a shaker the gel was washed with water. Afterwards the gel was scanned and dried between two cellophane films.

Molecular weight standard

Protein Molecular Weight Marker (Fermentas)

SDS running gel (12 %)

acrylamide stock solution	2	mL
Tris-HCl (1.5 M)	1.25	mL
H_2O_{dest}	1.75	mL
tetramethylen diamine (TEMED)	5	µL
APS solution	50	µL

in H_2O_{dest}; pH 8.8

SDS stacking gel (12 %)

acrylamide stock solution	0.5	mL
Tris-HCl (0.5 M)	0.62	mL
H_2O_{dest}	1.37	mL
TEMED	2.5	µL
APS solution	5	µL

in H_2O_{dest}; pH 6.8

APS solution

ammonium peroxodisulfate 10% (w/v)
in H_2O_{dest}

Acrylamide stock solution

Rotiphorese®Gel 30 (37.5:1) (Roth)

Electrophoresis buffer

glycine	380	mM
Tris-HCl	50	mM
SDS	0.1	% (w/v)

in H_2O_{dest}; pH 8.3

SDS-loading dye

Tris-HCl	100	mM
glycerol	40	% (v/v)
β-mercaptoethanol	10	% (v/v)
SDS	3.2	% (w/v)
bromphenol blue	0.2	% (w/v)

in H_2O_{dest}; pH 6.8

Staining solution

InstantBlue™	(Expedeon)

2.6.5 Western Blotting

This method serves for the transfer of proteins onto a polyvinylidenfluoride (PVDF)-membrane. The membrane binds the proteins by polar interactions. The first step was PVDF-membrane activation in methanol for 15 min. Afterwards, the membrane as well as the SDS-gel and blotting paper were incubated in Towbin-buffer. The assembly in the blotting apparatus was the following: Cathode, blotting paper, PVDF-membrane, SDS-gel, blotting paper, anode (Fig. 15). Proteins were blotted onto the membrane for 30 - 45 min at 15 V according to manufacturer's instruction. Non-specific binding sites of the membrane were saturated in blocking solution for 1 h at 4 ℃ under slight shaking. Proteins immobilized on a PVDF-membrane were specifically detected by antibodies. Primary antibodies were directed against the GST- or other tags while the secondary antibodies were directed against the primary antibody and were coupled to an alkaline phosphatase. Incubation with the first antibody was carried out in blocking solution for 1 h at RT and slight shaking. Three washing steps followed, 10 min for each with washing buffer. After incubation with the second antibody for 45 min and four additional washing steps with PBS/Tween buffer (10 min each), membranes were incubated for 5 min in alkaline phosphatase buffer and exposed to staining solution until bands became visible. During exposure alkaline phosphatase, the enzyme bound to the secondary antibody, catalyzes the reaction of 5-bromo-4-chloro-3-indolylphosphate (BCIP) with nitroblue-tetrazolium (NBT). Fig. 15 shows a schematic representation of the Western blotting assembly.

Fig. 15: Schematic representation of a Western blotting apparatus.

Towbin-buffer

Tris-HCl	25	mM
glycine	192	M
methanol	10	% (v/v)
in H_2O_{dest}; pH 8.5		

10 x Phosphate-buffered saline (PBS)

NaCl	1.37	M
KCl	27	mM
Na_2HPO_4	100	mM
KH_2PO_4	20	mM
in H_2O_{dest}		

Blocking solution

skim milk powder	5	% (w/v)
Tween20	0.1	% (v/v)
10 x PBS	10	% (v/v)
in H_2O_{dest}		

Washing solution

skim milk powder	0.5	% (w/v)
Tween20	0.1	% (v/v)
10 x PBS	10	% (v/v)
in H_2O_{dest}		

PBS/Tween buffer

10 x PBS	10	% (v/v)
Tween20	0.1	% (v/v)
in H_2O_{dest}		

Alkaline phosphatase buffer

Tris-HCl	100	mM
NaCl	100	mM
$MgCl_2$	5	mM
in H_2O_{dest}; pH 9.5		

Staining solution

NBT solution	0.33	% (v/v)
BCIP solution	0.33	%(v/v)
in alkaline phosphatase buffer		

NBT solution

nitroblue-tetrazolium	10	% (w/v)
dimethylenformamide (DMF)	70	% (v/v)
in H_2O_{dest}		

BCIP solution

5-brom-4-chloro-3-indolylphosphate	5	% (w/v)
in DMF solution		

Antibodies

Anti-Glutathione-S-Transferase (Rabbit-anti-GST)	1:2000
Anti-Rabbit IgG, Alkaline Phosphatase Conjugated	1:5000

2.7 Determination of ALAS Activity

The enzyme activity assay was performed as described previously (Hunter and Ferreira, 1995). In this assay the enzyme concentration ranged from 0.2 - 2 µM in a total volume of 200 µL. Data were taped using a Jasco V-550 UV/VIS spectrophotometer (Jasco®, Gross-Umstadt, Germany) and analyzed with SigmaPlot11 software (Systat, Erkrath, Germany).

2.7.1 Determination of Kinetic Parameters of ALAS

2.7.1.1 Steady State Kinetics

ALAS activity was determined on a Shimadzu UV2100 UV/VIS dual beam spectrophotometer in Florida, Tampa, USA in a coupled enzyme assay: the production of CoA (Equation (3)) was coupled to the reduction of nictotinamide adenine dinucleotide (NAD^+, Equation (4)). Experiments were carried out at 30 ℃ in a total volume of 150 µL over a time perio d of 5 min. The reaction mixture contained reaction buffer, ALAS, glycine and succinyl-CoA. The coupling enzyme, α-ketoglutarate dehydrogenase (α-KGD), was added directly to the assay as supplied by Sigma (St. Louis, MO, USA and Munich, Germany, respectively). The amount of NADH was analyzed by measuring the absorbance at 340 nm with an extinction coefficient of ε_{340} = 6'560 M^1 x cm^{-1} (Hunter and Ferreira, 1995). For the determination of the kinetic parameters K_M, k_{cat} and the 'real' v_{max}, the concentrations of the substrates were varied (in matrices of five glycine and five succinyl-CoA concentrations). The observed rates were fitted to the Michaelis-Menten equation using the nonlinear regression analysis software program SigmaPlot (SigmaPlot11, Systat Software Inc., Erkrath, Germany).

$$\text{glycine} + \text{succinyl-CoA} \xrightarrow{\text{ALAS}} \text{ALA} + \text{CoASH} + CO_2 \qquad (2)$$

$$\text{CoASH} + NAD^+ + \alpha\text{-ketoglutarate} \xrightarrow{\alpha\text{-KGD}} \text{succinyl-CoA} + \text{NADH} + CO_2 \qquad (3)$$

Equation 2 and 3: Coupled enzyme reaction of ALAS and α-KGD.
Equation (2) describes the reaction catalyzed by ALAS. It catalyzes the condensation of the amino acid glycine and succinyl-CoA with the products ALA, carbon dioxide and CoA. Equation (3) describes the ALAS-coupled α-KGD reaction with CoA, NAD^+ and α-ketoglutarate as educts as well as succinyl-CoA, NADH and carbon dioxide as products.

The reduction of NAD^+ to NADH is stoichiometric with ALA formation and succinyl-CoA was generated by α-KGD. The NADH concentration can be quantified *via* the Beer-Lambert law (Equation (4)):

$$A = \varepsilon * b * c \quad (4)$$

Equation 4: Beer-Lambert law.
The Beer-Lambert law relates the absorption of light to the properties of the material through which the light is traveling. It is useful for the determination of unknown concentrations in a solution. *A*: absorption; ε: extinction coefficient of NADH *[M^1cm^{-1}]*; *b*: cell diameter *[cm]*; *c*: concentration of NADH *[M].*

Kinetic parameters were calculated as follows:

$$v_{max} = (average\ of\ the\ apparent\ v'_{max}s) * c \quad (5)$$

Equation 5: Calculation of the 'real' v_{max}.
For the calculation of the 'real' v_{max} both v_{max} values for succinyl-CoA and glycine have to be determined. v_{max} = maximal velocity; *c* = concentration of NADH *[M^1cm^{-1}].*

For the calculation of the turnover number k_{cat}, the 'real' maximal velocity v_{max} was divided by the corresponding enzyme concentration (Equation (6)).

$$v_{max} = k_{cat} * [E] \longrightarrow k_{cat} = \frac{v_{max}}{[E]} \quad (6)$$

Equation 6: Calculation of the turnover number k_{cat}.
For the calculation of the turnover number k_{cat} the maximal velocity has to be divided by the enzyme concentration used in the assay. v_{max} = maximal velocity; *[E]* = enzyme concentration used in the assay *[µM]*; k_{cat} = catalytic constant *[s^{-1}]*.

K_M describes the substrate concentration where the rate of turnover is half of v_{max}. It is an approximation of the affinity of the enzyme for its substrate based on the rate constants within the reaction. A high K_M value denotes that the enzyme is half-saturated at high substrate levels; its substrate affinity is low. Contrary, a low K_M implies that the enzyme needs low levels of substrate to be half-saturated; its substrate affinity is high. The k_{cat} is the rate constant of a first order enzyme kinetic with its unit s^{-1}. It correlates to the amount of substrate molecules which are converted into product by one enzyme molecule per second. With the knowledge of the K_M and k_{cat} values the constante k_{cat}/K_M was calculated. The k_{cat}/K_M is the rate constant of second order ($s^{-1} * M^{-1}$) and describes the catalytic efficiency or specificity of the enzyme if more than one substrate is available. The factor k_{cat}/K_M cannot be higher than k_1 which is the rate constant for the formation of the enzyme-substrate-complex. This denotes that the decay of the enzyme-substrate-complex cannot occur more often than enzyme and substrate collide with each other. The k_{cat}/K_M is used to measure enzyme's substrate preference or its catalytic efficiency. The higher the k_{cat}/K_M ratio, the better the enzyme catalyzes the substrate conversion and the more efficient the enzyme works. Using the software SigmaPlot11 the rates of each reaction *[mAbs/min]* were plotted against the consumed glycine *[mM]* and succinyl-CoA *[µM]* concentrations, respectively, resulting in secondary plots for glycine and succinyl-CoA. The K_M values for both substrates resulted from these secondary plots as well as their v_{max} values.

Reaction buffer			
	Hepes	20	mM
	magnesium chloride	3	mM
	α-ketoglutaric acid sodium salt	1	mM
	nicotinamid adenine dinucleotide (NAD^+)	1	mM
	thyamine pyrophosphate (TPP)	0.25	mM
	in H_2O_{dest}; pH 7.5		
ALAS solution			
	ALAS	0.2-2	µM
Glycine solution			
	glycine in H_2O_{dest}	1	M
Succinyl-CoA solution			
	succinyl-CoA in H_2O_{dest}	1	mM

2.7.1.2 Single Turnover Reactions

ALAS catalysis to synthesize ALA is a multiple-step catalytic conversion ('Introduction', Fig. 7). In order to monitor single turnover reactions transient kinetic analyses were performed. Aim of these single turnover reactions is to have ALAS performs only one catalytic half cycle, *i.e.* each ALAS binds to one glycine molecule. This is achieved by using higher enzyme concentrations than the substrate concentration of succinyl-CoA.
Rapid scanning stopped flow measurements were performed under aerobic conditions by using an OLIS model RSM-1000 stopped-flow spectrophotometer (On-line Instrument Systems Inc., Bogart, USA). This instrument has a dead time of approximately 2 ms and an observation chamber path length of 4 mm. Spectral scans, covering a wavelength range of 200 - 600 nm, were collected at a rate of 1'000 scans/sec and then averaged to 62 scans/sec reducing time course data files to an appropriate size for global fit analyses. Stopped flow experiments were carried out at 30 ℃ with an exter nal water bath to maintain a constant temperature.
The stopped-flow was useful for those experiments because the reactants could be rapidly mixed in a small volume. The mixing solutions flow into an observation cell while the previous contents are flushed and replaced with freshly mixed reactants. A stop syringe is used to limit the volume of solution expended with each measurement (Fig. 16).
Syringe one contained the enzyme (127 – 442 µM) and a high concentration of the first substrate glycine (30 mM). The second syringe was filled with the second substrate, succinyl-CoA (60 µM), in a lower concentration than glycine and buffer-A. Both syringes contained a total volume of 1 mL. The

concentrations of reactants loaded into both syringes are in each experiment two-fold greater than in the reaction cell. The final concentrations of the reactants for the $ALAS_{Rc}$-catalyzed reactions were: 63.5 – 220.7 µM bacterial ALAS, 15 mM glycine and 30 µM succinyl-CoA. Fluorescence at 510 nm resulting from formation of the second quinonoid was recorded *via* excitation at 400 nm and emission measurement above 500 nm. Time courses were analyzed with the decomposition software (SIFIT) provided by OLIS.

$$A_t = \sum_{n=1}^{э} a_i \, e^{-k_i t} + c \qquad (7)$$

Equation 7: Fitting equation for time courses at wavelengths of interest (Hunter and Ferreira, 1999).
Time courses at wavelengths of interest were analyzed by fitting to equations for one to three exponentials. A_t = Absorbance at time t; a = amplitude of each phase; k = observed rate constant for each phase; c = final absorbance.

Single turnover reactions were evaluated using a three-step mechanism as described in Equation (8).

$$A \xrightarrow{k^1_{obs}} B \xrightarrow{k^2_{obs}} C \xrightarrow{k^3_{obs}} D \qquad (8)$$

Equation 8: Visualization of a three step reaction mechanism with its educt, product and intermediates.
A three step mechanism starts with an educt (A) followed by two intermediates (B and C) and ended with a product (D). The observed rates are described by k^1_{obs}, k^2_{obs} and k^3_{obs}.

Buffer-A	N-(1,1-Dimethyl-2-hydroxyethyl)-3-amino-2-hydroxypropanesulfonic acid (AMPSO) in H_2O_{dest}; pH 9.5	100	mM
Glycine solution	glycine in H_2O_{dest}	1	M
Succinyl-CoA solution	succinyl-CoA in H_2O_{dest}	1	mM
ALAS solution	ALAS	> 60	µM

Fig. 16 shows a schematic representation of a stopped-flow apparatus used for these measurements.

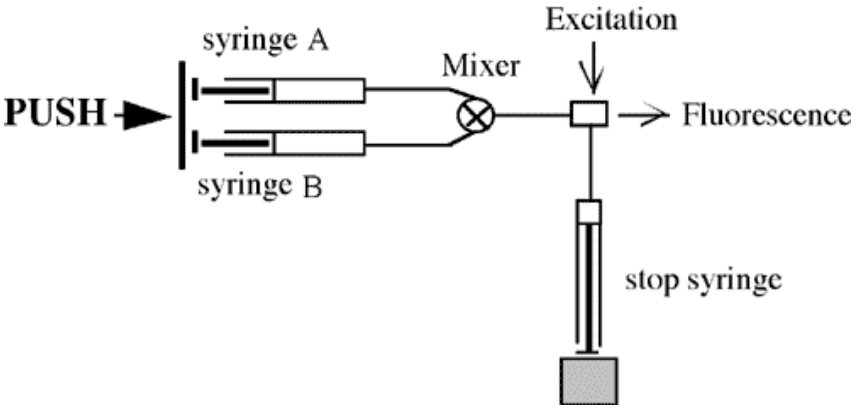

Fig. 16: Schematic representation of a stopped flow apparatus.
The syringes A and B contain the different solutions, *here:* the enzyme-glycine mixture in one syringe and the succinyl-CoA buffer mixture in the other one. By pushing both syringes at the same time, a defined volume of both solutions flow into a mixer and thus into the observation cell. The volume in this chamber is regulated by the stop syringe. The excitation is given by an UV-lamp and the fluorescence of the reacting solution could be observed in dependency on time.

2.7.2 Substrate Specificity

Substrate specificity determinations were carried out at 30 ℃. The experimental set-up was similar as for the steady state kinetics (2.7.1.1). The difference was the utilization of other amino acids than glycine, but with the physiological second substrate succinyl-CoA. In a further approach glycine served as first substrate, but different acyl-CoA derivatives were used as second substrate.

Amino acid solutions

D-alanine	1	M
L-alanine	1	M
L-cysteine	1	M
L-threonine	0.5	M
L-serine	1	M

Acyl-CoA solutions

succinyl-CoA	0.1	mM
octanoyl-CoA	0.1	mM
butyryl-CoA	0.1	mM

2.7.3 Quinonoid Formation

Experiments for detection of the second quinonoid in absorbance mode were carried out at 30 ℃ at a wavelength range from 650 to 200 nm in a total volume of 150 µL. Twenty µM enyzme was mixed with AMPSO-buffers with a pH of 7.5 or a pH of 9.5, respectively. ALA had to be neutralized with the same amount of sodium hydroxide (NaOH) solution before starting the reaction by adding 5 mM ALA (Sigma, Hamburg, Germany). A Shimadzu spectrophotometer served for data collection. Data were evaluated with SigmaPlot11 software (Systat, Erkrath, Germany).

AMPSO-buffer

AMPSO	100	mM
in H_2O_{dest}; pH 7.5 and pH 9.5		

NAOH solution

NaOH	100	mM
in H_2O_{dest}		

ALA solution

ALA	100	mM
In H_2O_{dest}		

2.7.4 Reaction of ALAS with Glycine-methylester and *O*-methylglycine

Identification of the 2-amino-3-beta-ketoadipate intermediate results from the reaction of ALAS with glycine-methylester and succinyl-CoA as described for AONS (Kerbarh *et al.*, 2006). In this reaction the reactive β-ketoacid PLP-aldimine will be trapped in the enzyme-bound form so it cannot undergo decarboxylation and thus will accumulate. The chemical nature of the putative β-ketoacid-methylester-aldimine intermediate is determined by reducing the unstable imine bond with sodium cyanoborohydride. Subsequently, the products were analyzed by electrospray mass spectrometry (Kerbarh *et al.*, 2006). These experiments were performed with the $ALAS_{Rc}$-N54 mutant enzymes as well as with the mouse ALAS2-N119 mutant in Florida by Greg Hunter (Prof. Dr. Gloria C. Ferreira's laboratory, Tampa, University of South Florida, Florida, USA). For the detection of the first quinonoid *O*-methylglycine was used as pseudosubstrate instead of glycine. The generated methylester of the β-ketoacid-aldimine complex does not decarboxylate to afford the second quinonoid intermediate. Similar to the reaction of the ALAS-glycine complex with succinyl-CoA (2.7.1.1), the kinetic trace for the reaction of the ALAS-*O*-methylglycine complex with succinyl-CoA was best described by a three-step process. These experiments also were performed with the $ALAS_{Rc}$-N54 mutant enzymes as well as with the mouse ALAS2-N119 mutant in

Florida by Greg Hunter (Prof. Dr. Gloria C. Ferreira's laboratory, Tampa, University of South Florida, Florida, USA).

2.7.5 Glycine Binding Experiments

The ALAS shows a characteristical peak at 420 nm. If glycine is bound changes in this absorption peak were observable. Glycine binding experiments were carried out at 30 ℃ at a wavelength range from 650 to 200 nm in a total volume of 150 µL. Twenty µM enyzme was mixed with AMPSO-buffer, pH 9.5. After a spectrum of enzyme only was taken, 5 mM glycine was added and a new spectrum was recorded. A Shimadzu served for data collection. Data were evaluated with SigmaPlot11 software (Systat, Erkrath, Germany).

AMPSO-buffer

AMPSO in H_2O_{dest}; pH 9.5	100	mM

Glycine solution

glycine in H_2O_{dest}	100	mM

2.7.6 Dynamic Loop Experiments

In the $ALAS_{Rc}$ crystal structure two different conformations were observed, an open and a closed conformation. The open enzyme conformation differs from the closed one in two areas located between amino acids 358 - 374 and 332 - 348 (Astner, 2007). The closed conformation is comparable to the product-bound structure of AONS. In dynamic loop experiments carried out in Tampa, Florida, USA (Ferreira and coworkers) the movement of the dynamic loop should be analyzed. For this purpose, a cysteine-free $ALAS_{Rc}$-T365C mutant (correspond to the murine T430 residue) was labelled on the cysteine with a fluorophore for studying the kinetics of the change from open to closed conformation (data not shown; still in progress).

2.8 Crystallization of *Rhodobacter capsulatus* Aminolevulinic Acid Synthase

The holo form of the $ALAS_{Rc}$ was crystallized and the X-ray crystal structure was solved at 2.1 Á resolution (Astner *et al.,* 2005) as well as enzyme-substrate complexes with glycine and succinyl-CoA, respectively.

2.8.1 Crystallization Conditions

For the crystallization of purified $ALAS_{Rc}$ the vapour diffusion method was applied allowing a slow and controlled growth of protein crystals. Crystallization experiments with cysteine-less wild-type $ALAS_{Rc}$ and the $ALAS_{Rc}$ mutant variants N54D and N54Q were carried out under aerobic and anaerobic conditions at 17 ℃. An MACS MG 1000 anaerobic work station was used for anaerobic attempts (Don Whitley Scientific, Lähden-Holte, Germany). A variety of buffers, precipitants and salts were used, provided from Qiagen (Hilden, Germany) within 96-well sitting drop CrystalClear strip racks (Greiner bio-one, Frickenhausen, Germany) with 100 µL reservoir solution. For enzyme-substrate attempts 1 µL reservoir and 2.3 µL enzyme-substrate-mix were used while for enzyme approaches 1.5 µL reservoir and 1.5 µL enzyme-DTT solution were used. An enzyme concentration between 115 µM and 230 µM (5 - 10 mg/mL) was used in each assay. Furthermore, crystallization experiments were carried out with enzyme only, but also with both substrates. For both substrates 1 µM stock solutions were prepared, in the assay they had a final concentration between 0.1 µM and 0.25 µM. Additionally, a 70 mM stock solution of DTT was prepared and added to each enzyme or enzyme-substrate-mixture right prior to usage in the crystallization experiments. The final DTT concentration for all crystallization approaches were 0.15 mM. For each variant and the wild-type $ALAS_{Rc}$ we conducted three 96-well plates with enzyme only as well as with an enzyme-substrate-mixture under aerobic and anaerobic conditions with four different crystal screens (Qiagen, Tab. 2). A total of approximately fourty 96-well plates were prepared.

3 RESULTS AND DISCUSSION

Based on the solved crystal structure of $ALAS_{Rc}$ and previous biophysical investigation the question for the formation of a potential 2-amino-3-ketoadipate intermediate in ALAS catalysis, the recognition of the succinyl-CoA and glycine substrates, and finally the molecular basis of ALAS-βSCS interaction were investigated.

For this purpose amino acid residues potentially involved in these processes were exchanged in $ALAS_{Rc}$. Mutant enzymes were recombinantly produced, purified and subjected to advanced steady state kinetic and single turnover analyses. Selected $ALAS_{Rc}$ variants were employed in substrate specificity assays and crystallization attempts.

3.1 Rationale for Amino Acid Exchanges in $ALAS_{Rc}$ for the Demonstration of the 2-amino-3-ketoadipate Intermediate

In the ALAS reaction mechanism three different reaction intermediates occur. The first and the third one are quinonoids (first and second quinonoid) while the second one is a potential ketoadipate (2-amino-3-ketoadipate). The ALAS reaction is fast, so that only the second quinonoid is spectroscopically detectable. $ALAS_{Rc}$-N54 corresponds to the N119 residue of the mouse ALAS2 enzyme and to N197 of the human ALAS2. Hunter and coworkers (Hunter *et al.*, 2007) suggested that the N119 residue of murine ALAS2 plays an important role in stabilizing or destabilizing the potential 2-amino-3-ketoadipate intermediate. The β-ketoadipate was modeled into a murine ALAS2 active site model with the conservation of the hydrogen bond interactions found for the succinyl-CoA. The found arrangement of hydrogen bonds in this model was similar to that observed for the product-bound structure of the homologous enzyme AONS (Alexeev *et al.*, 1998) as well as with the product-bound crystal structure of $ALAS_{Rc}$ (Astner *et al*., 2005). Based on the relative orientation of the nitrogen and oxygen atoms of the murine ALAS2-N119 side chain amide, which is typically ambiguous in crystal structures (Word *et al.*, 1999; McDonald and Thornton, 1995), it was proposed that the murine ALAS2 residue N119 and

analogously the $ALAS_{Rc}$-N54 either stabilize or destabilize the 2-amino-3-ketoadipate intermediate. With the $ALAS_{Rc}$-N54 variant we intended to prove this assumption by performing the $ALAS_{Rc}$ reaction with glycine-methylester, a glycine analog. The ALAS is able to bind but not catalyze this molecule as substrate. The reaction mechanism should pause at the step of the 2-amino-3-ketoadipate intermediate and thus prove its formation.

Furthermore, special consideration was given to the cysteine residues of $ALAS_{Rc}$, because these amino acids are known to hinder crystallization procedures by intermolecular disulfide bridge formation and by their reaction with molecular oxygen. C400 is a residue at the surface of the protein and located at the C-terminal domain of the $ALAS_{Rc}$ enzyme and possibly responsible for the oxidation sensibility. The residues C52 and C201 are not surface exposed. It was suggested that an amino acid exchange of either of these both residues affects protein folding and results in an inactive or instable protein (Astner, 2007). Therefore, $ALAS_{Rc}$ variants were produced in which the cysteines 400, 201 and 52 were exchanged to serines. Additionally, in two of the cysteine-free $ALAS_{Rc}$ variants the N54 residue was exchanged to aspartic acid and glutamine for trapping the 2-amino-3-ketoadipate during crystallization.

3.2 Substrate Recognition and Coordination in $ALAS_{Rc}$

3.2.1 Rationale of Amino Acid Exchanges in $ALAS_{Rc}$ for Functional Investigation of Substrate Recognition

Several residues are responsible for a correct substrate recognition and coordination in the ALAS active site. The succinyl-CoA carboxylate group is coordinated *via* a salt bridge in the $ALAS_{Rc}$ crystal structure by the R21 residue (‘Introduction’, Fig. 8). Further stabilization is due to two hydrogen bonds to T83 and N85 as well as van der Waals interactions with I86. The result of the tight binding of the succinyl-CoA carboxylate group is suggested to be responsible for the slow release of the resulting product ALA. This step is the rate-limiting one in ALAS catalysis (Hunter and Ferreira, 1999). By performing $ALAS_{Rc}$

reactions with substrate analogs we wanted to verify the influence of the selected residues on substrate recognition and coordination. Furthermore, the hypothesis that the ALA release is the rate-limiting step in ALAS catalysis should be analyzed by the characterization of $ALAS_{Rc}$ carrying these mutated residues.

3.2.2 Rationale for Amino Acid Exchanges in $ALAS_{Rc}$ for the Investigation of Enzyme Dynamics during Substrate Recognition

During ALAS catalysis the enzyme undergoes a conformational change due to substrate binding and active site loop movement. Ferreira and coworkers assume that the major conformational change between the open and closed form of the enzyme occurs at the 'active site loop' with T365 (T430 in murine ALAS2) at its tip (Lendrihas *et al.*, 2010). Furthermore, T365 bridges the carboxyl acid moiety of succinyl-CoA and the side chain of R21 to complete a hydrogen bonding triad. Thus, the substrate entry into the active site seems to be defined by the chemical characteristics of the acyl-tail of succinyl-CoA. In 'loop dynamic' experiments we wanted to clarify the role of the T365 residue in the outlined processes using a fluorescent-tag labeled $ALAS_{Rc}$-T365 cysteine-free mutant enzyme. For the investigation of these assumptions we collaborated with Prof. Dr. Gloria C. Ferreira's laboratory in Tampa, Florida, USA. Two $ALAS_{Rc}$-T365 cysteine-free variants were generated in the framework of this thesis and purified proteins were sent to Tampa, Florida, USA (T365S-C52S-C201S-C400S; T365C-C52S-C201S-C400S). Ferreira and coworkers performed the fluorescent labeling and the 'loop dynamic' experiments by studying the enzyme kinetics for the time from the open to the closed conformations. With the achieved results we wanted to get a more detailed look in the conformational change of ALAS due to substrate binding.

3.3 Rationale for Amino Acid Exchanges in $ALAS_{Rc}$ for the Investigation of ALAS-βSCS Interaction

The $ALAS_{Rc}$-D47 and M309 (correspond to D190 and R452 in human ALAS2) residues are positioned at the surface of the protein. In humans they play a role in interaction with the β-subunit of SCS. Previously, Furuyama and coworkers (Furuyama and Sassa, 2000) characterized a D190V variant for the human ALAS2 enzyme. This mutation led to a modification of the solvent exposed surface of the ALAS2 and seemed to be responsible for decreased protein stability while enzyme activity was not affected. The decreased protein stability of this ALAS2 variant is currently subject of discussion for the cause of the outbreak of XLSA disease. However, treatment of patients with pyridoxine did not mitigate the disease. Currently, it is speculated about a disturbed protein-protein interaction to another protein of importance. With the generation of the both $ALAS_{Rc}$ variants $ALAS_{Rc}$-D47 and -M309, we performed interaction studies with βSCS of *R. capsulatus* ($βSCS_{Rc}$) to give evidence for the involved residues of the interaction with this enzyme. For the $ALAS_{Rc}$-D47 and -M309 variants carrying conservative amino acid exchanges we expected to yield enzymes where the interaction with $βSCS_{Rc}$ is not affected. In contrast in $ALAS_{Rc}$ with non-conservative amino acid exchanges the interaction of both enzymes should be interrupted. With the results of these experiments we are able to understand the influence of D47 and M309 on the interaction with βSCS and in triggering XLSA in humans.

Tab. 9: Generated $ALAS_{Rc}$ variants.
Listed are the different generated $ALAS_{Rc}$ variants. For each residue of interest one conservative and one non-conservative amino acid exchange were generated.
Conservative amino acid exchanges were highlighted in light pink.

residue	conservative amino acid exchange	non-conservative amino acid exchange	interaction with/ responsible for
N54	N54Q	N54D	stabilize/destabilize 2-amino-3-ketoadipate intermediate
C52-C201-C400	C52S-C201S-C400S	-	C400: oxidization sensitivity C52/C201: protein folding
N54-C52-C201-C400	N54D-C52S-C201S-C400S	N54Q-C52S-C201S-C400S	stabilize/destabilize 2-amino-3-ketoadipate intermediate; C400: oxidization sensitivity C52/C201: protein folding
R21	R21K	R21E	succinyl-Coenzyme A carboxylate
T83	T83S	T83L	succinyl-Coenzyme A carboxylate
N85	N85Q	N85F	succinyl-Coenzyme A carboxylate
I86	I86L	I86H	succinyl-Coenzyme A carboxylate
T365-C52-C201-C400	T365S-C52S-C201S-C400S	-	involved in change of enzyme conformation during catalysis.
	T365C-C52S-C201S-C400S	-	involved in change of enzyme conformation during catalysis.
D47	D47E	D47S	succinyl-Coenzyme A synthetase
M309	M309L	M309W	succinyl-Coenzyme A synthetase

3.4 Production and Purification of Recombinant Wild-type $ALAS_{Rc}$

3.4.1 Construction of an Expression Vector for Wild-type $ALAS_{Rc}$

First, the *R. capsulatus hemA* gene was amplified *via* PCR and cloned into the expression vector pGEX-6P-1. Consequently, all proteins were produced as fusion proteins with an N-terminal GST-tag. The genomic DNA of *R. capsulatus* for amplification of the *hemA* gene was received from the DSMZ (‘Deutsche Sammlung von Mikroorganismen und Zellkulturen GmbH, Braunschweig-Stöckheim, Germany). Oligonucleotide primers for *hemA* amplification contained *Bam*HI and *Xho*I restriction sites for cloning purposes.

3.4.2 Production of Recombinant Wild-type ALAS$_{Rc}$

To analyze the best protein production host several different *E. coli* strains were tested. Therefore, the wild-type ALAS$_{Rc}$ expression vector p*Rc*-A was transformed into the selected *E. coli* strains. Recombinant protein production studies revealed best results in BL21(DE3)pLysS at 25 ℃ after 20 h after gene induction with 200 µM IPTG. Cell free extracts were separated *via* SDS-PAGE. Fig. 17 shows an SDS gel with the results from recombinant protein production experiments for wild-type ALAS$_{Rc}$.

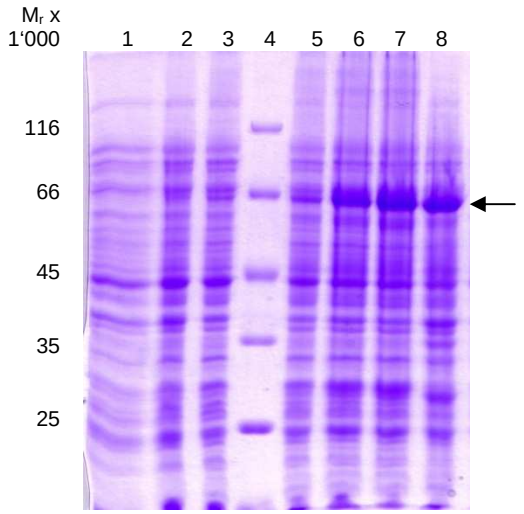

Fig. 17: Recombinant wild-type ALAS$_{Rc}$ production studies.
Cell free extracts were loaded onto a 12 % SDS-PAGE. Proteins were separated and afterwards visualized by staining with Instant*Blue*™. The SDS-PAGE shows recombinant protein production of p*Rc*-A in BL21(DE3)pLysS at 25 ℃.
Lane 1: before induction of gene expression using IPTG; lane 2: 1 h after induction; lane 3: 2 h after induction; lane 4: molecular weight marker; lane 5: 3 h after induction; lane 6: 4 h after induction; lane 7: 5 h after induction; lane 8: 20 h after induction.

The observed dominant protein with a relative molecular mass of approximately M_r = 66'000 (Fig. 17, lane 6 - 8) was in good agreement with the calculated molecular mass of the ALAS-GST-tag-fusion protein of M_r = 68'575.

3.4.3 Detection of Recombinantly Produced Wild-type ALAS$_{Rc}$ *via* Western Blotting

To test whether the dominant protein visible in the SDS gel (Fig. 17, lane 6 - 8) with a relative molecular mass of approximately M_r = 66'000 really was the wild-type ALAS$_{Rc}$, we performed protein detection *via* Western Blotting ('Material and Methods', 2.6.5). For this approach we used several protein samples of a test

protein production of two different *R. capsulatus* wild-type *hemA* clones in two *E. coli* strains, BL21(DE3)RIL and BL21(DE3)pLysS, which were cultivated at three different temperatures.

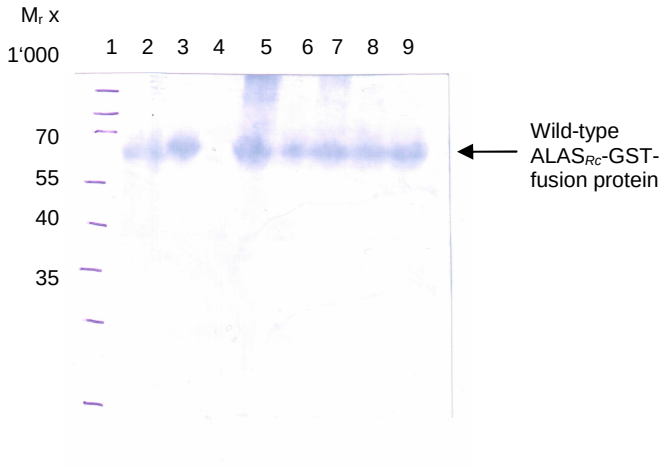

Fig. 18: Detection of wild-type ALAS$_{Rc}$ *via* Western Blotting.
PVDF-membrane with blotted proteins from *E. coli* cell free extracts were incubated with anti-GST antibodies. Visualization was *via* the alkaline phosphate catalyzed reaction of 5-bromo-4-chloro-3-indolylphosphate (BCIP) with nitroblue-tetrazolium (NBT). A dominant protein band with a relative molecular mass of approximately M_r = 65'000 became visible.
Lane 1: molecular weight marker; lane 2: positive control (*T. elongatus* uroporphyrinogen III synthase-GST-fusion protein); lane 3: *hemA*-clone-2 in BL21(DE3)RIL, 37 °C, 5 h after induction of gene expression; lane 4: *hemA*-clone-2 in BL21(DE3)pLysS, 37 °C, before induction; lane 5: *hemA*-clone-2 in BL21(DE3)pLysS, 37 °C, 5 h after induction; lane 6: *hemA*-clone-2 in BL21(DE3)RIL, 25 °C, 5 h after induction; lane 7: *hemA*-clone-11 in BL21(DE3)pLysS, 25 °C, 5 h after induction; lane 8: *hemA*-clone-2 in BL21(DE3)RIL, 17 °C, 20 h after induction; lane 9: *hemA*-clone-11 in BL21(DE3)pLysS, 17 °C, 20 h after induction.

The results of the Western Blot analysis (Fig. 18) verified that the dominant protein with a relative molecular mass of M_r = 66'000 of the test protein production (Fig. 17) was the induced wild-type ALAS$_{Rc}$, in this case produced as GST-fusion protein.

3.4.4 Purification of Recombinant Wild-type ALAS$_{Rc}$

Recombinant wild-type ALAS$_{Rc}$ was produced as GST-fusion-protein with an N-terminal GST-tag. Resulting protein was purified to apparent homogeneity by column chromatography with Econo-Pac columns containing glutathione sepharose at 4 °C. After chromatography as described in 'Material and Methods' (2.6.1.2) and incubation with PreScission™Protease for 40 h at 4 °C,

the protein was eluted and columns regenerated with a GST-containing buffer. Washing and elution fractions were analyzed *via* SDS-PAGEs.

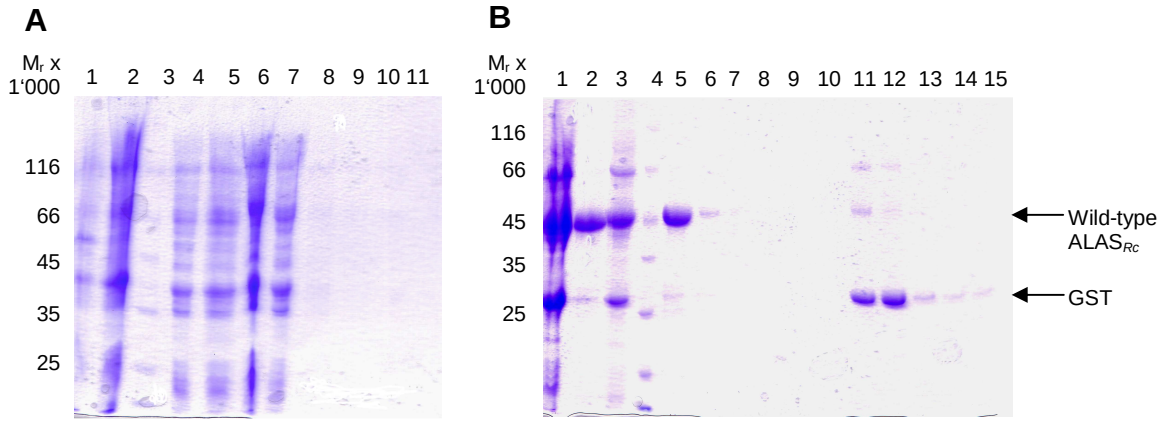

Fig. 19: Purification of wild-type $ALAS_{Rc}$ with GST column chromatography.
After cell disruption and centrifugation, the soluble fractions were separated by 12 % SDS-PAGE. Proteins were visualized by staining with Instant*Blue*™. The SDS-PAGEs shows protein purification of wild-type $ALAS_{Rc}$ at 4 ℃. **A**: Lane 1: sediment after cell disruption and centrifugation; lane 2: supernatant after cell disruption and centrifugation; lane 3: molecular weight marker; lane 4: first flow through fraction after incubation of resin and supernatant; lane 5: second flow through fraction after incubation of resin and supernatant; lane 6: first washing fraction with elution buffer; lane 7: second washing fraction with elution buffer; lane 8: third washing fraction with elution buffer; lane 9: fourth washing fraction with elution buffer; lane 10: fifth washing fraction with elution buffer; lane 11: sixth washing fraction with elution buffer. **B**: Lane 1: sediment of flow through fraction after 40 h incubation of PreScission™Protease and protein solution; lane 2: supernatant of flow through fraction; lane 3: sediment of first elution fraction after 40 h incubation with PreScission™Protease; lane 4: molecular weight marker; lane 5: supernatant of first elution fraction; lane 6: second elution fraction; lane 7: third elution fraction; lane 8: fourth elution fraction; lane 9: fifth elution fraction; lane 10: sixth elution fraction; lane 11: first washing fraction with regeneration buffer; lane 12: second washing fraction with regeneration buffer; lane 13: third washing fraction with regeneration buffer; lane 14: fourth washing fraction with regeneration buffer; lane 15: fifth washing fraction with regeneration buffer.

The first column chromatography resulted in isolation of an almost pure protein solution (Fig. 19B, lane 5). For further purification two different columns were chosen: an anion exchange column chromatography on MonoQ (2.6.1.4) and a GPC on Superdex-200 (2.6.1.5). GPC also was used to determine the oligomerization state of the protein. After the first purifying GST column chromatography samples were dialyzed against low salt buffer prior to the MonoQ column chromatography which was performed using a salt gradient starting from 0 mM to 1 M sodium chloride at RT. The wild-type $ALAS_{Rc}$ had an eluting salt concentration of 260 mM (data not shown) but showed no further purification. Due to the handling at RT where $ALAS_{Rc}$ was not as stable as at

4 ℃ the wild-type ALAS$_{Rc}$ only was purified with the GST column chromatography.

3.4.5 Oligomerization State of Recombinant Wild-type ALAS$_{Rc}$

For the determination of the oligomerization state of the wild-type ALAS$_{Rc}$ we used a GPC on Superdex-200. It was shown earlier that ALAS$_{Rc}$, but also of other bacteria and mouse, occurs as homodimers (Tan and Ferreira, 1996; Bolt *et al*., 1999; Astner *et al.*, 2005). The sizes of the monomers were described having a relative molecular mass between M_r = 43'000 and M_r = 66'000. The chromatography was carried out as described in 'Materials and Methods' (2.6.1.5). The elution volume of wild-type ALAS$_{Rc}$ was approximately 14.25 mL. With the calibration curve (Fig. 20) we determined a relative molecular mass of approximately M_r = 91'000. This value was in good agreement with the calculated relative molecular mass of the ALAS$_{Rc}$ homodimer of M_r = 87'332.

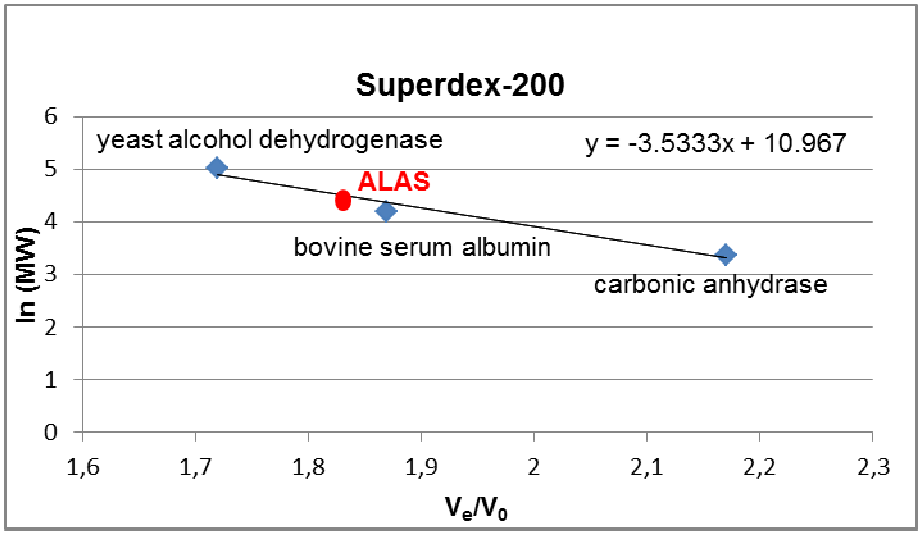

Fig. 20: Determination of the oligomerization state of wild-type ALAS$_{Rc}$.
The natural logarithm of the molecular weight (ln (MW)) of the marker proteins was plotted against their elution volume (V_e) divided with the 'dead volume' (V_0) of the column. A molecular mass of approximately M_r = 91'000 was determined for ALAS$_{Rc}$ matching with the calculated molecular mass of M_r = 87'332. The column was calibrated using carbonic anhydrase (M_r = 29'000), bovine serum albumin (M_r = 66'000) and yeast alcohol dehydrogenase (M_r = 150'000) as marker proteins.

3.5 Generation, Production and Purification of Recombinant ALAS$_{Rc}$ Enzyme Variants

The expression vector p*Rc*-A carrying the wild-type *hemA* gene of *R. capsulatus* served as template for site-directed mutagenesis. For each residue of interest (Tab. 9) we developed one conservative and one non-conservative amino acid exchange whereby one, three or four amino acid exchanges were conducted. The resulting constructs were verified for their correct gene sequence. Analogously to the wild-type ALAS$_{Rc}$ protein, we tested two different *E. coli* strains, BL21(DE3)RIL and BL21(DE3)pLysS, for each ALAS$_{Rc}$ variant with regard to best protein production. Tab. 10 shows a summary of obtained results.

Tab. 10: ALAS$_{Rc}$ variants, their best protein producing *E. coli* strain and optimal growth temperature.
The time point of highest protein production was identical for all ALAS$_{Rc}$ variants (20 h), but they differed in the growth temperature of the producing strain and in the protein producing *E. coli* strain itself. Conservative amino acid exchanges were highlighted in light pink.
n/a: non-available.

ALAS$_{Rc}$ variant	*E. coli* strain	temperature	growth time
N54Q	BL21(DE3)pLysS	17 ℃	20 h
N54D	BL21(DE3)pLysS	17 ℃	20 h
C52S-C201S-C400S	BL21(DE3)pLysS	17 ℃	20 h
N54Q-C52S-C201S-C400S	BL21(DE3)pLysS	25 ℃	20 h
N54D-C52S-C201S-C400S	BL21(DE3)pLysS	25 ℃	20 h
R21K	BL21(DE3)pLysS	17 ℃	20 h
R21E	BL21(DE3)pLysS	17 ℃	20 h
T83S	BL21(DE3)pLysS	17 ℃	20 h
T83L	*n/a*	*n/a*	*n/a*
N85Q	BL21(DE3)RIL	25 ℃	20 h
N85F	BL21(DE3)pLysS	17 ℃	20 h
I86L	*n/a*	*n/a*	*n/a*
I86H	BL21(DE3)RIL	25 ℃	20 h
T365S-C52S-C201S-C400S	BL21(DE3)pLysS	17 ℃	20 h
T365C-C52S-C201S-C400S	BL21(DE3)pLysS	17 ℃	20 h
D47E	BL21(DE3)pLysS	17 ℃	20 h
D47S	BL21(DE3)pLysS	17 ℃	20 h
M309L	*n/a*	*n/a*	*n/a*
M309W	BL21(DE3)RIL	17 ℃	20 h

Induction of protein production of each $ALAS_{Rc}$ variant was carried out with 200 µM IPTG. As an example, the SDS-PAGEs in Fig. 21 show the results from recombinant protein production for $ALAS_{Rc}$-D47E and the fourfold $ALAS_{Rc}$ variant T365S-C52S-C201S-C400S. The SDS gels for all generated $ALAS_{Rc}$ variants showed similar results like these two mutants (Fig. 21) and the wild-type $ALAS_{Rc}$ (Fig. 17).

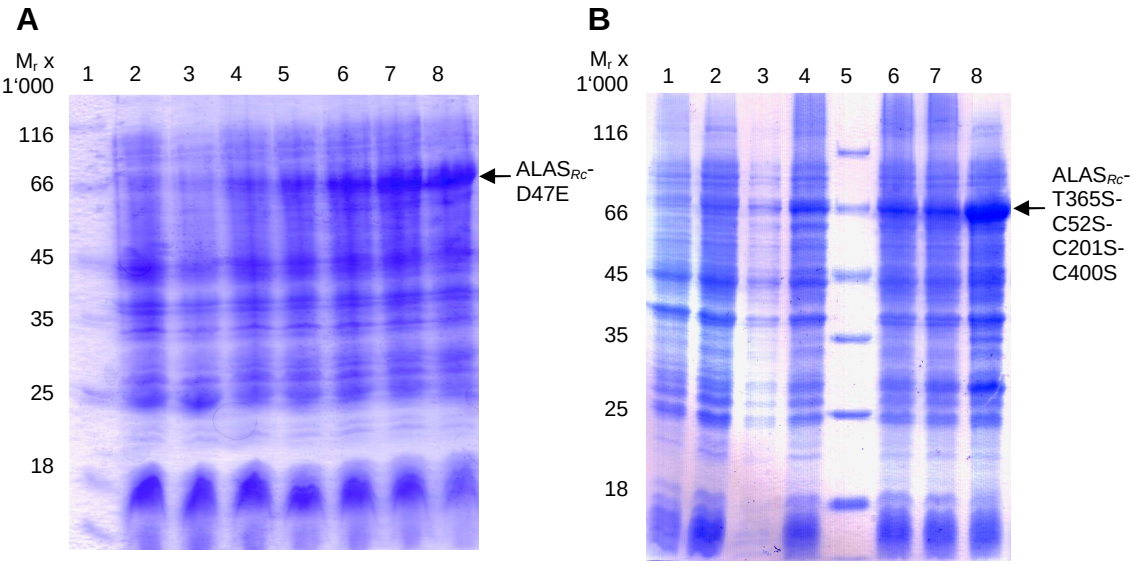

Fig. 21: Recombinant protein production studies for the $ALAS_{Rc}$ variants D47E and T365S-C52S-C201S-C400S.
Cell free extracts were loaded onto a 12 % SDS-PAGE. Proteins were separated and afterwards visualized by staining with Instant*Blue*™. The SDS-PAGEs show recombinant protein production of p*Rc*-A-D47E and p*Rc*-A-T365S-C52S-C201S-C400S in BL21(DE3)pLysS at 25 °C. **A**: D47E variant; lane 1: molecular weight marker; lane 2: before induction of gene expression using IPTG; lane 3: 1 h after induction; lane 4: 2 h after induction; lane 5: 3 h after induction; lane 6: 4 h after induction; lane 7: 5 h after induction; lane 8: 20 h after induction. **B**: T365S-C52S-C201S-C400S; lane 1: before induction; lane 2: 1 h after induction of gene expression using IPTG; lane 3: 2 h after induction; lane 4: 3 h after induction; lane 5: molecular weight marker; lane 6: 4 h after induction; lane 7: 5 h after induction; lane 8: 20 h after induction.

The observed dominant protein with a relative molecular mass of approximately M_r = 66'000 (Fig. 21A: lanes 5 - 8; Fig. 21B: lanes 6 - 8) was in good agreement with the calculated relative molecular mass of the $ALAS_{Rc}$-GST-fusion protein of M_r = 68'575. Astner and coworkers (Astner, 2007) mentioned that only the $ALAS_{Rc}$-C400S enzyme was stable enough for protein production. With our results (Fig. 21B) in protein production studies for the $ALAS_{Rc}$-T365S-C52S-C201S-C400S variant we demonstrated that this fourfold mutant $ALAS_{Rc}$ enzyme was also stable and suited for protein production. This indicated that

the amino acid exchanges of C52 and C201 did not have a notable effect on protein folding.

3.5.1 Purification of ALAS$_{Rc}$ Variants *via* GST Column Chromatography

Analogously to the wild-type ALAS$_{Rc}$ affinity column chromatography using GST column chromatography was performed for each of the developed ALAS$_{Rc}$ variants. Fig. 22 shows the obtained results with the example of the ALAS$_{Rc}$-D47S variant. The other generated, produced and purified ALAS$_{Rc}$ variants revealed almost identical behavior.

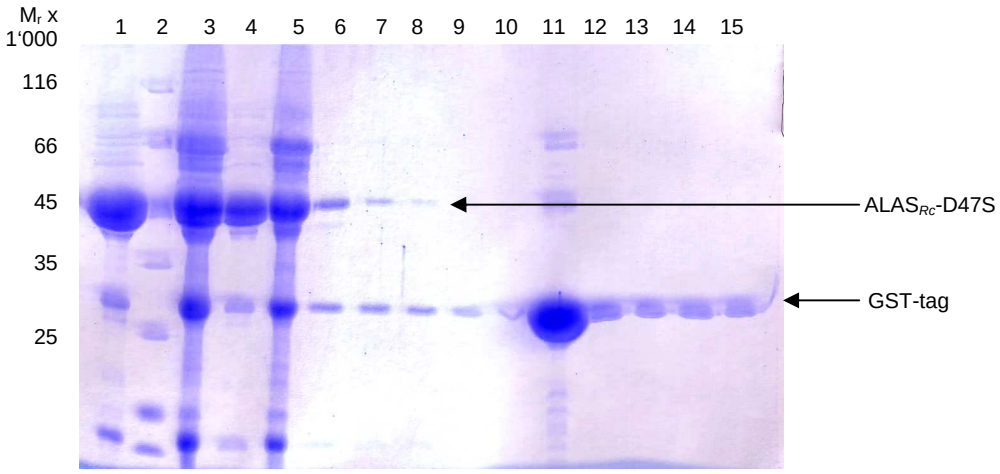

Fig. 22: Purification of the ALAS$_{Rc}$-D47S variant *via* GST column chromatography.
After cell disruption and centrifugation, the soluble fractions were separated by 12 % SDS-PAGE. Proteins were visualized by staining with Instant*Blue*™. The SDS-PAGE shows protein purification of ALAS$_{Rc}$-D47S variant at 4 ℃. Lane 1: supernatant of flow through after 40 h-incubation of PreScission™Protease and protein solution; lane 2: molecular weight marker; lane 3: sediment of flow through after incubation with PreScission™Protease; lane 4: supernatant of first elution fraction after 40 h-incubation with PreScission™Protease; lane 5: sediment of first elution fraction; lane 6: second elution fraction; lane 7: third elution fraction; lane 8: fourth elution fraction; lane 9: fifth elution fraction; lane 10: sixth elution fraction; lane 11: first washing fraction with regeneration buffer; lane 12: second washing fraction with regeneration buffer; lane 13: third washing fraction with regeneration buffer; lane 14: fourth washing fraction with regeneration buffer; lane 15: fifth washing fraction with regeneration buffer.

After this first affinity chromatography we obtained an almost pure protein solution (Fig. 22, lane 4). Protein containing fractions were pooled and concentrated using a VIVASPIN concentrator. We recovered protein solutions with recombinant ALAS$_{Rc}$ enzyme amounts between 1 mg/mL (= 23 µM) and 20 mg/mL (= 460 µM) per 10 liter cell culture depending on the ALAS$_{Rc}$ variant.

Fractions containing $ALAS_{Rc}$ had a yellowish color which is characteristic for PLP-dependent enzymes. Fig. 23 shows a yellowish enzyme solution using the $ALAS_{Rc}$-R21E variant as an example with a concentration of 455 µM (= 19.8 mg/mL). The yellowish color is due to a Schiff'base linkage between the PLP-cofactor and the ε-amino group of an active site lysine residue.

Fig. 23: Yellowish color of purified $ALAS_{Rc}$-R21E solution.
The yellow color of ALAS solutions is characteristic for PLP-dependent enzymes. It was a reliable visible indicator for a first estimation if a purification procedure was successful. The yellowish color is the result of a Schiff'base linkage between the PLP-cofactor and the ε-amino group of an active site lysine residue.

Further purification attempts using ion exchange chromatography on MonoQ and GPC on Superdex-200 failed to improve enzyme purity. The different enzyme solutions could not be concentrated to the same protein amount per mL because of differences in their stability at 4 °C and their stability during the concentrating procedure. Stored at -80 °C protein solutions showed no detectable degradation and were stable for more than several months.

3.6 Experimental Approach

3.6.1 Used Test Systems

3.6.1.1 Approach 1: Steady State Kinetics

Steady state kinetics are useful for the detection of the slowest step in enzyme reactions. In case of mouse ALAS2 it is the conformational change of the enzyme while ALA is released as it was shown by Hunter and coworkers (Hunter and Ferreira, 1999). For the measurement of $ALAS_{Rc}$ steady state kinetics a coupled enzyme assay with the NADH-dependent α-KGD was used. Consequently, the stoichiometry of the overall reaction requires one molecule of

NADH made for every ALA molecule. The Michaelis Menten constant (K_M), the maximal velocity (v_{max}) and the catalytic constant (k_{cat}) were determined from substrate velocity plots by measuring the constant velocity formation of NADH over a substrate range from 0 – 100 mM glycine and 0 – 20 µM succinyl-CoA. The NADH concentration was calculated with the Beer-Lambert law with *A* is the Absorption, *c* is the concentration of NADH [M] *and ε is the* extinction coefficient of NADH [M^1cm^{-1}] (2.7.1.1).

$$\frac{A}{\varepsilon} = c = \frac{0.001}{6560\frac{c}{mol}} = \frac{152\,nM}{min} = \frac{1.52439 * 10^{-7} mol}{min}$$

The concentration of NADH was 1.52439 * 10^{-7} mol/min and necessary for the calculation of the 'real' v_{max}. Steady state kinetic parameters were calculated as described in ‚Material and Methods' (2.7.1.1).

By performing steady state kinetics for the $ALAS_{Rc}$ enzyme and mutant variants we wanted to verify the significance of selected residues in enzyme catalysis.

Tab. 11: Kinetic parameters for mouse ALAS2 and wild-type $ALAS_{Rc}$ as well as generated $ALAS_{Rc}$ variants.

V_{max} was the velocity at maximal substrate concentrations; K_M was the substrate concentration that leads to half-maximal velocity; k_{cat} was the turnover number and k_{cat}/K_M was the catalytic efficiency of the enzyme. The conservative amino acid exchanges were highlighted in light pink. Data for the mouse wild-type ALAS2 enzyme were determined in Tampa, Florida, USA with purified enzyme of Professor Dr. Ferreira's group matching with published values for the murine ALAS2.

nd = non-detectable. Enzyme concentrations varied from 0.2 to 2 µM.

enzyme/ $ALAS_{Rc}$ variant	v_{max} [µM/min]	$K_M^{succinyl\text{-}CoA}$ [µM]	K_M^{gly} [mM]	k_{cat} [s^{-1}]	$k_{cat}/K_M^{succinyl\text{-}CoA}$ [$s^{-1} * µM^{-1}$]	k_{cat}/K_M^{gly} [$s^{-1} * mM^{-1}$]
mouse ALAS2	6.38	2.26	9.89	0.053	0.023	0.005
Wild-type $ALAS_{Rc}$	3.74	0.221	0.273	0.31	1.401	1.136
N54D	*nd*	*nd*	*nd*	*nd*	*nd*	*nd*
N54Q	9.5	0.846	1.7	0.32	0.378	0.188
R21E	*nd*	*nd*	*nd*	*nd*	*nd*	*nd*
R21K	2.62	4.66	13.54	0.021	0.005	0.002
T83S	2.28	0.68	0.034	0.019	0.028	0.559
N85F	18.8	7.46	3.53	1.57	0.21	0.445
N85Q	5.57	11.06	1.16	0.185	0.017	0.159
I86H	0.78	0.43	2.93	0.0065	0.015	0.002
D47E	11.02	0.672	0.362	0.367	0.546	1.014
D47S	2.95	0.066	0.475	0.163	2.485	0.344

The in Tab. 11 listed steady state kinetic parameters will be discussed in detail later, together with the subsequently obtained results on the respective single turnover experiments.

3.6.1.2 Approach 2: Quinonoid Formation and Single Turnover Reactions

In the ALAS reaction mechanism two different quinonoids occur but only the second one is detectable due to the rapid conversion of the first quinonoid (Fig. 24)

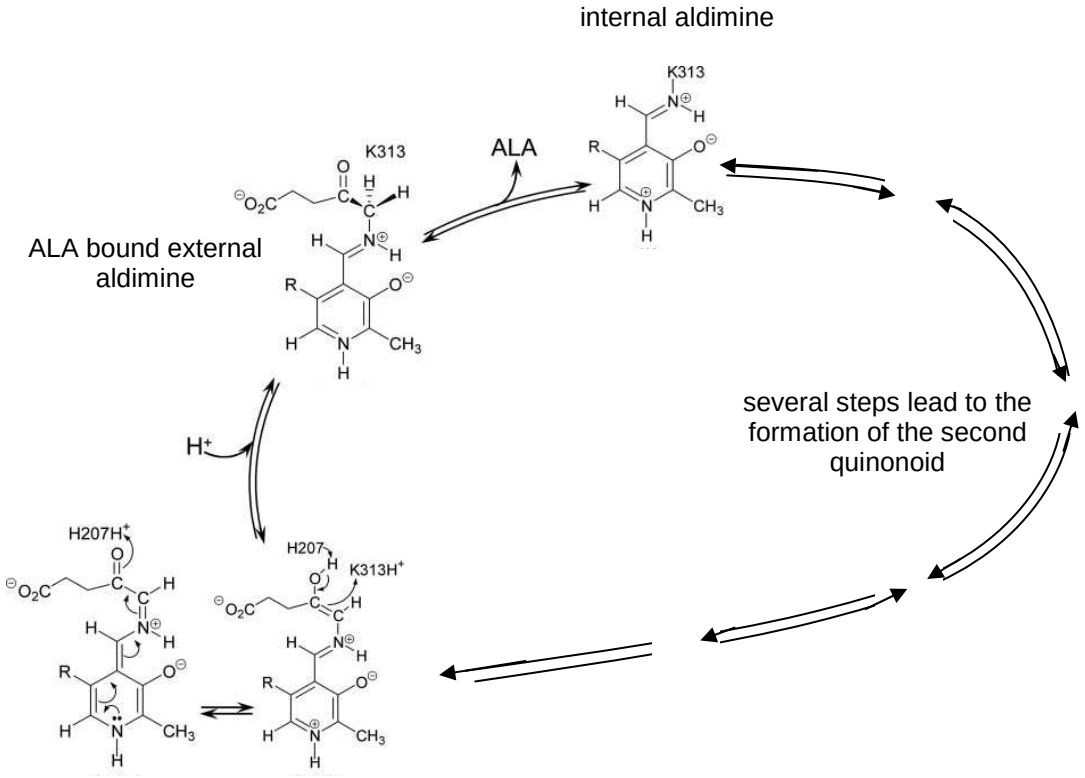

Fig. 24: Extract of the ALAS reaction mechanism for the mouse ALAS2 (adapted from Hunter *et al.*, 2007).
Formation of the second quinonoid, its quenching by protonation and ALA release.

To get a first impression we determined the pH-dependency of the formation of this second quinonoid of $ALAS_{Rc}$. Therefore, the $ALAS_{Rc}$ was spectroscopically analyzed. The experimental set-up was carried out as described in 'Materials and Methods' (2.7.3). The second quinonoid was observed at an absorption at 510 nm solely at a pH of 9.5 (Fig. 25).

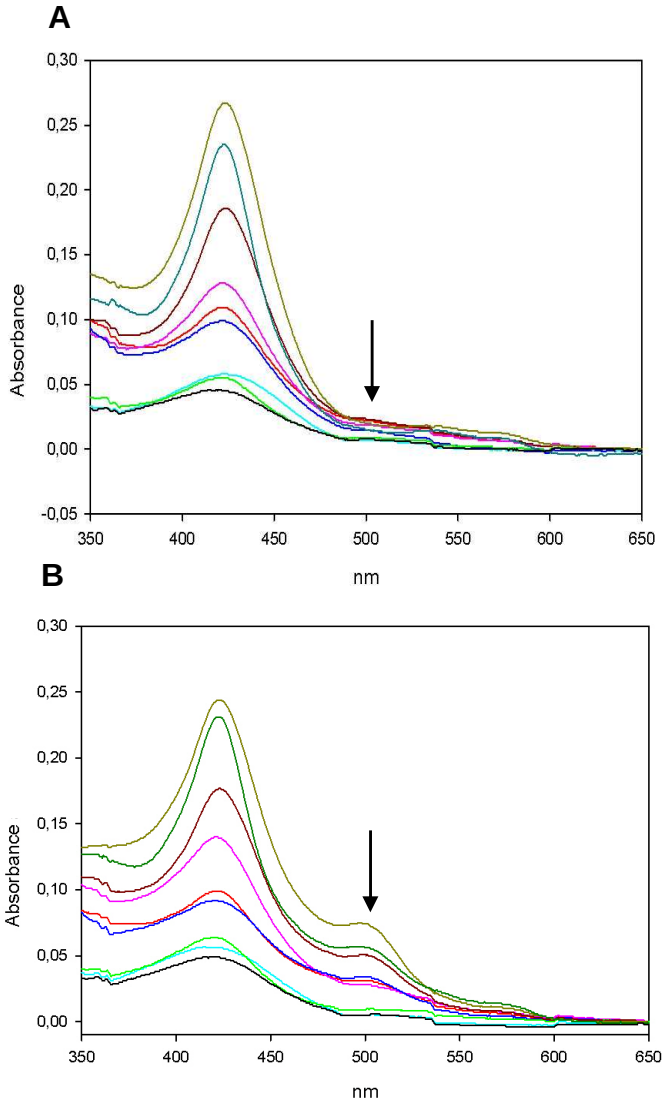

Fig. 25: Formation of the second quinonoid for the wild-type $ALAS_{Rc}$ and various $ALAS_{Rc}$ variants
In the $ALAS_{Rc}$ reaction mechanism two different quinonoid intermediates are generated but only the second one is detectable at 510 nm. Enzyme concentrations were 20 µM in a total volume of 150 µL. Two different pH's were tested.
A. Quinonoid formation measurements at a pH of 7.5. **B.** Quinonoid formation measurements at a pH of 9.5.
Black line: N54D; pink line: N54Q; green line: R21K; blue line: N85F; cyan line: R21E; dark red line: T83S; green-yellow line: D47E; dark green line: wild-type.

Subsequently, fluorescence stopped-flow experiments for detection of single turnover experiments were performed as described in 'Materials and Methods' (2.7.1.2).

The formation of the second quinonoid is a three-step mechanism. The first step (Fig. 26, (I)) is the decarboxylation of the second intermediate 2-amino-3-ketoadipate (= α-amino-β-ketoadipate) to form the second quinonoid (Q_f with k_1). The decay occurs in two steps (Q_{d1} and Q_{d2}): First, quenching of the quinonoid is due to its protonation (Fig. 26, (II)). The product ALA is bound at the active site (Q_{d1} with k_2). Finally, the ALA release (Fig. 26, (III)) occurs and a conformational change of the enzyme takes place (Q_{d2} with k_3). For pre-steady state kinetic experiments 60 µM succinyl-CoA were mixed with buffer in one syringe of the stopped flow apparatus and 30 mM glycine with enzyme

concentrations ranging from 60 µM to 220 µM in the second one. Collection time was 60 seconds, 3'750 scans were collected with 62 scans/sec. Rapid scanning stopped-flow experiments of murine ALAS2 demonstrated that the reaction of the enzyme with glycine and succinyl-CoA resulted in a pre-steady state burst of quinonoid intermediate formation (Hunter and Ferreira, 1999). Thus, a step following binding of substrates and initial quinonoid intermediate formation is rate-determining. At the very beginning of reactions, known as pre-steady state or transient phase kinetics, the enzyme-substrate-complex concentration rises from zero to its steady state value. In contrast to steady state kinetics, in transient phases the rate of the enzyme catalyzed reaction is not defined since the reactants are not used at a one-to-one stoichiometry. Nevertheless, for measurements of such fast reactions including the pre-steady states special high resolution methods and assay setups are necessary. A stopped-flow apparatus was employed where the first milliseconds (ms) of a reaction can be analyzed. In our case, we measured single turnover reactions by using high amounts of glycine to saturate the enzyme, but only a low concentration of succinyl-CoA, so that only one catalytic cycle can occur ('Materials and Methods', 2.7.1.2).

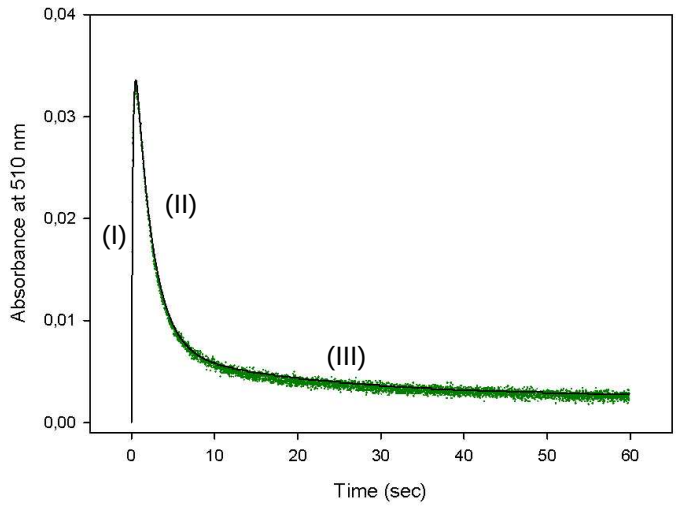

Fig. 26: Single turnover reaction of the ALAS$_{Rc}$ wild-type.
Single turnover reactions were carried out with a stopped flow apparatus. The time [sec] was plotted against the absorbance of the second quinonoid at 510 nm. Stopped flow measurements of second quinonoid formation, quenching and ALA release The first observable step is quinonoid formation (I), the decay occurs in two steps: quenching of the quinonoid (II) and ALA release (III). Green line: raw date; black line: fitted curve for a three-step reaction.

Fig. 26 shows the typical single turnover reaction using the wild-type ALAS$_{Rc}$ as example. After initiation of the reaction there exists an initial burst of second quinonoid formation, *i.e.* the assembly of enzyme-substrate-complexes.

3.6.2 Kinetics of Wild-type ALAS$_{Rc}$

The only available crystal structure for ALAS is for the enzyme from *R. capsulatus*. However, in contrast to the detailed structural picture available, almost nothing is known about the kinetic characteristics of the enzyme. For the wild-type ALAS$_{Rc}$ we expected a reaction mechanism with a similar kinetic behavior as observed for other well characterized ALAS enzymes.

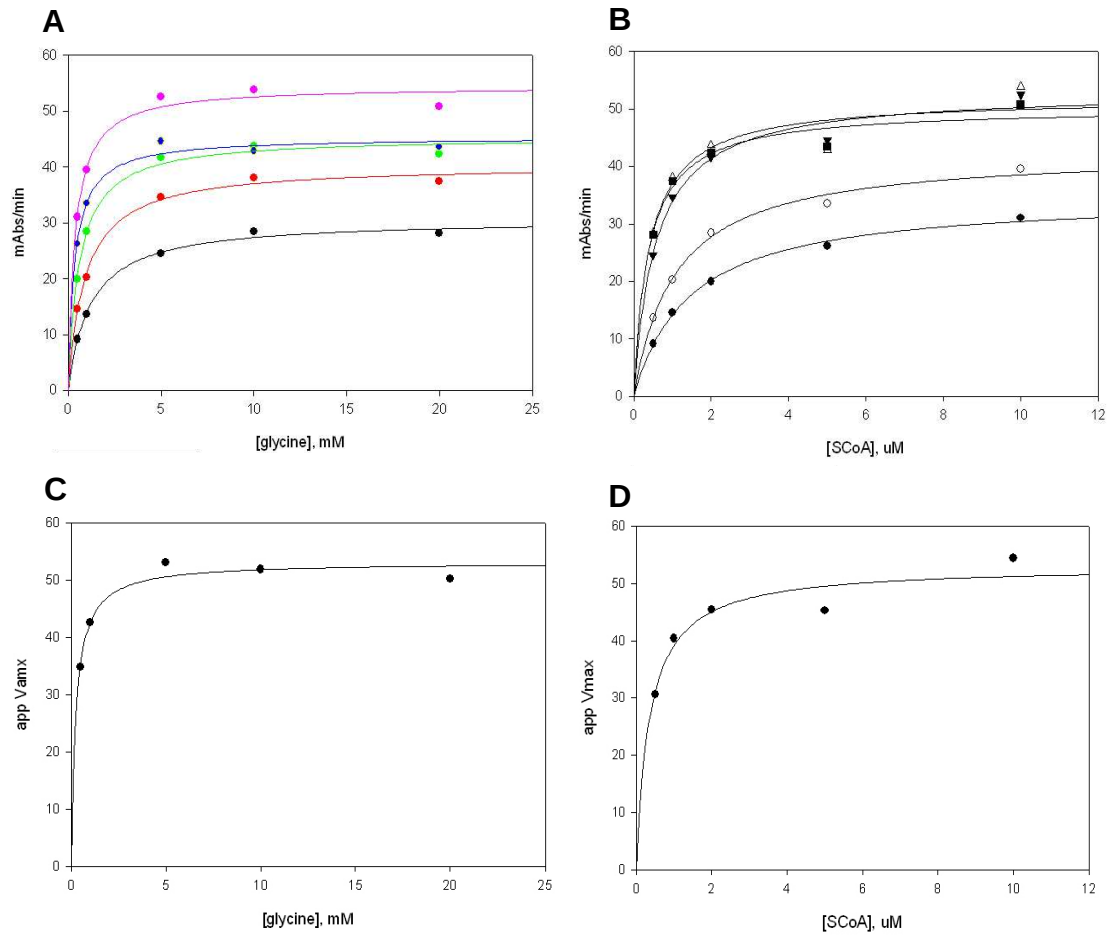

Fig. 27: Steady state kinetics of wild-type ALAS$_{Rc}$.
Steady state kinetics were determined with five different glycine and five different succinyl-CoA concentrations. Enzyme concentration was 0.2 µM in a total volume of 150 µL. **A.** Steady state kinetic data for succinyl-CoA. Black dots: 0.5 µM succinyl-CoA; red dots: 1 µM succinyl-CoA; green dots: 2 µM succinyl-CoA; blue dots: 5 µM succinyl-CoA; pink dots: 10 µM succinyl-CoA. **B.** Steady state kinetic data for glycine. Black dots: 0.5 mM glycine; white dots: 1 mM glycine; black triangles: 5 mM glycine; white triangles: 10 mM glycine; black squares: 20 mM glycine. **C.** Secondary plot for glycine with glycine concentrations ranging from 0.5 mM to 20 mM glycine. **D.** Secondary plot for succinyl-CoA with succinyl-CoA concentrations ranging from 0.5 µM to 10 µM succinyl-CoA.

Fig. 27 shows steady state kinetic mesaurements of wild-type $ALAS_{Rc}$. From these results the kinetic parameters were calculated (2.7.1.1). We compared these kinetic data for wild-type $ALAS_{Rc}$ with the well kinetically characterized mouse ALAS2 enzyme (Ferreira and coworkers). In Tab. 12 the corresponding kinetic parameters for the wild-type $ALAS_{Rc}$ and for the mouse ALAS2 are summarized.

Tab. 12: Kinetic parameters for mouse wild-type ALAS2 and wild-type $ALAS_{Rc}$.
V_{max} was the velocity at maximal substrate concentrations; K_M was the substrate concentration that leads to half-maximal velocity; k_{cat} was the turnover number and k_{cat}/K_M was the catalytic efficiency of the enzyme.

ALAS enzyme	v_{max} [µM/min]	$K_M^{succinyl\text{-}CoA}$ [µM]	K_M^{gly} [mM]	k_{cat} [s^{-1}]	$k_{cat}/K_M^{succinyl\text{-}CoA}$ [$s^{-1} * µM^{-1}$]	k_{cat}/K_M^{gly} [$s^{-1} * mM^{-1}$]
mouseALAS2	6.38	2.26	9.89	0.053	0.023	0.005
Wild-type $ALAS_{Rc}$	3.74	0.221	0.273	0.31	1.401	1.136

Compared to the mouse enzyme $ALAS_{Rc}$ showed lower K_M values for both substrates. In the literature the K_M's for glycine range from 0.2 mM (*Rhodopseudomonas sphaeroides;* Jordan and Laghai-Newton, 1986) to 51 mM (murine ALAS2; Ferreira and Dailey, 1993b) while the K_M's for succinyl-CoA range from 5 µM (*R. sphaeroides*; Jordan and Laghai-Newton, 1986) to 55 µM (murine ALAS2, Ferreira and Dailey, 1993b). For the wild-type $ALAS_{Rc}$ enzyme we measured a K_M for glycine of 0.273 mM and for succinyl-CoA 0.221 µM. The turnover number k_{cat} was 0.31 * s^{-1} and thus approximately six times higher than for the mouse enzyme. In contrast the v_{max} of wild-type $ALAS_{Rc}$ was two times lower (v_{max} for the wild-type $ALAS_{Rc}$ was 3.74 µM/min and for the mouse enzyme v_{max} was 6.38 µM/min). Furthermore, $k_{cat}/K_M^{succinyl\text{-}CoA}$ for the mouse ALAS2 was 61fold lower than the catalytic efficiency of the *R. capsulatus* enzyme while k_{cat}/K_M^{gly} even was 227fold lower. The k_{cat}/K_M ratio describes enzyme specificity if more than one substrate is available such as in the ALAS reaction mechanism. These values indicated that the murine ALAS2 showed a less high efficiency for both substrates glycine and succinyl-CoA than its bacterial counterpart. Consequently, the turnover number is lower for the mouse enzyme (k_{cat} = 0.053 * s^{-1}) than for *R. capsulatus* (k_{cat} = 0.31 * s^{-1}) indicating that the bacterial ALAS is more specific for its substrates resulting in a more efficient product formation. Although the mouse ALAS2 enzyme needed higher amounts

of glycine and succinyl-CoA to be half-saturated (K_M for glycine was 9.89 mM and K_M for succinyl-CoA was 2.26 µM) the reaction occurred fast, but product release was slow. This phenomenon could be the result of a tighter product binding in the mouse wild-type ALAS2 enzyme. The conclusion is that, although the mouse enzyme showed a faster reaction, the product formation is less efficient. In contrast, the wild-type $ALAS_{Rc}$ enzyme needed low substrate amounts to be half-saturated, but although the reaction is not as fast as the mouse ALAS2 reaction the product binding is more loosely and occurred faster with the bacterial ALAS enzyme.

With the measured kinetic parameters (Tab. 12) we now knew substrate concentrations necessary for the wild-type $ALAS_{Rc}$ single turnover reaction. Getting further impressions of the kinetic behavior of the $ALAS_{Rc}$ enzyme quinonoid formation was determined spectroscopically prior to use fluorescence stopped-flow.

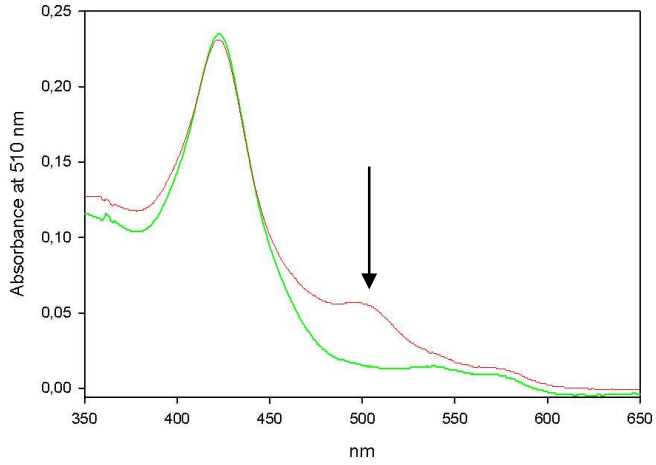

Fig. 28: Formation of the second quinonoid in wild-type $ALAS_{Rc}$ reaction.
The formation of the second quinonoid in the $ALAS_{Rc}$ reaction mechanism is detectable at 510 nm. Enzyme concentration was 20 µM in a total volume of 150 µL. Two buffer solutions with a different pH were tested.
Red line: pH 9.5; green line: pH 7.5.

As outlined before, the wild-type $ALAS_{Rc}$ enzyme showed a distinct quinonoid formation at 510 nm but only at a pH of 9.5 (Fig. 28). At a lower pH less intermediate was detectable. *R. capsulatus* is a bacterium that occurs in fresh water, marine and hypersaline habitats (Stahl *et al.*, 1992), *i.e.* biotopes with more reduced pH values (5 - 7). However, pH-dependent spectroscopy clearly showed that ALA was preferably produced at pH 9.5. An explanation for the detection of the second quinonoid at higher pH's might be provided by a deceleration of the $ALAS_{Rc}$ reaction in more alkaline solutions. This slowdown enabled the detection of the quinonoid at 510 nm. The $ALAS_{Rc}$ was not the only

recombinant produced enzyme which was tested for second quinonoid formation. For the mouse wild-type ALAS2 *e.g.* also could be shown that quinonoid formation is better at a higher pH (Prof. Dr. Gloria C. Ferreira, personal communication). With these results we now could perform fluorescence single turnover reactions for the detection of the second quinonoid. In single turnover reactions for the wild-type $ALAS_{Rc}$ the three steps (I, II, III) of quinonoid formation and decay were clearly visible. They are shown and explained in Fig. 26 on page 78.

Tab. 13: Stopped-flow single turnover rates for $ALAS_{Rc}$ wild-type.
The $ALAS_{Rc}$ reaction was fitted to a three-step reaction with three observable rates. k_1: rate of the decarboxylation step of the 2-amino-3-ketoadipate intermediate, formation of second quinonoid. The decay occurs in two steps. k_2: rate of second quinonoid quenching; k_3: ALA release.

$ALAS_{Rc}$ variant	k_1 [s^{-1}]	k_2 [s^{-1}]	k_3 [s^{-1}]
Wild-type $ALAS_{Rc}$	5.4 ± 1	0.48 ± 0.03	0.0050 ± 0.0009

In Tab. 13 the observable rates of second quinonoid formation and decay for the wild-type $ALAS_{Rc}$ are summarized. The second step of quinonoid decay (Q_{d2}, ALA release and conformational change of the enzyme, with the rate k_3) should have the same value as the turnover number (k_{cat}) of steady state kinetics (Tab. 12). Q_{d2} with its rate k_3 describes the ALA release while k_{cat} is the amount of ALA formed in one second. This means both values describe the same parameter, *i.e.* the amount of formed ALA. The consequence for the $ALAS_{Rc}$ catalysis seems to be that the ALA release is not the rate-limiting step. It should be considered that steady state kinetics were performed at a pH of 7.5 and transient kinetic analysis at a pH of 9.5 due to a better quinonoid observation at higher pH's. For a final conclusion concerning the rate-limiting step of the $ALAS_{Rc}$ reaction it is necessary to peform steady state kinetics as well as transient kinetic analysis at a higher pH. The pH optimum of the coupling enzyme α-KGD ranging from 5.7 for *Bos taurus* (Bunik *et al.*, 2005) to 8.5 for *Aspergillus niger* (Meixner-Monori *et al.*, 1985) should be taken into account. However, we also have to consider the instability of NADH at higher pH's. We tried to perform steady state kinetics at a pH of 9.5 where the buffer already showed a yellow color after 1 h incubation in assay buffer indicating the conversion of NAD^+ into NADH. Therefore, it was not possible to determine

steady state kinetics at a pH of 9.5. For this reason steady state kinetics for all constructed $ALAS_{Rc}$ variants had to be performed at a pH of 7.5 and single turnover reactions at a pH of 9.5.

3.6.3 Kinetics of $ALAS_{Rc}$ Variants Involved in Ketoadipate Formation

In the $ALAS_{Rc}$ reaction cycle three different intermediates are proposed to be generated: 1. first quinonoid, 2. 2-amino-3-ketoadipate, 3. second quinonoid. The ALAS reaction is fast, so that only the third intermediate, *i.e.* second quinonoid is detectable. Kerbarh and coworkers (Kerbarh *et al.*, 2006) provided the first definitive evidence for a β-ketoacid intermediate in the α-oxoamine synthase mechanism of AONS. They were able to trap the reactive β-ketoacid PLP-aldimine formed in the condensation step of the AONS by carrying out the reaction with L-alanine-methylester and pimeloyl-CoA generating the more stable methylester of the putative intermediate. Given that AONS and ALAS belong to the same α-oxoamine synthase family, they also catalyze the same chemical reaction consisting of the unusual cleavage of two α-carbon bonds in a Claisen condensation reaction between amino acids and acyl-CoA thioesters (Kikuchi *et al.*, 1958; Alexeev *et al.*, 1998).

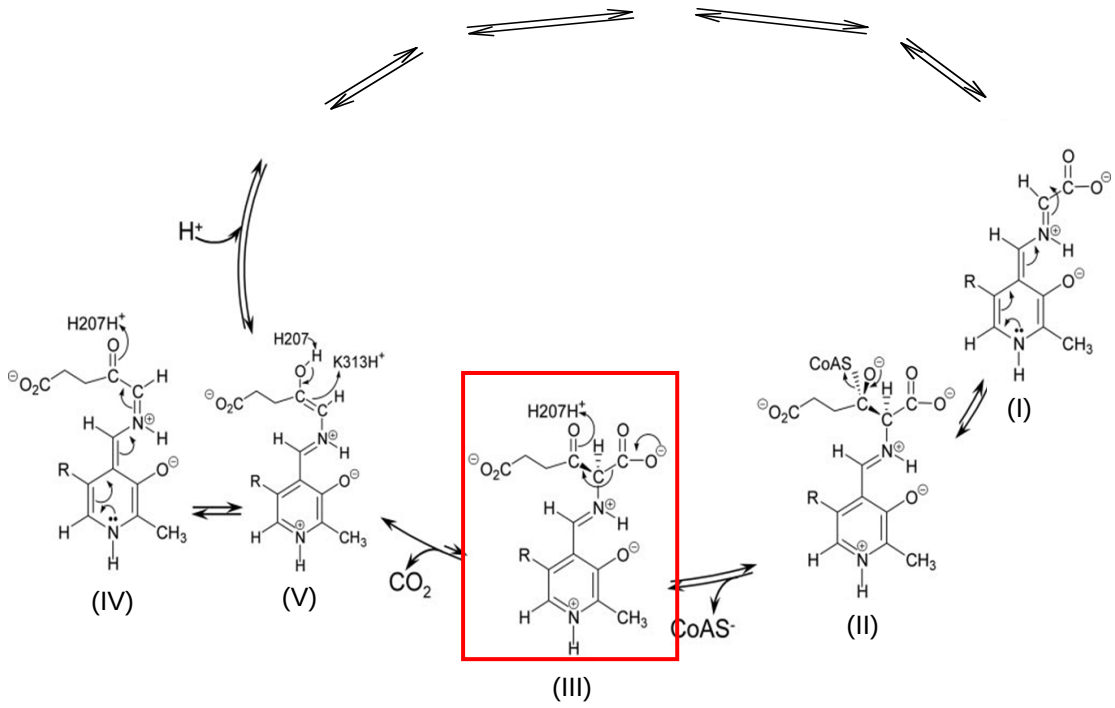

Fig. 29: Extract of the ALAS reaction mechanism for the mouse ALAS2 enzyme (adapted from Hunter *et al.*, 2007).
In the murine ALAS2 reaction mechanism the first quinonoid (I) was formed after condensation of the enzyme-glycine bound structure (external aldimine) with succinyl-CoA. Next, the 2-amino-3-ketoadipate intermediate (III) was formed after $CoAS^-$ release. The second quinonoid (IV) was in equilibrium with its enol (V) and was generated by decarboxylation of the ketoadipate.

From the analysis of the $ALAS_{Rc}$ crystal structure, we deduced that the $ALAS_{Rc}$-N54 variant (corresponds to N119 of murine ALAS2) might be a good target for site-directed mutagenesis. We hypothesized that $ALAS_{Rc}$-N54 (or mouse ALAS2-N119) has a role in stabilizing (or destabilizing) the 2-amino-3-ketoadipate intermediate. To get a first impression of enzyme activity we performed steady state kinetics for both generated $ALAS_{Rc}$-N54 variants (Tab. 14).

Tab. 14: Kinetic parameters for wild-type $ALAS_{Rc}$ and $ALAS_{Rc}$-N54 variants.
V_{max} was the velocity at maximal substrate concentrations; K_M was the substrate concentration that leads to half-maximal velocity; k_{cat} was the turnover number and k_{cat}/K_M was the catalytic efficiency of the enzyme. The conservative amino acid exchanges were highlighted in light pink. *nd = non-detectable.* Enzyme concentrations varied from 0.2 to 2 µM.

$ALAS_{Rc}$ variant	**v_{max} [µM/min]**	**$K_M^{succinyl\text{-}CoA}$ [µM]**	**K_M^{gly} [mM]**	**k_{cat} [s^{-1}]**	**$k_{cat}/K_M^{succinyl\text{-}CoA}$ [$s^{-1} * µM^{-1}$]**	**k_{cat}/K_M^{gly} [$s^{-1} * mM^{-1}$]**
Wild-type $ALAS_{Rc}$	3.74	0.221	0.273	0.31	1.401	1.136
N54D	*nd*	*nd*	*nd*	*nd*	*nd*	*nd*
N54Q	9.5	0.846	1.7	0.32	0.378	0.188

It was understandable that the amino acid exchange from asparagine to aspartic acid (N54D) led to a completely inactive enzyme. Aspartic acid has an additional carboxyl group while asparagine harbors an amino group. The change from a polar to an acidic amino acid seemed to be that dramatic that no enzyme activity was traceable. The conservative $ALAS_{Rc}$ variant with glutamine instead of asparagine (N54Q) yielded a protein with a similar turnover number (k_{cat} = 0.32 * s^{-1}) as the wild-type $ALAS_{Rc}$. Glutamine has a carbon backbone with five carbon atoms while in asparagine the backbone consists of only four carbon atoms. N54 coordinates the PLP-glycine intermediate *via* a hydrogen bond (2.9 Å). If asparagine is replaced by a longer amino acid the distance to the intermediate is reduced. Although the substrate affinities were higher than in the wild-type $ALAS_{Rc}$ enzyme (N54Q K_M^{gly} = 1.7 mM; $K_M^{succinyl\text{-}CoA}$ = 0.846 µM), the amino acid exchange had no drastic effect on enzyme activity. This means that N54 cannot be replaced by other amino acids unless it is of similar chemical nature. The result of these experiments was that the amino acid exchange to glutamine led to a protein with higher K_M values for both substrates but a similar k_{cat}. The conclusion was that a polar amino acid in position 54 is necessary for enzyme catalysis.

The second step in analyzing $ALAS_{Rc}$-N54 acitivity was the measurement of formation of the second quinonoid spectroscopically as well as with fluorescence single turnover experiments.

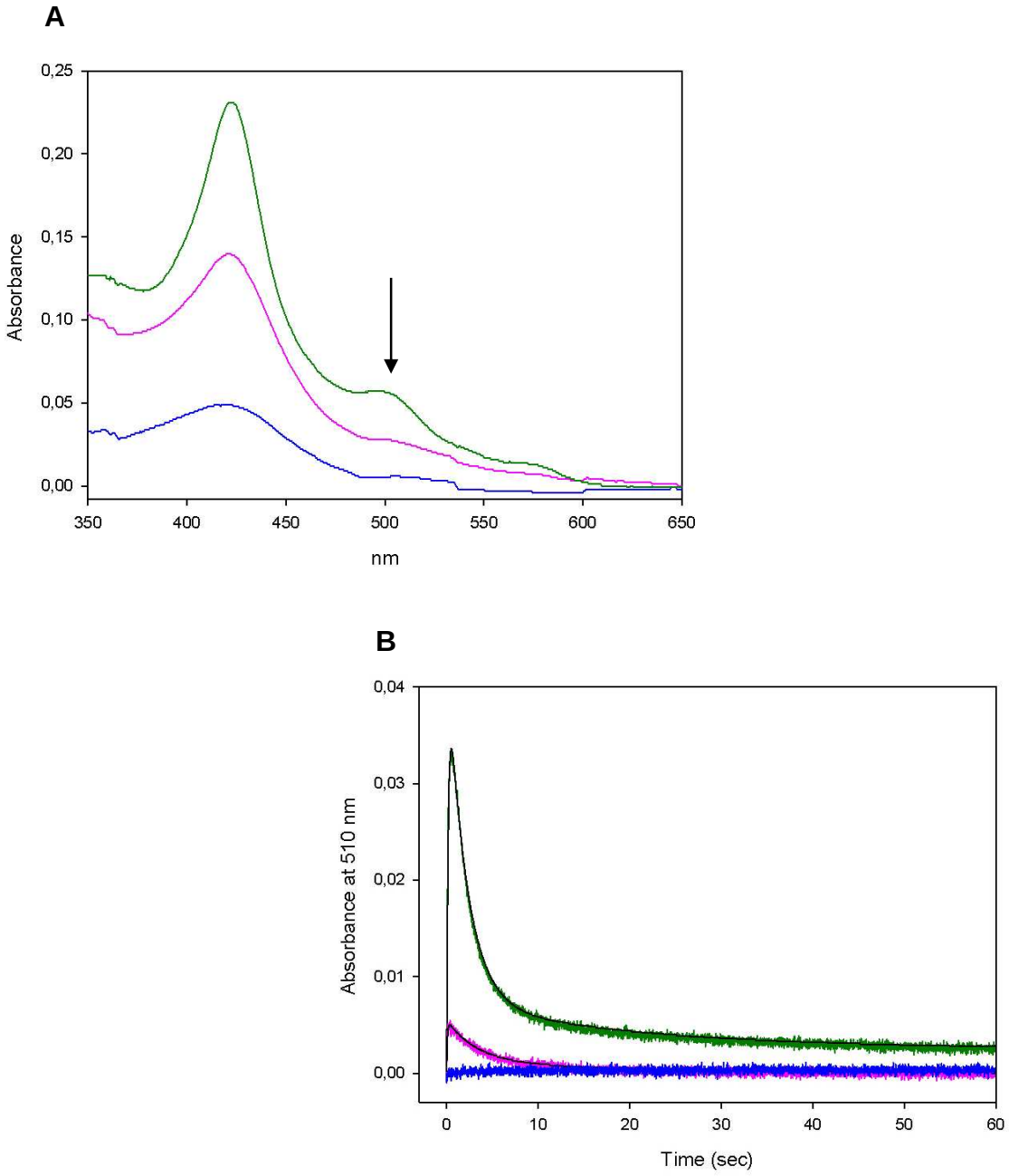

Fig. 30: Detection of the second quinonoid in the reaction mechanism of the ALAS$_{Rc}$ wild-type and ALAS$_{Rc}$-N54 variants.
The second quinonoid is the third intermediate in the ALAS reaction cycle. The first two intermediates are not detectable due to a fast conversion into the second quinonoid which shows an absorption at 510 nm. **A.** Detection of the second quinonoid using absorbance spectroscopy. **B.** Detection of the second quinonoid using a fluorescence stopped-flow apparatus. Raw data and fitting curves (black lines, three-step reaction fits). The first observable step is quinonoid formation, the decay occurs in two steps: quenching of the quinonoid and ALA release.
ALAS$_{Rc}$-N54Q: pink line; ALAS$_{Rc}$-N54D: blue line; wild-type ALAS$_{Rc}$: dark-green line.

In Tab. 15 the corresponding rates of second quinonoid formation and decay are listed. The non-conservative amino acid exchange N54D resulted in an

almost inactive enzyme which did not yield any detectable quinonoid formation (Fig. 30A and Fig. 30B, blue line) at 510 nm.

Tab. 15: Stopped-flow single turnover rates for wild-type $ALAS_{Rc}$ and N54-$ALAS_{Rc}$ variants.
The $ALAS_{Rc}$ reaction was fitted to a three-step reaction with three observable rates. k_1: rate of the decarboxylation step of the 2-amino-3-ketoadipate intermediate; formation of second quinonoid. The decay occurs in two steps. k_2: rate of second quinonoid quenching; k_3: ALA release.
nq:no quinonoid. Conservative amino acid exchanges were highlighted in light pink.

$ALAS_{Rc}$ variant	k_1 [s^{-1}]	k_2 [s^{-1}]	k_3 [s^{-1}]
Wild-type $ALAS_{Rc}$	5.4 ± 1	0.48 ± 0.03	0.0050 ± 0.0009
N54Q	11 ± 2	3 ± 0.3	0.038 ± 0.007
N54D	*nq*	*nq*	*nq*

It was not possible to fit the $ALAS_{Rc}$-N54D reaction to a three step mechanism like the wild-type $ALAS_{Rc}$ or the $ALAS_{Rc}$-N54Q variant. In contrast, the single turnover reaction of the $ALAS_{Rc}$-N54Q variant (Fig. 30A und 30B, pink line) showed fast quinonoid formation. This residue is also necessary for the coordination of glycine *via* a hydrogen bond. Glycine is the first substrate required for the ALA formation and a prerequisite for onset of the reaction process. The reaction is slowed down or interrupted once the amino acid substrate cannot bind in such a manner that the reaction can occur. The conclusion of both approaches is that the N54 residue is important for $ALAS_{Rc}$ activity. To test whether the $ALAS_{Rc}$-N54 variants trapped the second intermediate, 2-amino-3-ketoadipate, we wanted to take a similar experimental approach like Kerbarh and coworkers did. They conducted the AONS reaction using the methylester of L-alanine as a pseudosubstrate which forms a stable quinonoid species after proton abstraction (Kerbarh *et al.*, 2006). Thus, this species also might undergo condensation with pimeloyl-CoA integrating the methylester into β-ketoacid-aldimine complex. Hence, the complex cannot undergo decarboxylation and thus it should accumulate. Previously, amino acid methylester analogs were successfully used in studies of PLP-dependent enzymes (Hayashi *et al.*, 1993; Moore *et al.,* 1997; Olmo *et al.*, 2002; Ikushiro *et al.*, 2004). During the reaction of AONS with the amino acid methylester in the presence of pimeloyl-CoA a new enzyme bound intermediate accumulated which had an absorbance maximum at 454 nm. To verify that the 454 nm

absorption had been due to the β-ketoacid-methylester aldimine complex, a sodium cyanoborohydride reduction was carried out to reduce the unstable imine bond of the complex (Kerbarh *et al.*, 2006). Additionally, in electrospray mass spectrometry experiments of the products a new peak had occurred, which had not corresponded to the peaks of the apo- and holoenzyme, but to AONS monomer plus the reduced β-ketoacid-methylester aldimine. This was the evidence for the β-ketoacid intermediate in the reaction mechanism. A similar approach to identify the β-ketoacid intermediate was undertaken for the ALAS$_{Rc}$-N54 variant using glycine-methylester as amino acid pseudosubstrate.

To get a first impression of the behavior of the wild-type ALAS$_{Rc}$ and the ALAS$_{Rc}$-N54D and –N54Q variants in glycine-methylester binding experiments we measured their absorption changes due to glycine binding capacity. The spectra covered a wavelength range from 200 to 600 nm. At first view the spectra looked similar but zooming in identified differences at 420 nm.

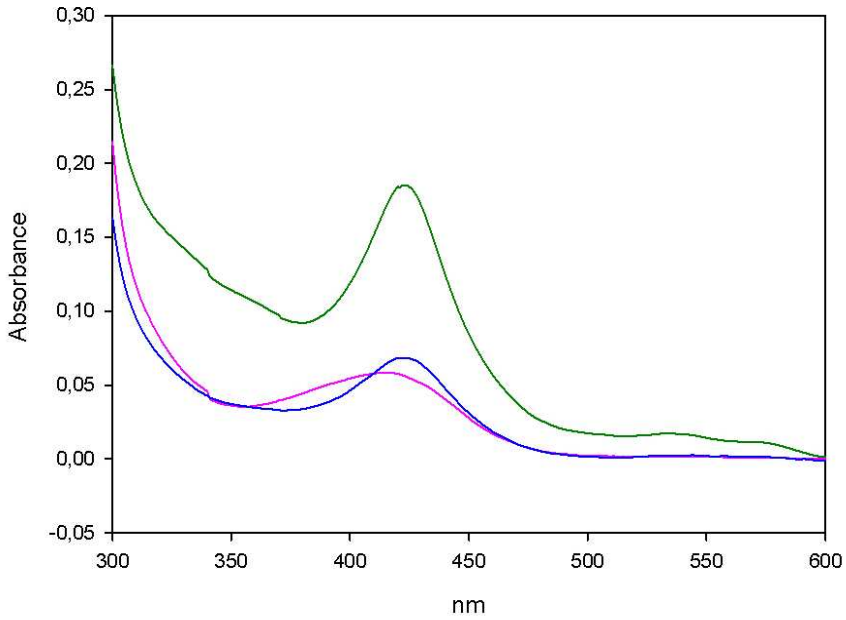

Fig. 31: Absorbance spectra of the wild-type ALAS$_{Rc}$ enzyme and ALAS$_{Rc}$-N54 variants.
For the wild-type ALAS$_{Rc}$ enzyme and the ALAS$_{Rc}$-N54 variants, N54D and N54Q, absorbance spectra were recorded within a wavelength range from 200 to 600 nm.
Green line: wild-type ALAS$_{Rc}$; pink line: N54D; blue line: N54Q.

The absorbance spectrum of the ALAS$_{Rc}$-N54D mutant (Fig. 31, pink line) indicated why this amino acid exchange led to an inactive enzyme. The protein lacked the characteristical peak at 420 nm. Usually, in glycine binding experiments a change in peak height was observable (Fig. 32).

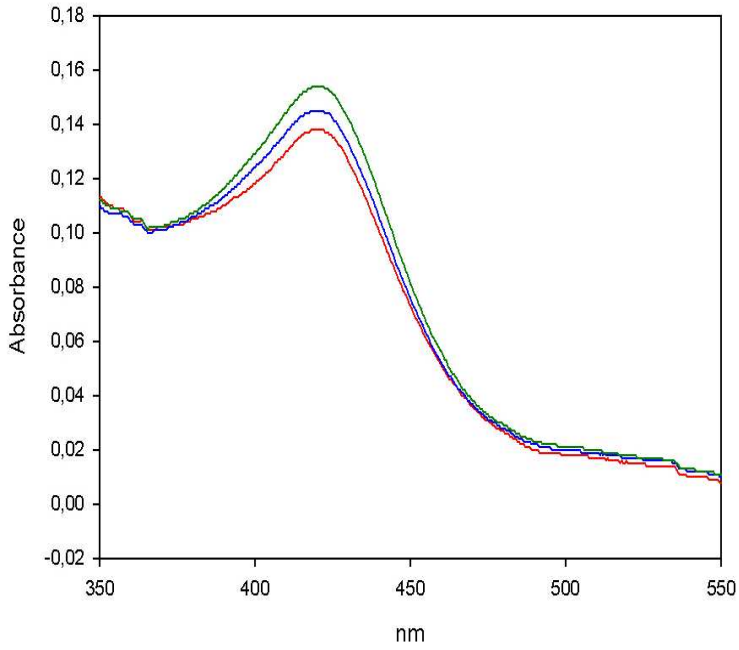

Fig. 32: Glycine binding experiments with the ALAS$_{Rc}$-N54Q variant. Glycine binding experiments were carried out with the ALAS$_{Rc}$-N54Q mutant at 30 °C. Different glycine concentrations were used and changes at 420 nm were recorded.

With these results it became apparent why the ALAS$_{Rc}$-N54D variant was inactive. The amino acid exchange from asparagine to aspartic acid destroyed the glycine binding ability of the enzyme. For this reason experiments with glycine-methylester for trapping the β-ketoadipate only were conducted with the ALAS$_{Rc}$-N54Q variant. In Prof. Dr. Gloria Ferreira's laboratory in Tampa, Florida, USA the reaction with glycine-methylester was conducted and compared to the results given with the corresponding mutation in the mouse ALAS2 enzyme (N119Q). These experiments are under current performance. Furthermore, reactions with *O*-methylglycine had been executed with the focus on the formation and decay of the first generally difficult to detect quinonoid. The *O*-methylglycine pseudosubstrate was used instead of glycine, since the generated methylester of the β-ketoacid-aldimine complex does not decarboxylate to afford the second quinonoid intermediate. Similar to the reaction of the ALAS-glycine complex with succinyl-CoA, the kinetic trace for the reaction of the ALAS-*O*-methylglycine complex with succinyl-CoA was best

described by a three-step process (data not shown). The ALAS reaction was similar to that of the AONS where the second intermediate, 2-amino-3-ketoadipate, was detected. By trapping the first and the second quinonoid we were now able to assume the occurrence of this β-ketoadipate intermediate in the $ALAS_{Rc}$ reaction mechanism.

The ultimate experiment giving the evidence of the occurrence of the β-ketoadipate would be its trapping in a crystal structure of a $ALAS_{Rc}$ variant. Although the $ALAS_{Rc}$-C400S was crystallized earlier (Astner *et al.*, 2005), crystals with substrates incorporated in the active site only were achieved with impregnation experiments of before obtained substrate-less $ALAS_{Rc}$ crystals with substrate solutions. Here, direct enzyme-substrate crystallization experiments were conducted with the N54 variants of the $ALAS_{Rc}$ enzyme as well as with enzyme only. First crystallization tests were executed using same buffers identical to crystallization experiments of $ALAS_{Rc}$ carried out before (Astner *et al.*, 2005; Astner, 2007). However, with these buffers no results were achieved why a variety of different buffers, precipitants and salts provided from Qiagen were tested under aerobic and anaerobic conditions at 17 ℃. The PEGs II Suite, the Cryos Suite, the Classics II Suite and the Classics Lite Suite (Qiagen, Nextal) were tested with enzyme only as well as with enzyme together with both substrates, glycine and succinyl-CoA. We performed crystallization assays with the wild-type $ALAS_{Rc}$ but also with the $ALAS_{Rc}$-N54Q and $ALAS_{Rc}$-N54D mutant enzymes. Crystallization experiments were carried out as described in ‘Materials and Methods’ (2.8.1) with the following enzyme concentrations: wild-type $ALAS_{Rc}$: 6 mg/mL and 9.8 mg/mL; $ALAS_{Rc}$-N54Q: 6.7 mg/mL and 11.25 mg/mL as well as $ALAS_{Rc}$-N54D: 9.6 mg/mL, respectively. If substrates were added they had concentrations between 0.1 µM and 0.25 µM. After six to eight weeks crystals of the cysteine-free wild-type $ALAS_{Rc}$ (9.8 mg/mL) were obtained under following conditions: Classics Suite A11 containing 200 mM ammonium acetate, 100 mM Tris-HCl pH 8.5 and 30 % v/v 2-propanol as well as with Classics Suite B10 containing 100 mM Hepes pH 7.5 and 70 % v/v 2-methyl-2,4-pentandiol under aerobic atmosphere. Further crystals were observed in Classics Suite B11 containing 100 mM Tris pH 8.5

and 25 % v/v tert-Butanol. X-ray diffractions were performed at the HZI (Helmholzzentrum für Infektionsforschung, Braunschweig, Stöckheim, Germany) with crystals grown in Classics Suite A11 and B10 due to low dimensions of the other achieved crystals. After fishing crystals were frozen in liquid nitrogen. Unfortunately, the crystals (Fig. 33) diffracted poorly. All crystallization attempts are still routinely screened to obtained better diffracting $ALAS_{Rc}$ crystals.

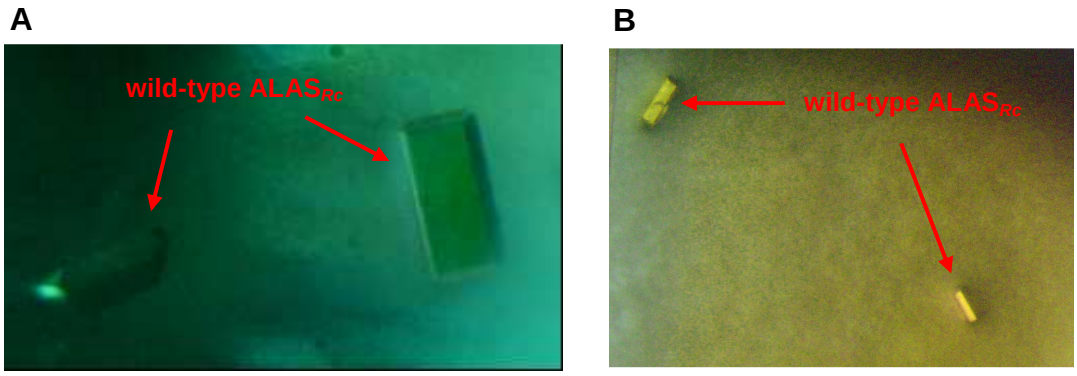

Fig. 33: Cysteine-less wild-type $ALAS_{Rc}$ crystals under aerobic conditions.
Wild-type $ALAS_{Rc}$ crystals were achieved within conditions A11, B10 and B11 of Classics Suite (Qiagen) after approximately five to eight weeks and aerobic conditions at 17 °C. **A.** Achieved wild-type $ALAS_{Rc}$ crystals in Classics Suite condition A11. **B.** Acieved wild-type $ALAS_{Rc}$ crystals in Classics Suite condition B10. Unfortunately, X-ray diffraction revealed poor diffraction.

3.6.4 Kinetics of $ALAS_{Rc}$ Variants Involved in Substrate Recognition

The $ALAS_{Rc}$ enzyme utilizes two different substrates for the formation of its product ALA. On the basis of the solved crystal structure several residues were suggested to be involved in substrate recognition and coordination. With the possibility of measuring enzyme kinetics we wanted to functionally prove these structural assumptions. Fig. 8 of the introduction shows that R21 forms a salt bridge to to the carboxylate group of succinyl-CoA while T83, N85 and I86 coordinate this group *via* hydrogen bonds. After generating $ALAS_{Rc}$ variants of the residues R21, T83, N85 and I86 we performed steady state kinetics for the determination of their activities and kinetic parameters. Fig. 34 shows steady state kinetics with the example of the $ALAS_{Rc}$-N85F variant. The steady state kinetics for all other $ALAS_{Rc}$ variants were performed analogously and looked similar to the steady state kinetics for the $ALAS_{Rc}$-N85F variant.

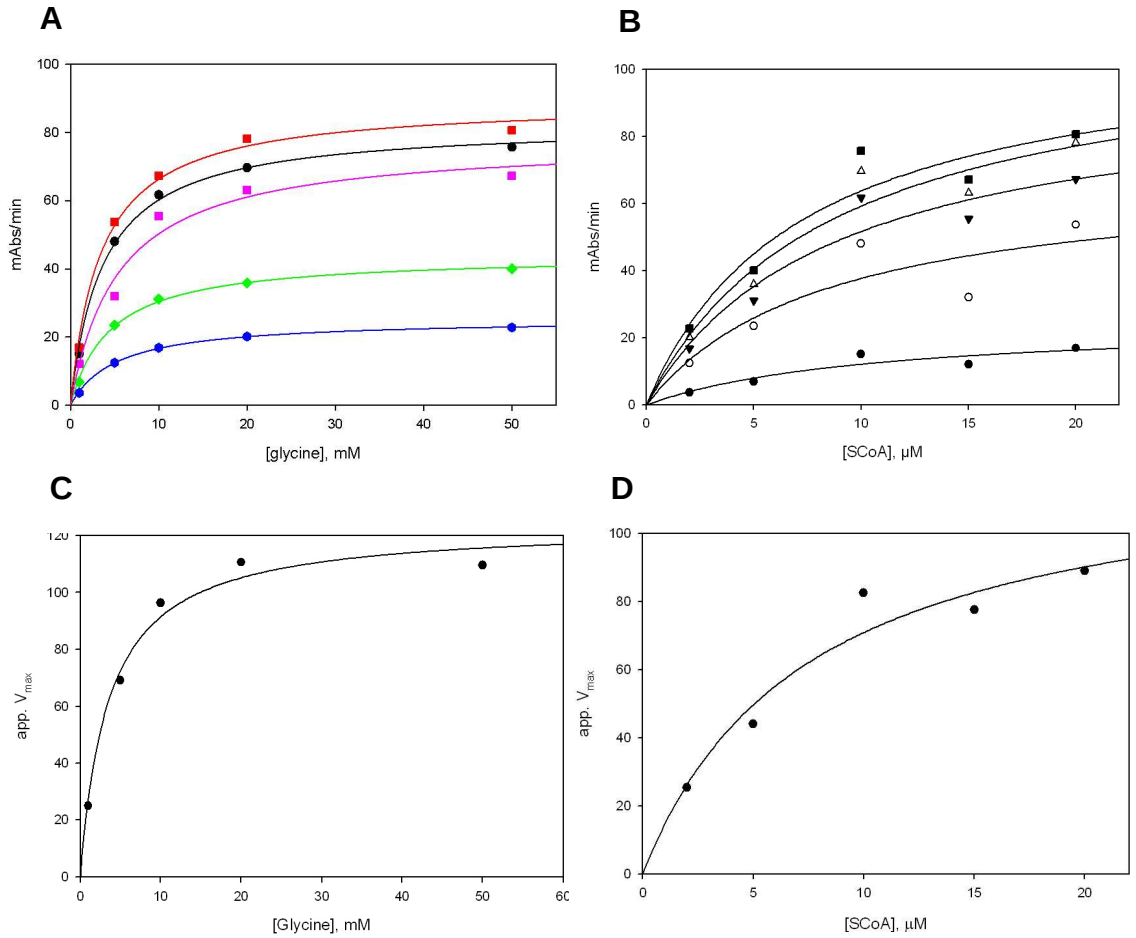

Fig. 34: Steady state kinetics of the ALAS$_{Rc}$-N85F variant.
Steady state kinetics were determined with five different glycine and five different succinyl-CoA concentrations. Enzyme concentration was 0.2 µM in a total volume of 150 µL.
A. Steady state kinetic data for succinyl-CoA. blue dots: 2 µM succinyl-CoA; green dots: 5 µM succinyl-CoA; pink dots: 10 µM succinyl-CoA; black dots: 15 µM succinyl-CoA; red dots: 20 µM succinyl-CoA. **B.** Steady state kinetic data for glycine. Black dots: 1 mM glycine; dots: 5 mM glycine; black triangles: 10 mM glycine; triangles: 20 mM glycine; black squares: 50 mM glycine. **C.** Secondary plot for glycine with glycine concentrations ranging from 1 mM to 50 mM glycine. **D.** Secondary plot for succinyl-CoA with succinyl-CoA concentrations ranging from 2 µM to 20 µM succinyl-CoA.

The achieved kinetic constants, v_{max}, k_{cat} and K_M values for both substrates, respectively, are summarized in Tab. 16 as well as the catalytic efficiencies for succinyl-CoA and glycine ($k_{cat}/K_M^{succinyl\text{-}CoA}$ and k_{cat}/K_M^{gly}).

Tab. 16: Kinetic parameters for wild-type $ALAS_{Rc}$ and $ALAS_{Rc}$ variants involved in substrate recognition and coordination.
V_{max} was the velocity at maximal substrate concentrations; K_M was the substrate concentration that leads to half-maximal velocity; k_{cat} was the turnover number and k_{cat}/K_M was the catalytic efficiency of the enzyme. The conservative amino acid exchanges were highlighted in light pink. *nd = non-detectable.* Enzyme concentrations varied from 0.2 to 2 µM.

$ALAS_{Rc}$ variant	v_{max} [µM/min]	$K_M^{succinyl\text{-}CoA}$ [µM]	K_M^{gly} [mM]	k_{cat} [s^{-1}]	$k_{cat}/K_M^{succinyl\text{-}CoA}$ [$s^{-1} * µM^{-1}$]	k_{cat}/K_M^{gly} [$s^{-1} * mM^{-1}$]
Wild-type $ALAS_{Rc}$	3.74	0.221	0.273	0.31	1.401	1.136
R21K	2.62	4.66	13.54	0.021	0.005	0.002
R21E	*nd*	*nd*	*nd*	*nd*	*nd*	*nd*
T83S	2.28	0.68	0.034	0.019	0.028	0.559
N85F	18.8	7.46	3.53	1.57	0.21	0.445
N85Q	5.57	11.06	1.16	0.185	0.017	0.159
I86H	0.78	0.43	2.93	0.0065	0.015	0.002

Furthermore, formation of the second quinonoid was detected by absorbance spectroscopy and further with single turnover experiments using fluorescence spectroscopy (Fig. 35).

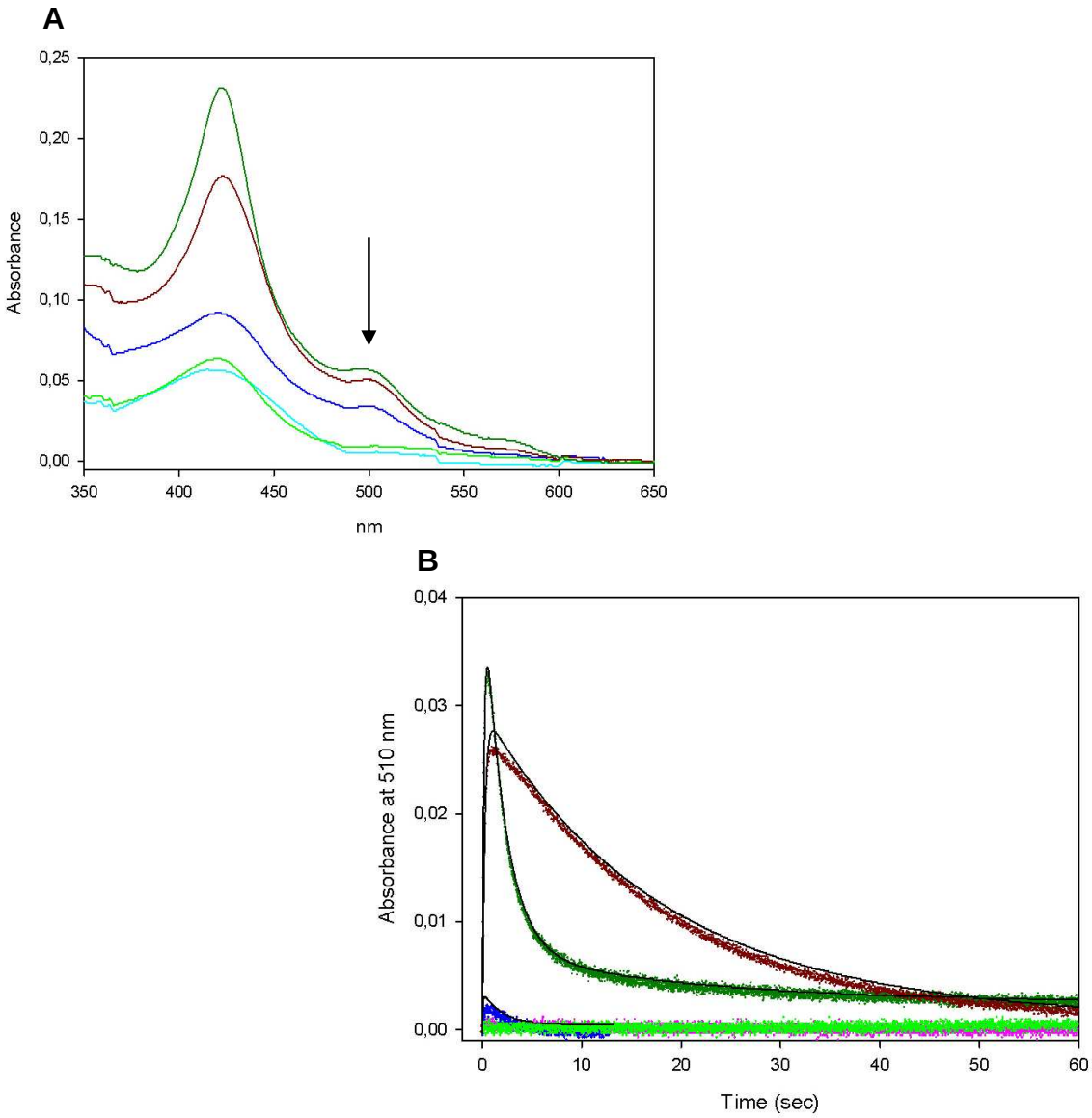

Fig. 35: Detection of the second quinonoid in the reaction mechanism of the ALAS$_{Rc}$ wild-type and ALAS$_{Rc}$ variants involved in substrate recognition and coordination.
The second quinonoid is the third intermediate in the ALAS reaction cycle. The first two intermediates are not detectable due to a fast conversion into the second quinonoid which shows an absorption at 510 nm. **A.** Detection of the second quinonoid using absorbance spectroscopy. **B.** Detection of the second quinonoid using fluorescence spectroscopy. The first observable step is the formation of the second quinonoid; the decay occurs in two steps: quenching of the second quinonoid and ALA release. Raw data and fitting curves (black lines, three step reaction fits).
ALAS$_{Rc}$-R21K: green line; ALAS$_{Rc}$-R21E: cyan line; ALAS$_{Rc}$-T83S: dark red line; ALAS$_{Rc}$-N85F: blue line; wild-type ALAS$_{Rc}$: dark-green line.

In Tab. 17 the corresponding rates of second quinonoid formation and decay are listed.

Tab. 17: Stopped-flow single turnover rates for wild-type $ALAS_{Rc}$ and developed $ALAS_{Rc}$ variants.
The $ALAS_{Rc}$ reaction was fitted to a three-step reaction with three observable rates. k_1: rate of the decarboxylation step of the 2-amino-3-ketoadipate intermediate, quinonoid formation. The decay occurs in two steps. k_2: rate of quinonoid quenching; k_3: ALA release.
nq:no quinonoid. Conservative amino acid exchanges were highlighted in light pink.

$ALAS_{Rc}$ variant	k_1 [s^{-1}]	k_2 [s^{-1}]	k_3 [s^{-1}]
Wild-type $ALAS_{Rc}$	5.4 ± 1	0.48 ± 0.03	0.0050 ± 0.0009
R21K	*nq*	*nq*	*nq*
R21E	*nq*	*nq*	*nq*
T83S	4 ± 0.4	0.057 ± 0.003	0.013 ± 0.001
N85F	14 ± 2	0.49 ± 0.02	0.003 ± 0.002

Arginine 21 is a residue coordinating the carboxylate group of succinyl-CoA *via* a salt bridge (2.8 Å). The non-conservative exchange from arginine to glutamic acid (R21E) led to an inactive enzyme. Arginine possesses a guanidine group ($HN=C(NH_2)$-NH-R) at its carbon backbone instead of a carboxyl group as in glutamic acid. Once, the guanidine group is lacking, the residue is unable to coordinate the carboxylate group of succinyl-CoA correctly which results in an inactive enzyme. The conservative amino acid exchange to lysine (R21K) yielded an enzyme with an approximately fifteen times lower k_{cat} value of 0.021 * s^{-1} than the wild-type $ALAS_{Rc}$ (k_{cat} = 0.31 * s^{-1}). Additionally, high amounts of both substrates were necessary for half saturating the enzyme (K_M^{gly} = 13.54 mM; $K_M^{succinyl\text{-}CoA}$ = 4.66 µM). This amino acid exchange led to an enzyme where the active site and thus the binding of both substrates was negatively affected. Due to single amino group of the lysine residue, the coordination of the carboxylate group of succinyl-CoA becomes difficult. Furthermore, R21 is located close to T365, a residue positioned at the tip of the dynamic active site loop which is responsible for the conformational change between the open and closed enzyme conformation. Once the hydrogen bond triad responsible for the correct succinyl-CoA coordination (s. 'Introduction', Fig. 8) in the active site cannot be formed due to the lysine residue in the $ALAS_{Rc}$-R21K variant, enzyme catalysis is dramatically affected. Thus, R21 is essential in this position since modification even of the length of the carbon backbone yielded an enzyme reduced in its activity. R21 is consequently a residue that is necessary for correct substrate coordination. This $ALAS_{Rc}$-R21E variant contained the non-conservative amino acid exchange of arginine to

glutamate. For the $ALAS_{Rc}$-R21E variant no steady state kinetics could be determined. In single turnover reactions both $ALAS_{Rc}$ variants carrying amino acid exchanges of the R21 residue did not show any detectable second quinonoid formation at 510 nm although steady state kinetic analyses of the $ALAS_{Rc}$-R21K yielded an active enzyme (Tab. 16). Their single turnover curves overlapped each other and could not been fit to a three step mechanism like the wild-type $ALAS_{Rc}$. The undetectable second quinonoid could be explained by a reaction mechanism with a fast occurring decarboxylation step. The consequence is that the protonation of the quinonoid intermediate, the penultimate step in this reaction cycle, could occur immediately. Thus, the ALA release is not the rate-limiting step in the reaction of $ALAS_{Rc}$-R21K rather the saturation of the enzyme with the first substrate glycine. The K_M value for this variant was determined with 13.54 mM and was 50fold higher than the wild-type $ALAS_{Rc}$.

The $ALAS_{Rc}$ residues T83 and I86 from the second monomer coordinate the carboxylate group of succinyl-CoA *via* a hydrogen bond (2.6 Å) and van der Waals interactions, respectively. The conservative amino acid exchange of threonine to serine (T83S) yielded an enzyme with a sixteen fold lower k_{cat} (k_{cat} = 0.019 * s^{-1}). Its side-chain methyl group is in direct van der Waals contact (3.9 Å) with the C_α-atom of the PLP-glycine intermediate (Astner *et al.*, 2005). A reason for the slower enzyme reaction could lie in the decreased binding of the substrate due to the lacking methyl group in serine compared to threonine. Although the $ALAS_{Rc}$-T83S variant only needed small amounts of glycine to be half-saturated (K_M = 0.034 mM), it required a 3fold higher succinyl-CoA concentration (K_M = 0.68 µM) than the wild-type $ALAS_{Rc}$. However, the glycine binding was faster and the binding of succinyl-CoA was decreased resulting in an enzyme with a lower k_{cat}. In single turnover experiments T83S (Fig. 35, dark red line) also revealed a slower reaction than the wild-type $ALAS_{Rc}$. Less tight binding of succinyl-CoA should also lead to a slowed down release of the resulting product. The residue can be designated as super particular concerning its amino acid exchange against other amino acids.

The amino acid substitution of isoleucine to histidine (I86H) also resulted in a less active protein (k_{cat} = 0.0065 * s^{-1}). The I86 residue from the second monomer is responsible for the coordination of the carboxylate group of succinyl-CoA *via* van der Waals interaction. Here, the measured turnover number was so low that the enzyme could be denoted as *de facto* inactive. Histidine lacks the methyl groups necessary for the formation of important van der Waals interaction. Due to small amounts of enzyme soluable we were not able to perform single turnover reactions with this variant.

N85 from the second monomer also coordinates the succinyl-CoA carboxylate group *via* a hydrogen bond with a distance of 3.1 Å (Astner *et al.*, 2005). Unexpectedly, a non-conservative amino acid exchange (N85F; Fig. 35, blue line) led to an enzyme with a faster reaction course compared to wild-type $ALAS_{Rc}$. This might be explained by a less tight binding of the carboxylate group. Usually, a non-conservative amino acid exchange should result in interrupted catalysis due to an incorrect protein folding or an insufficient binding of the required substrates. The conservative exchange from asparagine to glutamine (N85Q) showed a nearly 1.5 fold lower k_{cat} (k_{cat} = 0.185 * s^{-1}) than the wild-type (k_{cat} = 0.31 * s^{-1}). The only difference between asparagine and glutamine is one more carbon atom in the backbone of glutamine. This extension seems to be responsible for a less enzyme affinity for its second substrate succinyl-CoA yielding to a 50fold greater K_M value ($K_M^{succinyl\text{-}CoA}$ = 11.06 µM) for this molecule. The smaller distance between the interacting groups in the $ALAS_{Rc}$-N85Q variant seemed to be accountable for a tighter binding of the second substrate and thus for a retarded catalysis. The non-conservative amino acid exchange to phenylalanine (N85F) yielded a protein with a 5fold increased k_{cat} (k_{cat} = 1.57 * s^{-1}). In this case the substitution from a polar to a non-polar amino acid generated an $ALAS_{Rc}$ enzyme with higher activity, most likely due to a less tight coordination of the carboxylate group of succinyl-CoA. Phenylalanine is a more bulky residue and lacks the coordinating carbon acid amide group (R-$CONH_2$). If the succinyl-CoA carboxylate group was bound less tightly than in the wild-type ALAS enzyme all following steps after succinyl-CoA binding can occur faster. As a result a faster ALA release

was possible and thus the enzyme showed a higher turnover number than the wild-type. In summary, an $ALAS_{Rc}$ enzyme with a higher activity than the naturally occurring enzyme, however, with less affinity for both substrates (N85F: K_M^{gly} = 3.53 mM; $K_M^{succinyl\text{-}CoA}$ = 7.46 µM) was generated. Furthermore, this mutation allows the loop in the active site to move forward and backward very fast. In single turnover experiments and in comparison to wild-type $ALAS_{Rc}$ the reaction with $ALAS_{Rc}$-N85F was over after approximately 10 sec instead of more than 20 sec for wild-type $ALAS_{Rc}$ (Fig. 35B).

In summary, the residues R21, T83 and I86 seemed to be essential for catalysis and their substitution resulted in enzymes less active than the wild-type. In case of N85 a variant was generated that was more active with a non-conservative amino acid exchange than the wild-type $ALAS_{Rc}$ while with a similar amino acid in this position the activity was slowed down. This residue appeared not to be essential for catalytic activity because both substitutions led to an active protein.

The third approach to the question of substrate recognition by $ALAS_{Rc}$ were reactions of the $ALAS_{Rc}$ variants with substrate analogs. In the past, several assumptions have been made and experiments have been executed to determine substrate specificity of ALAS enzymes of different organisms. On the one hand the residue T83 was shown to be responsible for the coordination of the carboxylate group of succinyl-CoA *via* a hydrogen bond and on the other hand the methyl group in its side chain was necessary for the specific recognition of the substrate glycine (Astner, 2007). Shoolingin-Jordan and coworkers (Shoolingin-Jordan *et al.*, 2003) showed that the T83S variant of *R. sphaeroides* ALAS accepted other amino acids as substrate like threonine, serine and alanine. For the wild-type $ALAS_{Rc}$ it was shown that other substrates than glycine are bound in the active site. There, they block the access for the second substrate, succinyl-CoA based on the X-ray crystal structure of wild-type $ALAS_{Rc}$ (Astner, 2007). To prove these presumptions we conducted activity assays (steady state kinetics) with the wild-type $ALAS_{Rc}$ and the $ALAS_{Rc}$-T83S variant with the amino acids L-serine, L-cysteine, L-threonine, L-alanine and D-alanine as alternative substrates instead of glycine (Fig. 36). Generally, all

organisms use L-amino acids in their proteins, but bacteria also utilize some D-amino acids such as D-alanine or D-glutamate as components of their cell walls (Lam *et al.*, 2009).

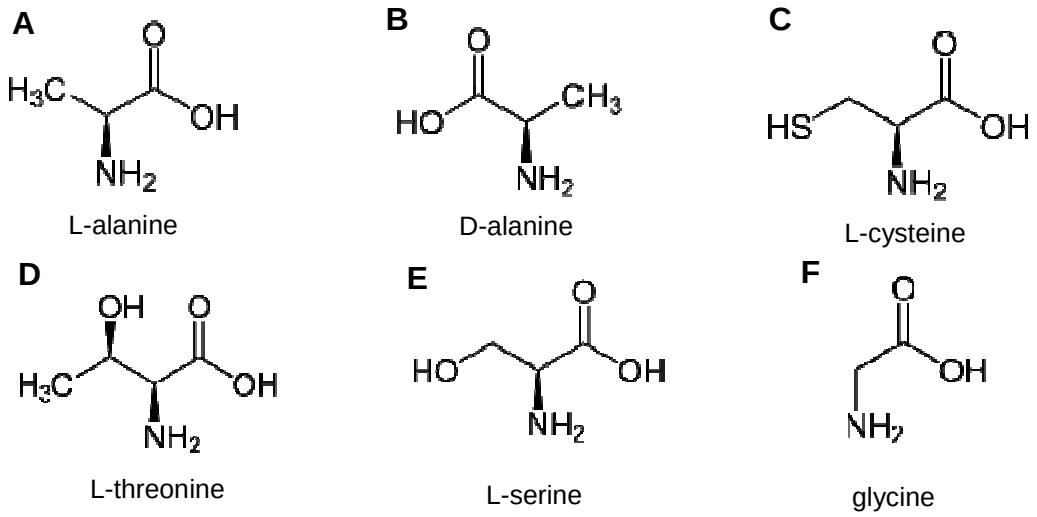

Fig. 36: Structures of amino acids used for substrate specificity assays compared to glycine.
Structures of amino acids used in substrate specificity assays. **A.** L-alanine. **B.** D-alanine. **C.** L-cysteine. **D.** L-threonine. **E.** L-serine. **F.** glycine. All amino acids, instead of glycine which is non-chiral, have a 'D' and an 'L' form (lat: D = *dexter* = 'right', L = *laevus* = 'left'). Usually, amino acids are only useful in their 'L-form', but bacteria also use D-alanine *e.g.* as a component of their cell walls.

Substrate specificity assays revealed that the wild-type $ALAS_{Rc}$ was specific for glycine as first substrate. Even with a high amount of succinyl-CoA (20 µM) no notable activity was observed with the other tested amino acids (data not shown). In contrast the $ALAS_{Rc}$-T83S variant showed enzyme activity with L-alanine, but not with the other tested amino acids.

Tab. 18 shows the determined kinetic parameters for the wild-type $ALAS_{Rc}$ and $ALAS_{Rc}$-T83S variant reaction with glycine as well as with L-alanine. The reaction of the $ALAS_{Rc}$-T83S mutant enzyme with L-alanine showed a 1.5fold higher k_{cat} (k_{cat} = 0.029 * s^{-1}) than the reaction with the physiological substrate glycine although the $K_M^{L\text{-}alanine}$ was much higher ($K_M^{L\text{-}alanine}$ = 0.143 mM). The affinity of the mutant enzyme for succinyl-CoA was approximately the same in both reactions. Thus, the rate-limiting factor seems to be the binding of the first substrate while the condensation with the second one was not affected. The conclusion is that the wild-type $ALAS_{Rc}$ enzyme is specific for glycine.

Furthermore, it was shown that $ALAS_{Rc}$-T83S plays an important role in glycine binding as assumed from Astner and coworkers (Astner, 2007) and shown by our kinetic investigations. Interestingly, L-alanine was also the only alternative substrate used by AONS of *E. coli* (Alexeev *et al.*, 1998). Alanine habors a methyl group lacking in serine. The difference between the two amino acids L-alanine and glycine also lies only in one additional methyl group in L-alanine. The other tested amino acids were most likely too bulky for binding in the active site and hence, avoided binding of the second substrate succinyl-CoA.

Tab. 18 Substrate specificity tested for the $ALAS_{Rc}$-T83S variant with glycine and L-alanine.
Different amino acids were tested as glycine alternative with the wild-type $ALAS_{Rc}$ and the $ALAS_{Rc}$-T83S variant. For T83S only the reaction with L-alanine as substrate showed enzyme activity.

	reaction with L-alanine	**reaction with glycine**
$K_M^{succinyl\text{-}CoA}$ *[µM]*	0.81	0.68
K_M^{gly} *[mM]*	-	0.034
$K_M^{L\text{-}alanine}$ *[µM]*	0.143	-
v_{max} *[µM/min]*	4.47	2.28
k_{cat} *[s^{-1}]*	0.029	0.019
k_{cat}/K_M^{gly} *[$s^{-1} * mM^{-1}$]*	-	0.56
$k_{cat}/K_M^{L\text{-}alanine}$ *[$s^{-1} * mM^{-1}$]*	0.203	-
$k_{cat}/K_M^{succinyl\text{-}CoA}$ *[$s^{-1} * µM^{-1}$]*	0.036	0.028

Furthermore, we performed single turnover reactions with the $ALAS_{Rc}$-T83S mutant as described in ‘Materials and Methods’ (2.7.1.2) with the physiological substrate succinyl-CoA and the amino acid alternative L-alanine. For both approaches 60 µM succinyl-CoA were mixed with buffer in one syringe of the stopped flow apparatus and 30 mM glycine with 70 µM protein in the second one. Collection time was 300 seconds, 3’125 scans were collected with 10 scans/sec. Fig. 37 illustrates the results of these experiments indicating that the reaction with L-alanine took more than 250 sec instead of approximately 50 sec for the reaction with glycine.

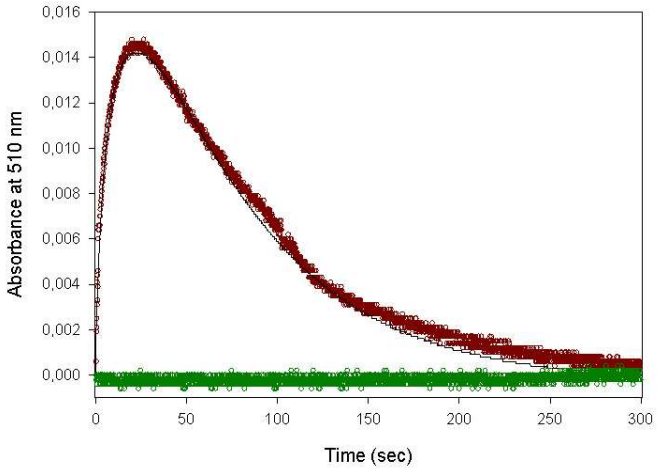

Fig. 37: Single turnover reaction for the wild-type $ALAS_{Rc}$ and the $ALAS_{Rc}$-T83S variant with L-alanine as first substrate.
Single turnover reactions were conducted with a stopped-flow apparatus. L-alanine was added in excess so that only one reaction cycle occurred. The absorbance at 510 nm was plotted against the time in sec. The picture shows the raw data (dotted lines) for wild-type $ALAS_{Rc}$ (dark green line) as well as for the $ALAS_{Rc}$-T83S variant (dark red line) and fitting curve (T83S, straight black line, three step reaction fit).

As steady state kinetics for the wild-type $ALAS_{Rc}$ had revealed, the enzyme did not show any detectable second quinonoid formation with L-alanine as amino acid alternative. In contrast the $ALAS_{Rc}$-T83S variant was able to use L-alanine as first substrate (Fig. 37).

Comparison of the $ALAS_{Rc}$-T83S single turnover reactions using the physiological substrates glycine and succinyl-CoA with L-alanine and succinyl-CoA (Fig. 38) indicated that the reaction occurred slower with L-alanine due to a slower binding of the amino acid in the active site. Both reactions of $ALAS_{Rc}$-T83S with glycine and L-alanine showed identical rates for the quinonoid decay (k_2 and k_3), only the quinonoid formation (k_1) was 15fold lower when L-alanine was used as substrate. Furthermore, the L-alanine-reaction took more than 200 seconds compared to approximately 100 seconds in the glycine reaction (Fig. 38).

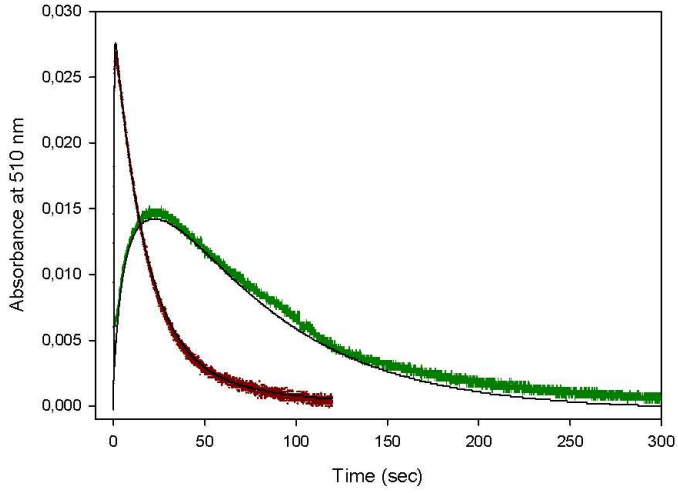

Fig. 38: Stopped flow reaction of $ALAS_{Rc}$-T83S variant with glycine and L-alanine as first substrates.
The absorbance at 510 nm was plotted against the time in seconds.
Green line: $ALAS_{Rc}$-T83S reaction with L-alanine; dark red line: $ALAS_{Rc}$-T83S reaction with glycine; black lines: three step reaction fits for both reactions.

In Tab. 19 the corresponding rates of second quinonoid formation and decay are listed.

Tab. 19: Stopped-flow single turnover rates for wild-type $ALAS_{Rc}$ and the $ALAS_{Rc}$-T83S variant with L-alanine or glycine.
The $ALAS_{Rc}$ reaction was fitted to a three step reaction with three observable rates. k_1: rate of the decarboxylation step of the 2-amino-3-ketoadipate intermediate; formation of second quinonoid. The decay occurs in two steps. k_2: rate of second quinonoid quenching; k_3: ALA release.
nq:no quinonoid

variant	k_1 [s^{-1}]	k_2 [s^{-1}]	k_3 [s^{-1}]
		Reaction with L-alanine	
Wild-type $ALAS_{Rc}$	*nq*	*nq*	*nq*
$ALAS_{Rc}$-T83S	0.26 ± 0.04	0.052 ± 0.005	0.015 ± 0.006
		Reaction with glycine	
Wild-type $ALAS_{Rc}$	5.4 ± 1	0.48 ± 0.03	0.0050 ± 0.0009
$ALAS_{Rc}$-T83S	4 ± 0.4	0.057 ± 0.003	0.013 ± 0.001

The second substrate, succinyl-CoA, binds in a hydrophobic pocket at the entrance of the first channel leading to the active site. Its carboxylate group is coordinated by several residues: T365 and R21 of the first monomer as well as by T83 of the second monomer (Astner, 2007). Shoolingin-Jordan and coworkers (Shoolingin-Jordan *et al.*, 1997) and Lendrihas and coworkers (Lendrihas *et al.*, 2009) tested different acyl-CoA derivatives with ALAS from *R. sphaeroides* and mouse, respectively. They found that acyl-CoA chain lengths and their hydrophobicity influences the position of the carboxylate group and thus ALAS acitivity. Lendrihas and coworkers tested four different acyl-CoA derivatives (octanoyl-CoA, butyryl-CoA, β-hydroxybutyryl-CoA and glutaryl-CoA) with three generated murine ALAS2 variants (R85L, R85K and R85L/T430V). They demonstrated that acyl-CoA substrates of increased hydrophobicity (*e.g.*, octanoyl-CoA and butyryl-CoA) showed greater affinity for the ALAS2 variants with a substituted aliphatic amino acid (R85L and R85L/T430V). They suggested that the chemical characteristics of the CoA-derived tail and the hydrogen-bonding potential of the invariant acyl-CoA binding residues are responsible for reaction specificity. In contrast, the replacement of arginine to lysine (R85K) yielded an enzyme similar to the murine wild-type ALAS2 due to the preservation of the positive charge and hydrogen bonding properties. With

regard to these results we executed substrate specificity assays with two different acyl-CoA derivatives (butyryl-CoA and octanoyl-CoA) with the $ALAS_{Rc}$-R21K variant and the wild-type $ALAS_{Rc}$, respectively. $ALAS_{Rc}$-R21E was not tested due to its catalytic failure. The obtained results are summarized in Tab. 20 and compared to the physiological acyl-CoA substrate succinyl-CoA.

Tab. 20: Comparison of steady state kinetic constants for wild-type $ALAS_{Rc}$ and its variant R21K with acyl-CoA derivatives as second substrate.
Steady state kinetic analysis were performed with two different acyl-CoA derivatives and compared to the kinetic constants for the physiological substrate succinyl-CoA.

	wild-type $ALAS_{Rc}$	$ALAS_{Rc}$-R21K
succinyl-CoA as substrate		
$K_M^{succinyl\text{-}CoA}$ [µM]	0.221	4.66
K_M^{gly} [mM]	0.273	13.54
V_{max} [µM/min]	3.74	2.617
k_{cat} [min^{-1}]	18.6	1.26
$k_{cat}/K_M^{succinyl\text{-}CoA}$ [$min^{-1} * \mu M^{-1}$]	84.16	0.27
k_{cat}/K_M^{gly} [$min^{-1} * mM^{-1}$]	68.13	0.09
butyryl-CoA as substrate		
$K_M^{butyryl\text{-}CoA}$ [µM]	1.213	3.049
K_M^{gly} [mM]	0.483	14.73
V_{max} [µM/min]	10.96	2.334
k_{cat} [min^{-1}]	21.9	1.165
$k_{cat}/K_M^{butyryl\text{-}CoA}$ [$min^{-1} * \mu M^{-1}$]	18.05	0.382
k_{cat}/K_M^{gly} [$min^{-1} * mM^{-1}$]	45.34	0.08
octanoyl-CoA as substrate		
$K_M^{octanoyl\text{-}CoA}$ [µM]	0.954	0.727
K_M^{gly} [mM]	0.124	20.01
V_{max} [µM/min]	5.79	1.5
k_{cat} [min^{-1}]	2.88	0.78
$k_{cat}/K_M^{octanoyl\text{-}CoA}$ [$min^{-1} * \mu M^{-1}$]	3.019	1.073
k_{cat}/K_M^{gly} [$min^{-1} * mM^{-1}$]	23.23	0.039

The results of steady state kinetics revealed enzyme activity independent of the used acyl-CoA substrate. The wild-type $ALAS_{Rc}$ exhibited high values for the reaction with succinyl-CoA: $k_{cat}/K_M^{succinyl\text{-}CoA}$ = 84.16 $min^{-1} * \mu M^{-1}$. The high substrate specificity was still visible with butyryl-CoA ($k_{cat}/K_M^{butyryl\text{-}CoA}$ = 18.05 $min^{-1} * \mu M^{-1}$). The only difference of these two molecules is the terminal

carboxyl group of succinyl-CoA lacking in the butyryl-CoA structure (Fig. 39C). In contrast, substrate specificity was decreased using octanoyl-CoA as second substrate. Here, $k_{cat}/K_M^{octanoyl\text{-}CoA}$ ($k_{cat}/K_M^{octanoyl\text{-}CoA}$ = 3.019 min^{-1} * μM^{-1}) was approximately thirty times lower than with the physiological substrate ($k_{cat}/K_M^{succinyl\text{-}CoA}$ = 84.16 min^{-1} * μM^{-1}). The tail of octanoyl-CoA consists of seven methyl-groups, two more than in succinyl-CoA, but lacks the carboxyl group (Fig. 39B). A consequence of this larger tail is a positive charge due to the electron shifting properties of the methyl groups towards the oxygen atom. The conservative replacement from arginine to lysine retains the positive charge. This positive charge at the active site could be responsible for a decreased binding ability of the positive charged octanoyl-CoA due to a rejecting effect. In contrast to the results of the wild-type $ALAS_{Rc}$, the R21K variant revealed another phenomenon. Here, the substrate specificity increased during utilization of the alternative substrates in the following order: succinyl-CoA; butyryl-CoA and octanoyl-CoA. $k_{cat}/K_M^{succinyl\text{-}CoA}$ were 0.27 min^{-1} * μM^{-1} in contrast to the higher values of $k_{cat}/K_M^{butyryl\text{-}CoA}$ = 0.382 min^{-1} * μM^{-1} for butyryl-CoA and $k_{cat}/K_M^{octanoyl\text{-}CoA}$ = 1.073 min^{-1} * μM^{-1} for octanoyl-CoA, respectively.

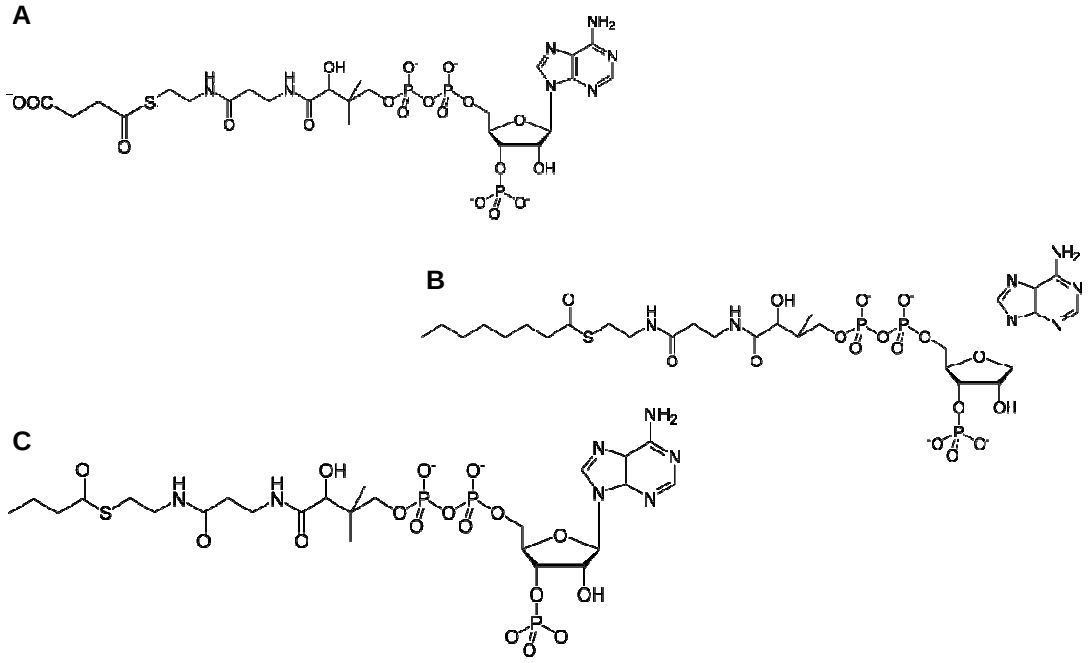

Fig. 39: Structures of succinyl-CoA and its derivatives octanoyl-CoA and butyryl-CoA. The different acyl-CoA molecules differ in their length of the acyl-residue. A similarity is the Coenzyme A consisting of (from right to left) a 3'-phosphorylated adenosine, diphosphate, 2,4-dihydroxy-3,3-dimethyl-butyric acid, β-alanine and cysteamine. **A.** succinyl-CoA. **B.** octanoyl-CoA. **C.** butyryl-CoA.

This phenomenon could be the result of the difference in the amino acid backbone between arginine and lysine which lacks an imine and amino group (Fig. 40).

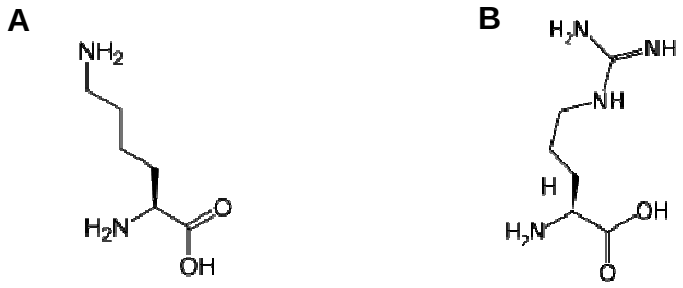

Fig. 40: Structures of the amino acids lysine and arginine.
Both amino acids belong to the group of alkaline amino acids. Arginine has an additional amino and imine group in one of its side chains. **A.** lysine. **B.** arginine.

The consequence of these lacking imine and amino groups is a more positively charged side chain end due to an electron pushing effect of the methyl groups towards the nitrogen atom at the α-C-atom. The carboxylate group of succinyl-CoA is coordinated by one amino group of the arginine residue whereas the lysine residue overall only possesses one amino group in this position. This could be the reason for a reduced binding of the physiological substrate succinyl-CoA by the $ALAS_{Rc}$-R21K variant. Furthermore, due to the lacking carboxylate group in octanoyl-CoA and butyryl-CoA the coordination of the acyl-CoA derivatives was hindered. Interestingly, the highest substrate specificity was measured for octanoyl-CoA which can be explained by the large tail widely extended into the active site so that the reaction can occur. Although the $ALAS_{Rc}$-R21K mutant variant is the conservative amino acid exchange significant difference in substrate coordination as observed. Results indicated that this residue is responsible for the recognition and correct coordination of the succinyl-CoA carboxylate group.

3.6.5 Kinetics of $ALAS_{Rc}$ Variants Involved in Loop Flexibility

In the ALAS reaction cycle two different enzyme conformations occur. In the open conformation the two loops at $ALAS_{Rc}$ amino residues 332 – 348 and

358 – 374 of the C-terminal domain move outwards, widening the active site channel and even opening a second one. In particular T365, located at the tip of second loop ($ALAS_{Rc}$ amino acid residues 358 – 375), moves inward by 3.5 Å during this transition. In the closed conformation T365 is firmly positioned among the residues of the active site stabilized by hydrogen bonds to R21 and by van der Waals interactions to I361 and M190. The functional consequences of the observed two conformations have not been analyzed yet.

Lendrihas and coworkers generated a mouse ALAS2-T430 variant (corresponds to T365 in $ALAS_{Rc}$) to study loop dynamics during the transition from the open to the closed enzyme conformation. The amino acid exchange from threonine to valine (T430V) resulted in a poorly expressed, unstable and proteolytically susceptible enzyme that could never be purified to homogeneity. The T430 amino acid exchange affected protein stability why Lendrihas and coworkers suggested that this residue is not only essential for optimal molecular recognition of succinyl-CoA but also necessary for stable folding. The threonine at position 430 is located at the tip of the active site loop where the major conformational changes seem to occur. Our laboratory in close cooperation with the laboratory of Prof. Dr. Gloria C. Ferreira wanted to functionally address the dynamics of this ALAS loop and corresponding conformational changes of the protein. The $ALAS_{Rc}$ enzyme seems to be a good reporter for these approaches. The threonine at position 365 of the bacterial ALAS enzyme was mutated to cysteine and serine, produced and purified in my work. The cysteine-containing mutant was labeled with a fluorescent tag and used in loop dynamic experiments in the laboratory of Prof. Dr. Gloria C. Ferreira in Tampa, Florida, USA. This mutation only makes sense if no other cysteines are present why we developed a cysteine-free T365C variant. First data were obtained (Ferrreira and coworkers, personal communication). Preliminary results indicated that the binding of the second substrate succinyl-CoA was responsible for a conformational change in the ALAS enzyme (data not shown), thereby initiating a loop movement opening the channel for the active site components.

3.6.6 Kinetics of $ALAS_{Rc}$ Variants Involved in Protein-protein Interaction with the βSCS_{Rc}

The SCS consists of two different subunits. In humans two different isoforms exist: one is specific for adenosine (A-SCS), the other for guanosine (G-SCS). In humans the β-subunit of the A-SCS interacts with the ALAS2 and an interruption in this interaction causes X-linked sideroblastic anemia. The *E. coli* SCS was already crystallized (Wolodko *et al.*; 1984; Fraser *et al.*, 1999). The β-subunits of mammalians and bacteria SCS showed high amino acid sequence identity of 45 %. Therefore, bacterial enzymes of ALAS and SCS can serve as good models for the determination of the ALAS-SCS-interactions. For this approach we designed three different $ALAS_{Rc}$ variants (D47E, D47S, M309W). The D47 residue is localized at the surface of the protein. First, enzyme activities and kinetic parameters were determined by measuring steady state kinetics. The results are summarized in Tab. 21.

Tab. 21: Kinetic parameters for wild-type $ALAS_{Rc}$ and $ALAS_{Rc}$-D47 variants.
V_{max} was the velocity at maximal substrate concentrations; K_M was the substrate concentration that leads to half-maximal velocity; k_{cat} was the turnover number and k_{cat}/K_M was the catalytic efficiency of the enzyme. The conservative amino acid exchanges were highlighted in light pink. Enzyme concentrations varied from 0.2 to 0.3 µM.

variant	v_{max} [µM/min]	$K_M^{succinyl\text{-}CoA}$ [µM]	K_M^{gly} [mM]	k_{cat} [s^{-1}]	$k_{cat}/K_M^{succinyl\text{-}CoA}$ [$s^{-1} * \mu M^{-1}$]	k_{cat}/K_M^{gly} [$s^{-1} * mM^{-1}$]
Wild-type $ALAS_{Rc}$	3.74	0.221	0.273	0.31	1.401	1.136
D47E	11.02	0.672	0.362	0.367	0.546	1.014
D47S	2.95	0.066	0.475	0.163	2.485	0.344

The conservative amino acid exchange of aspartic acid to glutamic acid (D47E) yielded a similar to wild-type $ALAS_{Rc}$ k_{cat} value of 0.367 * s^{-1}. Although the other kinetic parameters of this mutant differed from those of the wild-type, this amino acid exchange had no notable effect on the enzyme activity. Possibly, this conservative amino acid exchange led to a modification of the solvent exposed surface and seemed to be responsible for decreased protein stability while enzyme activity was not affected. This was also observed for the related human ALAS2 D190V mutant (Furuyama *et al.*, 1997). The non-conservative amino acid exchange of this residue, D47S, seemed to have a decreasing effect on enzyme activity with a k_{cat} of approximately half of that of the wild-type $ALAS_{Rc}$

(D47S k_{cat} = 0.163 * s^{-1}). In contrast to aspartic acid, serine harbors a hydroxl group instead of a carboxyl group. Possibly, the additional interaction of D47 with K35 (Astner, 2007) seemed to be changed in that way that the enzyme showed a more reduced affinity for glycine (K_M = 0.475 mM) than the wild-type enzyme. The affinity for succinyl-CoA was much higher with a K_M = 0.066 µM. However, glycine binding was the limitating factor since it has to be bound prior to succinyl-CoA. Thus, if glycine was bound to the active site, succinyl-CoA entering can occur fast but not as fast as in wild-type $ALAS_{Rc}$. Our results indicated that the D47 residue is necessary for optimal enzyme catalysis. Furthermore, the amount of protein of the produced variant M309W was not enough to determine its steady state kinetics. This might be due to decreased protein stability with this non-conservative amino acid exchange. This mutant protein variant could not be analyzed in further experiments.

Subsequently, experiments for the detection of the second quinonoid were performed using fluorescence stopped-flow. The $ALAS_{Rc}$ variants D47E and D47S showed good results in single-turnover reactions (Fig. 41, D47E: light green line, D47S: red line). The formation of the second quinonoid and its decay in two steps were clearly visible and detectable at 510 nm. The residue D47 located at the surface of the $ALAS_{Rc}$ protein should not have an effect on ALAS catalysis. The quinonoid decay of the wild-type $ALAS_{Rc}$ and the D47 variants took approximately 20 sec. In contrast to $ALAS_{Rc}$-D47E the $ALAS_{Rc}$-D47S variant revealed a faster quinonoid formation and decay although steady state kinetics (Tab. 21) showed that this mutant had a lower turnover number (k_{cat} = 0.163 * s^{-1}) than the wild-type and D47E. The consequence for D47S seemed to be a less tight binding of reaction intermediates and its product formation was limited by binding of the first substrate glycine.

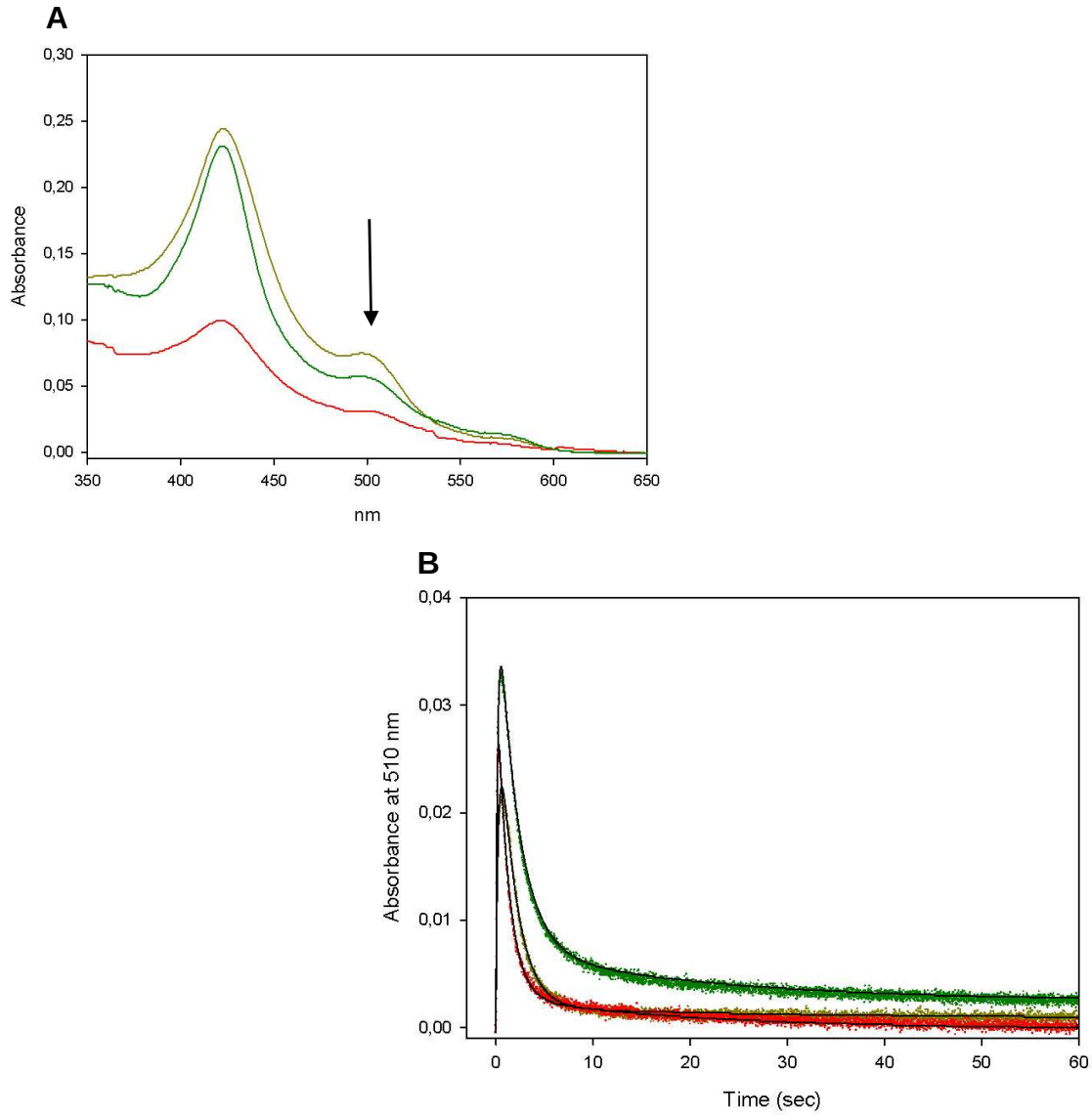

Fig. 41: Detection of the second quinonoid in the reaction mechanism of the ALAS$_{Rc}$ wild-type and the ALAS$_{Rc}$-D47variants.
The second quinonoid is the third intermediate in the ALAS reaction cycle. The first two intermediates are not detectable due to a fast conversion into the second quinonoid. It shows an absorption at 510 nm. **A.** Detection of the second quinonoid using absorbance spectroscopy. **B.** Detection of the second quinonoid using fluorescence spectroscopy. The first observable step is quinonoid formation, the decay occurs in two steps: quenching of the quinonoid and ALA release. Raw data and fitting curves (black lines, three-step reaction fits).
ALAS$_{Rc}$-D47S: red line; ALAS$_{Rc}$-D47E: light green line; wild-type ALAS$_{Rc}$: dark green line.

In Tab. 22 the corresponding rates of second quinonoid formation and decay are listed.

Tab. 22: Stopped-flow single turnover rates for wild-type $ALAS_{Rc}$ and developed $ALAS_{Rc}$-D47 variants.
The $ALAS_{Rc}$ reaction was fitted to a three-step reaction with three observable rates. k_1: rate of the decarboxylation step of the 2-amino-3-ketoadipate intermediate; formation of the second quinonoid. The decay occurs in two steps. k_2: rate of second quinonoid quenching; k_3: ALA release.
Conservative amino acid exchanges were highlighted in light pink.

$ALAS_{Rc}$ variant	k_1 [s^{-1}]	k_2 [s^{-1}]	k_3 [s^{-1}]
Wild-type $ALAS_{Rc}$	5.4 ± 1	0.48 ± 0.03	0.0050 ± 0.0009
D47E	3.4 ± 0.7	0.59 ± 0.06	0.003 ± 0.0005
D47S	10.1 ± 0.2	0.85 ± 0.07	0.048 ± 0.005

Next, for the determination of the $ALAS_{Rc}$-SCS_{Rc}-interaction we amplified the β-subunit of the *R. capsulatus* SCS gene (*sucC) via* PCR for its cloning into the expression vector pGEX-6P-1. The genomic DNA of *R. capsulatus* for amplification of the *sucC* gene was received from the DSMZ (‘Deutsche Sammlung von Mikroorganismen und Zellkulturen GmbH, Braunschweig, Stöckheim). When the project was started the nucleotide sequence for the $βSCS_{Rc}$ was not available in the Pubmed data base (updated September 2010). Hence, the disposable nucleotide sequence of the β-subunit of the *R. sphaeroides* SCS served as template for primer design. After cloning we were able to produce a protein with a relative molecular mass of approximately M_r = 60’000 expected to be the β-subunit of the *R. capsulatus* SCS. As a GST-fusion protein the enzyme should have a relative molecular mass of around M_r = 67’000 which is in good agreement with the achieved results (Fig. 42).

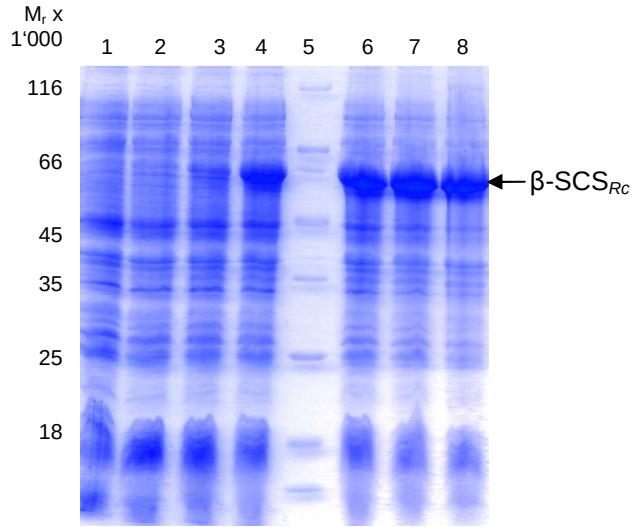

Fig. 42: Recombinant $βSCS_{Rc}$ production studies.
Proteins of cell free extracts were separated by 12 % SDS-PAGE and visualized by staining with Instant*Blue*™. The SDS-PAGE showed recombinant protein production with the p*Rc*-βSCS plasmid in BL21(DE3)RIL at 25 ℃.
Lane 1: before induction of gene expression using IPTG; lane 2: 1 h after induction; lane 3: 2 h after induction; lane 4: 3 h after induction; lane 5: molecular weight marker; lane 6: 4 h after induction; lane 7: 5 h after induction; lane 8: 20 h after induction.

Due to time constraints it was not possible to perform more experiments with this enzyme. However, with the recently submitted nucleotide sequence we were able to align both βSCS sequences of *R. sphaeroides* and *R. capsulatus*, respectively. The alignment showed a high sequence identity and revealed that the designed primers for the *R. sphaeroides* βSCS also matched for the amplification of the corresponding gene in *R. capsulatus*. Next, procedures should be βSCS solubilization tests, overproduction and purification as well as interaction studies together with $ALAS_{Rc}$.

4 SUMMARY

Aminolevulinic acid synthase (ALAS) is the initial enzyme of heme biosynthesis in humans, animals and some bacteria. It catalyzes the condensation of succinyl-CoA and glycine to yield aminolevulinic acid, Coenzyme A and CO_2. To clarify details of its catalytic mechanism thirteen *Rhodobacter capsulatus* ALAS ($ALAS_{Rc}$) variants were generated, purified and kinetically characterized. First, variants of $ALAS_{Rc}$ (N54D, N54Q) for trapping the second intermediate in the ALAS reaction mechanism, 2-amino-3-ketoadipate intermediate, in cysteine-free ALAS background were generated (C52S-C201S-C400S, N54D-C52S-C201S-C400S, N54Q-C52S-C201S-C400S). By performing single turnover experiments we were able to detect the second quinonoid. With the reaction with *O*-methylglycine we experimentally verified for the first time the occurrence of the first quinonoid as a clear indication for the presence of ketoadipate intermediate. Furthermore, crystallization and initial X-ray diffraction experiments were carried out. Second focus was on the binding and supply of the succinyl-CoA substrate. Amino acid residues interacting with the carboxylate group of succinyl-CoA were exchanged (R21E, R21K, T83S, N85F, N85Q, I86H). The results of stopped-flow kinetic analyses indicated that the residues R21, T83, N85 and I86 play a pivotal role in binding of the succinyl-CoA carboxylate group and contribute to a slow ALA release, the rate-limiting step of ALAS catalysis. Furthermore, substrate analog studies revealed the rather strict specificity of wild-type $ALAS_{Rc}$ for its substrates glycine and succinyl-CoA. Enzyme assays with different amino acid based glycine analogs failed to detect significant activity. Interestingly, acyl-CoA derivatives sustained partial ALAS acitivity indicating a less strong discrimination. The contribution of T365-$ALAS_{Rc}$ catalysis localized on the dynamic loop region between the amino acids 358 – 374 of the C-terminal domain was investigated. Mutant enzymes (T365S-C52S-C201S-C400S, T365C-C52S-C201S-C400S) were generated and first results indicate that the conformational change of the ALAS enzyme was due to succinyl-CoA binding. Finally, amino acid residues which were proposed to be responsible for the interaction with the β-subunit of the succinyl-Coenzyme A synthetase (βSCS) were exchanged (D47E, D47S, M309W) and

stand by for interaction studies. In summing crucial steps of ALAS catalysis, investigated with a combined kinetic and structural biology approach using mutant enzyme variants, were elucidated at the molecular level.

5 OUTLOOK

Interaction studies of Aminolevulinic acid synthase and succinyl-Coenzyme A synthetase of *R. capsulatus* variants

Previous studies showed that the interruption of interaction between human ALAS2 and the βSCS led to XLSA. To determine the contribution of D47 and M309 to this essential protein-protein interaction the following experiments should be conducted:

1) Production and purification of the βSCS_{Rc}
2) Interaction studies with generated $ALAS_{Rc}$ variants (D47E, D47S, M309W)

Further characterization of $ALAS_{Rc}$

Although the ALAS reaction cycle has been well characterized, it was not possible to finally proof the occurrence of the central intermediate, 2-amino-3-ketoadipate. Kerbarh and coworkers (Kerbarh *et al.*, 2006) provided the first experimental evidence for a β-ketoacid intermediate in the structurally and functionally related enzyme AONS. For the confirmation of the 2-amino-3-ketoadipate in the $ALAS_{Rc}$ reaction following approaches have to be taken:

1) Reaction of $ALAS_{Rc}$ with glycine-methylester.
2) Crystallization attempts with the generated N54Q and N54D $ALAS_{Rc}$ variants.

6 REFERENCES

Ajioka, R.S., Phillips, J.D., and Kushner, J.P. (2006) Biosynthesis of heme in mammals. *Biochim Biophys Acta* **1763:** 723-36.

Akhtar, M. (1991) Mechanism and stereochemistry of the enzymes involved in the conversion of uroporphyrinogen III into haem. Elsevier, Amsterdam.

Akhtar, M. (1994) The modification of acetate and propionate side chains during the biosynthesis of haem and chlorophylls: mechanistic and stereochemical studies. In *Ciba Foundation Symposium 180 - The Biosynthesis of the Tetrapyrrole Pigments*. Chadwick, D.J. and Ackrill, K. (eds). Chichester, UK: Wiley and Sons, pp. 131-151; discussion 152-135.

Altschul, S.F., Madden, T.L., Schaffer, A.A., Zhang, J., Zhang, Z., Miller, W., and Lipman, D.J. (1997) Gapped BLAST and PSI-BLAST: a new generation of protein database search programs. *Nucleic Acids Res* **25:** 3389-402.

Alexander, F.W., Sandmeier, E., Mehta, P.K., and Christen, P. (1994) Evolutionary relationships among pyridoxal-5'-phosphate-dependent enzymes. Regio-specific *α, β* and *γ* families. *Eur J Biochem* **219**: 953-960.

Alexeev, D., Alexeeva, M., Baxter, R.L., Campopiano, D.J., Webster, S.P., and Sawyer, L. (1998) The Crystal Structure of 8-Amino-7-oxononanoate Synthase: A Bacterial PLP-dependent, Acyl-CoA-condensing Enzyme. *J Mol Biol* **284**: 401-419.

Alexeev, D., Baxter, R.L., Campopiano, D.J., Kerbarh, O., Sawyer, L., Tomczyk, N., Watt, R., and Webster, S.P. (2006) Suicide inhibition of alpha-oxamine synthases: structures of the covalent adducts of 8-amino-7-oxononanoate synthase with trifluoroalanine. *Org Biomol Chem* **4**: 1209-1212.

Al-Karadaghi, S., Hansson, M., Nikonov, S., Jonsson, B., and Hederstedt, L. (1997) Crystal structure of ferrochelatase: the terminal enzyme in heme biosynthesis. *Structure* **5 (11)**: 1501-10.

Andrews, N.C. (1999) Disorders of iron metabolism. N Engl J Med **341**: 1986–1995.

Andrews, N.C. (2000) Iron Metabolism: Iron Deficiency and Iron Overload. *Annu Rev Genomics Hum Genet* **1**: 75-98.

Andrews, N.C. (2008) Forging a field: golden age of iron biology. *Blood* **112**: 219-230.

Astner, I., Schulze, J.O., van den Heuvel, J., Jahn, D., Schubert, W.-D., and Heinz, D.W. (2005) Crystal structure of 5-aminolevulinate synthetase, the first enzyme of heme biosynthesis, and its link to XLSA in humans. *EMBO J* **24**: 3166-3177.

Astner, I. (2007) Klonierung, Reinigung, Kristallisation und Strukturlösung der 5-Aminolävulinsäuresynthase und Untersuchung der Auswirkung und Behandelbarkeit von XLSA-Mutantionen. *Division of Structural Biology, Helmholtz Institut für Infektionsforschung (once: German Research Center for Biotechnology).* Doktorarbeit Braunschweig: Helmholtzzentrum für Infektionsforschung.

Awa, Y., Iwai, N., Ueda, T., Suzuki, K., Asano, S., Yamagishi, J., and Wachi, M. (2005) Isolation of a new antibiotic, alaremycin, structurally related to 5-aminolevulinic acid from *Streptomyces sp.* A012304. *Biosci Biotechnol Biochem* **69 (9)**: 1721-5.

Babilas, P., Landthaler, M., and Szeimies, R.M. (2006) Photodynamic therapy in dermatology. *Eur J Dermatol* **16 (4)**: 340-8.

Bailey, D.L., Wolodko, W.T., and Bridger, W.A. (1993) Cloning, characterization, and expression of the {beta} subunit of pig heart succinyl-CoA synthetase. *Prot Sci* **2**: 1255-1262.

Bailey, D.L., Fraser, M.E., Bridger, W.A., James, M.N.G., and Wolodko, W.T. (1999) A Dimeric Form of *Escherichia coli* Succinyl-CoA Synthetase Produced by Site-Directed Mutagenesis. *J Mol Biol* **285**: 1655-1666.

Banerjee, R., and Ragsdale, S.W. (2003) The many faces of vitamin B12: catalysis by cobalamin-dependent enzymes. *Annu Rev Biochem* **72**: 209-47.

Battersby, A.R., Fookes, C.J.R., Gustafson-Potter, K.E., McDonald, E., and Matcham, G.W.J. (1979) Biosynthesis of the natural porphyrins: experiments on the ring-closure steps and with the hydroxy-analogue of porphobilinogen. *J Chem Soc, Chem Commun:* 316-319.

Battersby, A.R., Fookes, C.J.R., Gustafson-Potter, K.E., McDonald, E. and Matcham, G.W.J., (1982) Biosynthesis of porphyrins and related macrocycles. Part 18. Proof by spectroscopy and synthesis that unrearranged hydroxymethylbilane is the product from deaminase and the substrate for cosynthetase in the biosynthesis of uroporphyrinogen-III. *J Chem Soc, Perkin Trans 1:* 2427-2444.

Beale, S.I., and Castelfranco, P.A. (1973) 14C incorporation from exogeneous compunds into δ-aminolevulinic acid by green cucumber cotyledons. *Biochem Biophys Res Commun* **52:** 143-149.

Beale, S.I., Foley, T., and Dzelzkalns, V. (1981) δ-Aminolevulinic acid synthase from *Euglena gracilis*. *Proc Natl Acad Sci USA* **78 (3)**: 1666-1669.

Beale, S.I. (1999) Enzymes of Chlorophyll biosynthesis. *Photosynthesis Research* **60:** 43-73.

Berg, K., Selbo, P.K., Weyergang, A., Dietze, A., Prasmickaite, L., Bonsted, A., Engesaeter, B.O., Angell-Petersen, E., Warloe, T., Frandsen, N., and Hogset, A. (2005) Porphyrin-related photosensitizers for cancer imaging and therapeutic applications. *J Microsc* **218** (Pt 2): 133-47.

Birney, M., Um, H.D., and Klein, C. (1997) Multiple Levels of Regulation of *Escherichia coli* Succinyl-CoA Synthetase. *Arch Biochem Biophys* **347**: 103-112.

Bishop, D.F., Henderson, A.S., and Astrin, K.H. (1990) Human delta-aminolevulinate synthase: assignment of the housekeeping gene to 3p21 and the erythroid-specific gene to the X chromosome. *Genomics* **7 (2)**: 207-14.

Blume, J.E., and Oseroff, A.R. (2007) Aminolevulinic acid photodynamic therapy for skin cancers. *Dermatol Clin* **25 (1):** 5-14.

Bollivar, D.W., Clauson, C., Lighthall, R., Forbes, S., Kokona, B., Fairman, R., Kundrat, L., and Jaffe, E.K. (2004) *Rhodobacter capsulatus* porphobilinogen synthase, a high activity metal ion independent hexamer. *BMC Biochem* **5**: 17.

Bolt, E.L., Kryszak, L., Zeilstra-Ryalls, J., Shoolingin-Jordan, P.M., and Warren, M.J. (1999) Characterization oft he *Rhodobacter shpaeroides* 5-aminolaevulinic acid synthase isoenzymes, HemA and HemT, isolated from recombinant *Escherichia coli*. *Eur J Biochem* **265**: 290-299.

Bottomley, S.S. (2004) Sideroblastic anaemias. In *Wintrobe's Clinical Hematology*, Greer, J., Foerster, J., Lukens, J.N., Rodgers, G.M. and Paraskevas, R., Glader Bertil (eds), pp 1012–1033. Philadelphia: Lippincott Williams & Wilkins.

Bradford, M.M. (1976). A Rapid and Sensitive Method for the Quantitation of Microgram Quantities of Protein Utilizing the Principle of Protein-Dye Binding. *Analytical Biochemistry* **72:** 248-254.

Breckau, D., Mahlitz, E., Sauerwald, A., Layer, G., and Jahn, D. (2003) Oxygendependent coproporphyrinogen III oxidase (HemF) from *Escherichia coli* is stimulated by manganese. *J Biol Chem* **278**: 46625-46631.

Buck, D., Spencer, M.E., and Guest, J.R. (1985) Primary Structure of the Succinyl-CoA Synthetase of *Escherichia coli*. *Biochem* **24**: 6245-6252.

Buck, D., and Guest, J.R. (1989) Overexpression and site-directed mutagenesis of the succinyl-CoA synthetase of *Escherichia coli* and nucleotide sequence of a gene (*g30*) that is adjacent to the *suc* operon. *Biochem* **260**: 737-747.

Bunik, V.I., Denton, T.T., Xu, H., Thompson, C.M., Cooper, A.J., and Gibson, G.E. (2005) Phosphonate analogues of alpha-ketoglutarate inhibit the activity of the alpha-ketoglutarate dehydrogenase complex isolated from brain and in cultured cells. *Biochem* **44 (31)**: 10552-61.

Burton, G., Fagerness, P.E., Hosozawa, S., Jordan, P.M., and Scott, A.I. (1979) 13C NMR evidence for a new intermediate, pre-uroporphyrinogen, in the enzymic transformation of porphobilinogen into uroporphyrinogens I and III. *J Chem Soc, Chem Commun:* 202-204.

Cassidy, M.A., Crockett, N., Leeper, F.J., and Battersby, A.R. (1996) Biosynthesis of porphyrins and related macrocycles. Part 44. Synthetic and stereochemical studies on the proposed spiro intermediate for biosynthesis of the natural porphyrins. *J Chem Soc Perkin Trans 1:* 384-386.

Cavaleiro, J.A.S., Kenner, G.W., and Smith, K.M. (1974) Pyrroles and related compounds. Part XXXII. Biosynthesis of protoporphyrin-IX from coproporphyrinogen-III. *J Chem Soc, Perkin Trans 1* **10***:* 1188-1194.

Cavallaro, G., Decaria, L., and Rosato, A. (2008) Genome-based analysis of heme biosynthesis and uptake in prokaryotic systems. *J Proteome Res* **7 (11)**: 4946-54.

Chadwick, D.J., and Ackrill, K. (eds.) (1994) The Biosynthesis of Tetrapyrrole Pigments, vol. **180**. Wiley and Sons, Chichester, UK.

Christen, P., and Mehta, P.K. (2001) From cofactor to enzymes. The molecular evolution of pyridoxal-5'-phosphate-dependent enzymes. *Chem Rec* **1**: 436–447.

Corey, E.J., and Sneen, R.A. (1956) Stereoelectronic Control in Enolization-Ketonization Reactions. *J Am Chem Soc* **78**: 6269-6278.

Corrigall, A.V., Siziba, K.B., Maneli, M.H., Shephard, E.G., Ziman, M., Dailey, T.A., Dailey, H.A., Kirsch, R.E., and Meissner, P.N. (1998) Purification of and kinetic studies on a cloned protoporphyrinogen oxidase from the aerobic bacterium *Bacillus subtilis. Arch Biochem Biophys* **358 (2)**: 251-6.

Cotter, P.D., May, A., Li, L., Al-Sabah, A.I., Fitzismons, E.J., Cazzola, M., and Bishop, D.F. (1999) Four New Mutations in the Erythroid-Specific 5-Aminolevulinate Synthase (ALAS2) Gene Causing X-Linked Sideroblastic Anemia: Increased Pyridoxine Responsiveness After Removal of Iron Overload by Phlebotomy and Coinheritance of Hereditary Hemochromatosis. *Blood* **93**: 1757-1769.

Cox, T.C, Bawden, M.J., Abraham, N.G., Bottomley, S.S., May, B.K., Baker, E., Chen, L.Z., and Sutherland, G.R. (1990) Erythroid 5-Aminolevulinate Synthetase Is Located on the X Chromosome. *Am J Hum Genet* **46**: 107-111.

Cox, T.C., Bawden, M.J., Martin, A., and May, B.K. (1991) Human erythroid 5-aminolevulinate synthetase: promoter analysis and identification of an iron-responsive element in the mRNA. *EMBO J* **10 (7)**: 1891-1902.

Cox, T.C., Bottomley, S.S., Wiley, J.S., Bawden, M.J., Matthews, C.S., and May, B.K. (1994) X-linked pyridoxine-responsive Sideroblastic anaemia due to a Thr^{388}-to-Ser substitution in erythroid 5-aminolevulinate synthetase. *N Engl J Med* **330 (10)**: 675-679.

Dailey, H.A., Finnegan, M.G., and Johnson, M.K. (1994) Human Ferrochelatase is an iron sulfur protein. *Biochemistry* **33**: 403-7.

Dailey, H. A. (2002) Terminal steps of haem biosynthesis. *Biochem Soc Trans* **30:** 590-5.

Dailey, H.A., and Dailey, T.A. (1996) Protoporphyrinogen oxidase of *Myxococcus xanthus*. Expression, purification, and characterization of the cloned enzyme. *J Biol Chem* **271 (15)**: 8714-8.

Dailey, T.A., and Dailey, H.A. (1997) Expression, purification, and characteristics of mammalian protoporphyrinogen oxidase. *Methods Enzymol* **281**: 340-9.

Dailey, T.A., and Dailey, H.A. (2002) Identification of [2Fe-2S] clusters in microbial ferrochelatases. *J Bacteriol* **184 (9)**: 2460-4.

Darlison, M.G., Spencer, M.E., and Guest, J.R. (1984) Nucleotide sequence of the sucA gene encoding the 2-oxoglutarate dehydrogenase of Escherichia coli K12. *Eur J Biochem* **141**: 351-359.

Day, A.L., Parsons, B.M., and Dailey, H.A. (1998) Cloning and characterization of *Gallus* and *Xenopus* ferrochelatases: presence of the [2Fe-2S] cluster in nonmammalian ferrochelatase. *Arch Biochem Biophys* **359 (2)**: 160-9.

Drew, P.D., and Ades, I.Z. (1989) Regulation of the stability of chicken embryo liver δ-aminolevulinate synthetase mRNA by hemin. *Biochem Biophys Res Commun* **162 (1)**: 102-107.

Dunathan, H.C. (1966) Conformation And Reaction Specificity In Pyridoxal Phosphate Enzymes. *Proc Natl Acad Sci USA* **55 (4)**: 712-6.

Elder, G.H. (1976). Acquired disorders of haem synthesis. *Essays Med Biochem* **2**: 75-114.

Elder, G.H., Evans, J.O., Jackson, J.R., and Jackson, A.H. (1978) Factors determining the sequence of oxidative decarboxylation of the 2- and 4-propionate substituents of coproporphyrinogen III by coproporphyrinogen oxidase in rat liver. *Biochem J* **169 (1)**: 215-23.

Eliot, A.C., and Kirsch, J.F. (2004) Pyridoxal Phosphate Enzymes: Mechanistic, Structural, and Evolutionary Considerations. *Annu Rev Biochem* **73**: 383-415.

Erskine, P.T., Coates, L., Newbold, R., Brindley, A.A., Stauffer, F., Wood, S.P., Warren, M.J., Cooper, J.B., Shoolingin-Jordan, P.M., and Neier, R. (2001) The X-ray structure of yeast 5-aminolaevulinic acid dehydratase complexed with two diacid inhibitors. *FEBS Lett* **503 (2-3)**: 196-200.

Erskine, P.T., Coates, L., Butler, D., Youell, J.H., Brindley, A.A., Wood, S.P., Warren, M.J., Shoolingin-Jordan, P.M., and Cooper, J.B. (2003) X-ray structure of a putative reaction intermediate of 5-aminolaevulinic acid dehydratase. *Biochem J* **373 (Pt 3)**: 733-8.

Fanica-Gaignier, M., and Clement-Metral, J. (1973a) 5-Aminolevulinic-Acid Synthetase of *Rhodopseudomonas spheroids* Y. Kinetic Mechanism and Inhibition by ATP. *Eur J Biochem* **40**: 19-24.

Fanica-Gaignier, M., and Clement-Metral, J. (1973b) 5-Aminolevulinic-Acid Synthetase of *Rhodopseudomonas spheroids* Y. Purification and Some Properties. *Eur J Biochem* **40**: 13-18.

Fenton, H.J.H. (1894) Oxidation of Tartaric Acid in presence of Iron. *J Chem Soc Trans* **65**: 899-911.

Ferreira, G.C., Neame, P.J., and Dailey, H.A. (1993a) Heme biosynthesis in mammalian systems: Evidence of a Schiff'base linkage between the pyridoxal 5'-phosphate cofactor and a lysine residue in 5-aminolevulinate synthetase. *Protein Sci* **2**: 1959-1965.

Ferreira, G.C., and Dailey, H.A. (1993b) Expression of Mammalian 5-Aminolevulinate Synthase in *Escherichia coli*. *J Biol Chem* **268**: 584-590.

Ferreira, G.C., Vajapey, U., Hafez, O., Hunter, G.A., and Barber, M.J. (1995a) Aminolevulinate synthetase: Lysine 313 is not essential for binding the pyridoxal phosphate cofactor but is essential for catalysis. *Protein Sci* **4**: 1001-1006.

Ferreira, G.C., and Gong, J. (1995b) 5-Aminolevulinate Synthase and the First Step of Heme Biosynthesis. *J Bioenerg Biomembr* **27 (2)**: 151-159.

Ferreira, G.C., and Zhang, J.S. (2002) Mechanism of 5-aminolevulinate synthetase and the role of the protein environment in controlling the cofactor chemistry. *Cell Mol Biol (Noisy-le-grand)* **48 (8)**: 827-33.

Frankenberg, N., Erskine, P.T., Cooper, J.B., Shoolingin-Jordan, P.M., Jahn, D., and Heinz, D.W. (1999a) High resolution crystal structure of a Mg2+-dependent porphobilinogen synthase. *J Mol Biol* **289:** 591-602.

Frankenberg, N., Heinz, D.W., and Jahn, D. (1999b) Production, purification, and characterization of a Mg2+-responsive porphobilinogen synthase from *Pseudomonas aeruginosa*. *Biochemistry* **38:** 13968-75.

Frankenberg, N., and Lagarias, J.C. (2003) Phycocyanobilin:ferredoxin oxidoreductase of *Anabaena sp*. PCC 7120. Biochemical and spectroscopic. *J Biol Chem* **278:** 9219-26.

Frankenberg, N., Moser, J., and Jahn, D. (2003) Bacterial heme biosynthesis and its biotechnological application. *Appl Microbiol Biotechnol* **63:** 115-27.

Fraser, M.E., James, M.N.G., Bridger, W.A., and Wolodko, W.T. (1999) A Detailed Structural Description of *Escherichia coli* Succinyl-CoA Synthetase. *J Mol Biol* **285**: 1633-1653.

Frere, F., Schubert, W.D., Stauffer, F., Frankenberg, N., Neier, R., Jahn, D., and Heinz, D.W. (2002) Structure of porphobilinogen synthase from *Pseudomonas aeruginosa* in complex with 5-fluorolevulinic acid suggests a double Schiff'base mechanism. *J Mol Biol* **320 (2)**: 237-47.

Frere, F., Nentwich, M., Gacond, S., Heinz, D.W., Neier, R., and Frankenberg-Dinkel, N. (2006) Probing the active site of *Pseudomonas aeruginosa* porphobilinogen synthase using newly developed inhibitors. *Biochemistry* **45 (27)**: 8243-53.

Fujita, H., Yamamoto, M., Yamagami, T., Hayashi, N., and Sassa, S. (1991a) Erythroleukemia differentiation. Distinctive responses of the erythroid-specific and the nonspecific delta-aminolevulinate synthase mRNA. *J Biol Chem* **266 (26)**: 17494-502.

Fujita, H., Yamamoto, M., Yamagami, T., Hayashi, N., Bishop, T.R.; De Verneuil, H., Yoshinaga, T., Shibahara, S., Morimoto, R., and Sassa, S. (1991b) Sequential activation of genes for heme pathway enzymes during erythroid differentiation of mouse Friend virus-transformed erythroleukemia cells. *Biochim Biophys Acta* **1090 (3)**: 311-6.

Fukuda, H., Casas, A., and Batlle, A. (2006) Use of ALA and ALA derivatives for optimizing ALA-based photodynamic therapy: a review of our experience. *J Environ Pathol Toxicol Oncol* **25 (1-2)**: 127-43.

Furuyama, K., Fujita, H., Nagai, T., Yomogida, K., Munakata, H., Kondo, M., Kimura, A., Kuramoto, A., Hayashi, N., and Yamamoto, M. (1997) Pyridoxine Refractory X-Linked Sideroblastic Anemia Caused by a Point Mutation in the Erythroid 5-Aminolevulinate Synthase Gene. *Blood* **90**: 822-830.

Furuyama, K., and Sassa, S. (2000) Interaction between succinyl CoA synthetase and the heme-biosynthetic enzyme ALAS-E is disrupted in sideroblastic anaemia. *J Clin Invest*v **105**: 757-764.

Furuyama, K., and Sassa, S. (2002) Multiple mechanisms for hereditary sideroblastic anaemia. *Cell Mol Biol (Noisy-le-grand)* **48 (1)**: 5-10.

Gibbs, P.N., Chaudhry, A.G., and Jordan, P.M. (1985) Purification and properties of 5-aminolaevulinate dehydratase from human erythrocytes. *Biochem J* **230 (1)**: 25-34.

Gong, J., Hunter, G.A., and Ferreira, G.C. (1998) Aspartate-279 in Aminolevulinate Synthetase Affects Enzyme Catalysis through Enhancing the Function of the Pyridoxal 5'-Phosphate Cofactor. *Biochem* **37**: 3509-3517.

Grzybowska, E., Gora, M., Plochocka, D., and Rytka, J. (2002) *Saccharomyces cerevisiae* ferrochelatase forms a homodimer. *Arch Biochem Biophys* **398 (2)**: 170-8.

Hamilton, J.W., Bement, W.J., Sinclair, P.R., Sinclair, J.F., Alcedo, J.A., and Wetterhahn, K.E. (1991) Heme Regulates Hepatic 5-Aminolevulinate Synthetase mRNA Expression by Decreasing mRNA Half-Life and Not by Altering Its Rate of Transcription. *Arch Biochem Biophys* **289 (2)**: 387-392.

Hansson, M., and Hederstedt, L. (1994a) *Bacillus subtilis* HemY is a peripheral membrane protein essential for protoheme IX synthesis which can oxidize coproporphyrinogen III and protoporphyrinogen IX. *J Bacteriol* **176**: 5962-70.

Hansson, M., and Hederstedt, L. (1994b) Purification and characterisation of a water-soluble ferrochelatase from *Bacillus subtilis*. *Eur J Biochem* **220 (1)**: 201-8.

Hansson, M., Gustafsson, M.C., Kannangara, C.G., and Hederstedt, L. (1997) Isolated *Bacillus subtilis* HemY has coproporphyrinogen III to coproporphyrin III oxidase activity. *Biochim Biophys Acta* **1340 (1)**: 97-104.

Harigae, H., Nakajima, O., Suwabe, N., Yokoyama, H., Furuyama, K., Sasaki, T., Kaku, M., Yamamoto, M., and Sassa, S. (2003) Aberrant iron accumulation and oxidized status of erythroid-specific δ-aminolevulinate synthetase (ALAS2)-deficient definitive erythroblasts. *Blood* **101 (3)**: 1188-93.

Hayashi, H., Mizuguchi, H., and Kagamiyama, H. (1993) Rat Liver L-Amino Acid Decaboxlyase: Spectroscopic and Kinetic Analysis of the Coenzyme and Reaction Intermediates. *Biochemistry* **32**: 812-818.

Heinemann, I.U., Diekmann, N., Masoumi, A., Koch, M., Messerschmidt, A., Jahn, M., and Jahn, D. (2007) Functional definition oft he tobacco protoporphyrinogen IX oxidase substrate-binding site. *Biochem J* **402 (3)**: 575-80.

Heinemann, I.U., Jahn, M., and Jahn, D. (2008) The biochemistry of heme biosynthesis. *Arch Biochem Biophys* **474 (2):** 238-51.

Henning, W.D., Upton, C., McFadden, G., Majumdar, R., and Bridger, W.A. (1988) Cloning and sequencing of the cytoplasmic precursor to the α subunit of rat liver mitochondrial succinyl-CoA synthetase. *Proc Natl Acad Sci USA* **85**: 1432-1436.

Herzberg, O., Chen, C.C.H., Kapadia, G., McGuire, M., Carroll, L., Noh, S.J., and Dunaway-Mariano, D. (1996) Swiveling-domain mechanism for enzymatic phosphotransfer between remote reaction sites. *Proc Natl Acad Sci USA* **93**: 2652-2657.

Heyl, D., Luz, E., Harris, S.A., and Folkers, K. (1951) Phosphates of the Vitamin B_6 Group. III. Pyridoxamine Phosphate. *J Am Chem Soc* **73**: 3436-3437.

Hungerer, C., Weiss, D.S., Thauer, R.K., and Jahn, D. (1996) The hemA gene encoding glutamyl-tRNA reductase from the archaeon Methanobacterium thermoautotrophicum strain Marburg. *Bioorg Med Chem* **4**: 1089-1095.

Hunter, G.A., and Ferreira, G.C. (1995) A Continuous Spectrophotometric Assay for 5-Aminolevulinate Synthetase That Utilizes Substrate Cycling. *Anal Biochem* **226**: 221-224.

Hunter, G.A., and Ferreira, G.C. (1999) Pre-steady-state Reaction of 5-Aminolevulinate Synthetase. *J Biol Chem* **274 (18)**: 12222-12228.

Hunter, G.A., Zhang, J., and Ferreira, G.C. (2007) Transient Kinetic Studies Support Refinements to the Chemical and Kinetic Mechanism of Aminolevulinate Synthetase. *J Biol Chem* **282 (32)**: 23025-23035.

Hunter, G.A., Sampson, M.P., and Ferreira, G.C. (2008) Metal ion substrate inhibition of ferrochelatase. *J Biol Chem* **283 (35)**: 23685-91.

Hunter, G.A., and Ferreira, G.C. (2009) 5-Aminolevulinate Synthetase: Catalysis Of The First Step Of Heme Biosynthesis. *Cell Mol Biol* **55 (1)**: 99-107.

Iida, K., Mimura, I., and Kajiwara, M. (2002) Evaluation of two biosynthetic pathways to delta-aminolevulinic acid in *Euglena gracilis. Eur J Biochem* **269 (1)**: 291-7.

Ikushiro, H., Hayashi, H., and Kagamiyama, H. (2004) Reactions of Serine Plamitoyltransferase with Serine and Molecular Mechanisms of the Actions of Serine Derivatives as Inhibitors. *Biochemistry* **43**: 1082-1092.

Ilag, L.L., and Jahn, D. (1992) Activity and spectroscopic properties of the *Escherichia coli* glutamate 1-semialdehyde aminotransferase and the putative active site mutant K265R. *Biochemistry* **31:** 7143-51.

Jacobs, N.J., and Jacobs, J.M. (1976). Nitrate, fumarate, and oxygen as electron acceptorsfor a late step in microbial heme synthesis. *Biochim Biophys Acta* **449**: 1-9.

Jaffe, E.K. (2004) The porphobilinogen synthase catalyzed reaction mechanism. *Bioorg Chem* **32 (5)**: 316-25.

Jahn, D., Michelsen, U., and Soll, D. (1991) Two glutamyl-tRNA reductase activities in *Escherichia coli*. *J Biol Chem* **266**: 2542-8.

Jahn, D., Verkamp, E., and Soll, D. (1992) Glutamyl-transfer RNA: a precursor of heme and chlorophyll biosynthesis. *Trends Biochem Sci* **17**: 215-8.

Jahn, D., Hungerer, C., and Troup, B. (1996) Unusual pathways and environmentally regulated genes of bacterial heme biosynthesis. *Naturwissenschaften* **83**: 389-400.

Jahn, D., and Heinz, D.W. (2009) Biosynthesis og 5-aminolevulinate acid. In *Tetrapyrroles: Birth, Life and Death*, Warren, M.J., Smith, A.G., Eds. Landes Bioscience: Austin, pp 29-42.

James, M.F.M., and Hift, R.J. (2000) Porphyrias. *Br J Anaest* **85**: 143-53.

Johnson, J.D., Mehus, J.G., Tews, K., Milavetz, B.I., and Lambeth, D.O. (1998a) Genetic evidence for the expression of ATP- and GTP-specific succinyl CoA synthetases in multicellular eucaryotes. *J Biol Chem* **273**: 27580-27586.

Johnson, J.D., Muhonen, W.W., and Lambeth, D.O. (1998b) Characterization of the ATP- and GTP-specific succinyl CoA synthetases in pigeon. The enzymes incorporate the same alpha subunit. *J Bio. Chem* **273**: 27572-27579.

Jordan, P.M., and Laghai-Newton, A. (1986) Purification of 5-Aminolevulinate Synthase. *Methods Enzymol* **123**: 435-443.

Jordan, P.M., and Warren, M.J. (1987) Evidence for a dipyrromethane cofactor at the catalytic site of *E. coli* porphobilinogen deaminase. *FEBS Lett* **225**: 87-92.

Jordan, P.M., and Woodcock, S.C. (1991) Mutagenesis of arginine residues in the catalytic cleft of *Escherichia coli* porphobilinogen deaminase that affects dipyrromethane cofactor assembly and tetrapyrrole chain initiation and elongation. *Biochem J* **280 (Pt 2)**: 445-449.

Kerbarh, O., Campopiano, D.J., and Baxter, R.L. (2006) Mechanism of α-oxoamine synthases: identification of the intermediate Claisen product in the 8-amino-7-oxononanoate synthase reaction. *Chem Commun (Camb)* **1**: 60-62.

Kikuchi, G., Kumar, A., Talmage, P., and Shemin, D. (1958) The Enzymatic Synthesis of δ-Aminolevulinic Acid *J Biol Chem* **233 (5)**: 1214-9.

Klausner, R.D., Rouault, T.A., and Harford, J.B. (1993) Regulating the Fate of mRNA: The Control of Cellular Iron Metabolism. *Cell* **72**: 19-28.

Koch, M., Breithaupt, C., Kiefersauer, R., Freigang, J., Huber, R., and Messerschmidt, A. (2004) Crystal structure of protoporphyrinogen IX oxidase: a key enzyme in haem and chlorophyll biosynthesis. *EMBO J* **23**:1720-8.

Labbe-Bois, R., and Labbe, P. (1990). Tetrapyrrole and heme biosynthesis in yeast. *In* HA Dailey, ed, Biosynthesis of Heme and Chlorophylls. *McGraw-Hill,* New York, 235-285.

Laemmli, U.K. (1970) Cleavage of structural proteins during the assembly of the head of bacteriophage T4. *Nature* **227**: 680-685.

Lam, H., Oh, D.C., Cava, F., Takacs, C.N., Clardy, J., de Pedro, M.A., and Waldor, M.K. (2009) D-amino acids govern stationary phase cell wall remodeling in bacteria. *Science* **325 (5947)**: 1552-5.

Lathrop, J.T., and Timko, M.P. (1993) Regulation by Heme of Mitochondrial Protein Transport Through a Conserved Amino Acid Motif. *Science* **259**: 522-525.

Layer, G., Verfurth, K., Mahlitz, E., and Jahn, D. (2002) Oxygen-independent coproporphyrinogen-III oxidase HemN from *Escherichia coli*. *J Biol Chem* **277**: 34136-42.

Layer, G., Moser, J., Heinz, D.W., Jahn, D., and Schubert, W.D. (2003) Crystal structure of coproporphyrinogen III oxidase reveals cofactor geometry of Radical SAM enzymes. *Embo J* **22 (23)**: 6214-24.

Layer, G., Reichelt, J., Jahn, D., and Heinz, D.W. (2010) Structure and function of enzymes in heme biosynthesis. *Protein Sci* **19**: 1137-1161.

Lecha, M., Puy, H., and Deybach, J.C. (2009) Erythropoietic protoporphyria. *Orphanet J Rare Dis* **4**: 19-28.

Leech, H.K., Raux-Deery, E., Heathcote, P., and Warren, M.J. (2002) Production of cobalamin and sirohaem in *Bacillus megaterium*: an investigation into the role of the branchpoint chelatases sirohydrochlorin ferrochelatase (SirB) and sirohydrochlorin cobalt chelatase (CbiX). *Biochem Soc Trans* **30**: 610-3.

Lendrihas, T., Zhang, J., Hunter, G.A., and Ferreira, G.C. (2009) Arg-85 and Thr-430 in murine 5-aminolevulinate synthase coordinate acyl- CoA-binding and contribute to substrate specificity. *Protein Sci* **18 (9)**: 1847-59.

Lendrihas, T., Hunter, G.A., and Ferreira, G.C. (2010) Targeting the Active Site Gate to Yield Hyperactive Variants of 5-Aminolevulinate Synthase. *J Biol Chem* **285 (18)**: 13704-11.

Lermontova, I., Kruse, E., Mock, H. P., and Grimm, B. (1997) Cloning and characterization of a plastidal and a mitochondrial isoform of tobacco protoporphyrinogen IX oxidase. *Proc Natl Acad Sci U S A* **94**: 8895-900.

Lewis, C.A., Jr., and Wolfenden, R. (2008) Uroporphyrinogen decarboxylation as a benchmark for the catalytic proficiency of enzymes. *Proc Natl Acad Sci U S A* **105 (45)**: 17328-33.

Lim, L., and McFadden, G.I. (2010) The evolution, metabolism and functions of the apicoplast. *Philos Trans R Soc Lond B Biol Sci* **365 (1541)**: 749-63.

Louie, G.V., Brownli, P.D., Lambert, R., Cooper, J.B., Blundell, T.L., Wood, S.P., Warren, M.J., Woodcock, S.C., and Jordan, P.M. (1992) Structure of porphobilinogen deaminase reveals a flexible multidomain polymerase with a single catalytic site. *Nature* **359**: 33-39.

Louie, G.V., Brownli, P.D., Lambert, R., Cooper, J.B., Blundell, T.L., Wood, S.P., Malashkevich, V.N., Hädener, A., Warren, M.J., and Shoolingin-Jordan, P.M. (1996) The Three-Dimensional Structure of *Escherichia coli* Porphobilinogen Deaminase at 1.76-Å Resolution. *Proteins* **25**: 48-78.

Luer, C., Schauer, S., Mobius, K., Schulze, J., Schubert, W. D., Heinz, D. W., Jahn, D., and Moser, J. (2005) Complex formation between glutamyl-tRNA reductase and glutamate-1-semialdehyde 2,1-aminomutase in *Escherichia coli* during the initial reactions of porphyrin biosynthesis. *J Biol Chem* **280**: 18568-72.

Luo, J., and Lim, C.K. (1993) Order of uroporphyrinogen III decarboxylation on incubation of porphobilinogen and uroporphyrinogen III with erythrocyte uroporphyrinogen decarboxylase. *Biochem J* **289 (Pt 2)**: 529-532.

Martins, B.M., Grimm, B., Mock, H.P., Huber, R., and Messerschmidt, A. (2001) Crystal structure and substrate binding modeling of the uroporphyrinogen-III decarboxylase from *Nicotiana tabacum*. Implications for the catalytic mechanism. *J Biol Chem* **276 (47)**: 44108-16.

Masoumi, A., Heinemann, I.U., Rohde, M., Koch, M., Jahn, M., and Jahn, D. (2008) Complex formation between protoporphyrinogen IX oxidase and ferrochelatase during haem biosynthesis in *Thermosynechococcus elongatus*. *Microbiology* **154**: 3707-3714.

Mathews, M.A., Schubert, H.L., Whitby, F.G., Alexander, K.J., Schadick, K., Bergonia, H.A., Phillips, J.D., and Hill, C.P. (2001) Crystal structure of human uroporphyrinogen III synthase. *EMBO J* **20 (21)**: 5832-9.

Matringe, M., Camadro, J.M., Labbe, P., and Scalla, R. (1989) Protoporphyrinogen oxidase as a molecular target for diphenyl ether herbicides. *Biochem J* **260 (1)**: 231-5.

May, B.K., Dogra, S.C., Sadlon, T.J., Bhasker, C.R., Cox, T.C., and Bottomley, S.S. (1995) Molecular regulation of heme biosynthesis in higher vertebrates. *Prog Nucleic Acid Res Mol Biol* **51**: 1-51.

May, A., and Bishop, D.F. (1998) The molecular biology and pyridoxine responsiveness of X-linked sideroblastic anaemia. *Haematologica* **83**: 56-70.

McDonald, I.K., and Thornton, J.M. (1995) The application of hydrogen bonding analysis in X-ray crystallography to help orientate asparagine, glutamine and histidine side chains. *Protein Eng* **8**: 217-224.

Medlock, A., Swartz, L., Dailey, T.A., and Dailey, H.A. (2007) Lanzilotta, W. N., Substrate interactions with human ferrochelatase. *Proc Natl Acad Sci U S A* **104 (6)**: 1789-93.

Medlock, A.E., Carter, M., Dailey, T.A., Dailey, H.A., and Lanzilotta, W.N. (2009) Product release rather than chelation determines metal specificity for ferrochelatase. *J Mol Biol* **393 (2)**: 308-19.

Mehta, P.K., and Christen, P. (1994) Homology of 1-Aminocyclopropane-1-carboxylate synthase, 8-Amino-7-oxononanoate synthase, 2- Amino-6-caprolactam racemase, 2,2-Dialkylglycine decarboxylase, Glutamate-1semialdehyde 2,1-Aminomutase and Isopenicillin-*N*-epimerase with Aminotransferases. *Biochem Biophys Res Commun* **198**: 138-143.

Meissner, P.N., Hift, R.J., and Kirsch, R.E. (2001) The porphyrias. In: Arias IM, Boyer JL, Chisari FV, Fausto N, Schacter D, Shafritz DA, eds. *The Liver: Biology and Pathobiology.* 4th ed. Philadelphia, Pa: LippincottWilliams andWilkins; 2001: 311–329.

Meixner-Monori, B., Kubicek, C.P., Habison, A., Kubicek-Pranz, E.M., and Röhr, M. (1985) Presence and regulation of the alpha-ketoglutarate dehydrogenase multienzyme complex in the filamentous fungud Aspergillus niger. *J Bacteriol* **161 (1)**: 265-71.

Melefors, Ö., Goossen, B., Johansson, H.E., Stripecke, R., Gray, N.K., and Hentze, M.W. (1993) Translational Control of 5-Aminolevulinate Synthetase mRNA by Iton-responsive Elements in Erythroid Cells. *J Biol Chem* **268 (8)**: 5974-5978.

Miles, J.S., and Guest, J.R. (1987) Molecular genetic aspects of the citric acid cycle of *Escherichia coli*. *Biochem Soc Symp* **54**: 45-65.

Mitchell, L.W., and Jaffe, E.K. (1993) Porphobilinogen synthase from *Escherichia coli* is a Zn(II) metalloenzyme stimulated by Mg(II). *Arch Biochem Biophys* **300 (1)**: 169-77.

Möbius, K., Arias-Cartin, R., Breckau, D., Hännig, A.L., Riedmann, K., Biedendieck, R., Schröder, S., Becher, D., Magalon, A., Moser, J., Jahn, M., and Jahn, D. (2010) Heme biosynthesis is coupled to electron transport chains for energy generation. *Proc Natl Acad Sci U S A* **107**: 10436-10441.

Mock, H.P., and Grimm, B. (1997) Reduction of Uroporphyrinogen Decarboxylase by Antisense RNA Expression Affects Activities of Other Enzymes Involved in Tetrapyrrole Biosynthesis and Leads to Light-Dependent Necrosis. *Plant Physiol* **113**: 1101-1112.

Mock, H.P., Heller, W., Molina, A., Neubohn, B., Sandermann, H., Jr., and Grimm, B. (1999) Expression of uroporphyrinogen decarboxylase or coproporphyrinogen oxidase antisense RNA in tobacco induces pathogen defense responses conferring increased resistance to tobacco mosaic virus. *J Biol Chem* **274**: 4231-4238.

Moore, P.S., Bertoldi, M., Dominici, P., and Voltattorni, C.B. (1997) Aromatic amino acid methyl ester analogs form quinonoidal species with Dopa decarboxylase. *FEBS Letters* **412**: 245-248.

Moser, J., Lorenz, S., Hubschwerlen, C., Rompf, A., and Jahn, D. (1999) *Methanopyrus kandleri* glutamyl-tRNA reductase. *J Biol Chem* **274**: 30679-85.

Moser, J., Schubert, W.D., Beier, V., Bringemeier, I., Jahn, D., and Heinz, D.W. (2001) Vshaped structure of glutamyl-tRNA reductase, the first enzyme of tRNA-dependent tetrapyrrole biosynthesis. *EMBO J* **20**: 6583-90.

Munro, A.W., Girvan, H.M., McLean, K.J., Cheesman, M.R., and Leys, D. (2009) Heme and hemoproteins. In *Tetrapyrroles: Birth, Life and Death*, Warren, M. J.; Smith, A. G., Eds. Landes Bioscience: Austin, pp 160-183.

Murphy, M.J., Siegel, L.M., Tove, S.R., and Kamin, H. (1974) Siroheme: a new prosthetic group participating in six-electron reduction reactions catalyzed by both sulfite and nitrite reductases. *Proc Natl Acad Sci U S A* **71 (3)**: 612-6.

Murzin, A.G. (1996) Structural classification of proteins: new superfamilies. *Curr Opin Struct Biol* **6**: 386-394.

Nandi, D.L. (1978a) Studies on δ-Aminolevulinic acid synthase of *Rhodopseudomonas spheroides*. *J Biol Chem* **253**: 8872-8877.

Nandi, D.L. (1978b) δ-Aminolevulinic acid synthase of *Rhodopseudomonas spheroides*. *Arch Biochem Biophys* **188 (2)**: 266-271.

Neidle, E.L., and Kaplan, S. (1993) 5-Aminolevulinic acid availability and control of spectral complex formation in hemA and hemT mutants of *Rhodobacter sphaeroides*. *J Bacteriol* **175**: 2304-2313.

O'Brian, M.R., and Thöny-Meyer, L. (2002) Biochemistry, regulation and genomics of haem biosynthesis in prokaryotes. *Adv Microb Physiol* **46**: 257-318.

Olmo, M.T., Sánchez-Jiménez, F., Medina, M.A., and Hayashi, H. (2002) Spectroscopic Analysis of Recombinant Rat Histidine Decarboxylase. *J Biochem* **132**: 433-439.

Padmanaban, G., and Rangarajan, P.N. (2000) Heme metabolism of *Plasmodium* is a major antimalarial target. *Biochem Biophys Res Commun* **268 (3)**: 665-8.

Panek, H., and O'Brian, M.R. (2002) A whole genome view of prokaryotic haem biosynthesis. *Microbiology* **148**: 2273-2282.

Percudani, R., and Peracchi, A. (2003) A genomic overview of pyridoxal-phosphate-dependent enzymes. *EMBO reports* **4 (9)**: 850-854.

Phillips, J.D., Whitby, F.G., Kushner, J.P., and Hill, C.P. (2003) Structural basis for tetrapyrrole coordination by uroporphyrinogen decarboxylase. *Embo J* **22 (23)**: 6225-33.

Pichon, C., Atshaves, B.P., Stolowich, N.J., and Scott, A.I. (1994) Evidence for an intermediate in the enzymatic formation of uroporphyrinogen III. *Bioorg Med Chem* **2 (3)**: 153-68.

Poblete-Gutierrez, P., Wiederholt, T., Merk, H.F., and Frank, J. (2006) The porphyrias: clinical presentation, diagnosis and treatment. *Eur J Dermatol* **16 (3)**: 230-40.

Puy, H., Gouya, L., and Deybach, J.D. (2010) Porphyrias. *Lancet* **375**: 924-37.

Rand, K., Noll, C., Schiebel, H.M., Kemken, D., Dulcks, T., Kalesse, M., Heinz, D.W., and Layer, G. (2010) The oxygen-independent coproporphyrinogen III oxidase HemN utilizes harderoporphyrinogen as a reaction intermediate during conversion of coproporphyrinogen III to protoporphyrinogen IX. *Biol Chem* **391 (1)**: 55-63.

Raux, E., Leech, H.K., Beck, R., Schubert, H.L., Santander, P.J., Roessner, C.A., Scott, A.I., Martens, J.H., Jahn, D., Thermes, C., Rambach, A., and Warren, M.J. (2003) Identification and functional analysis of enzymes required for precorrin-2 dehydrogenation and metal ion insertion in the biosynthesis of sirohaem and cobalamin in *Bacillus megaterium*. *Biochem J* **370**: 505-516.

Raux-Deery, E., Leech, H.K., Nakrieko, K.A., McLean, K.J., Munro, A.W., Heathcote, P., Rigby, S.E., Smith, A.G., and Warren, M.J. (2005) Identification and characterization of the terminal enzyme of siroheme biosynthesis from *Arabidopsis thaliana*: a plastid-located sirohydrochlorin ferrochelatase containing a 2FE-2S center. *J Biol Chem* **280**: 4713-21.

Riddle, R.D., Yamamoto, M., and Engel, J.D. (1989) Expression of δ-aminolevulinate synthase in avian cells: Separate genes encode erythroid-specific and nonspecific isozymes. *Proc Natl Acad Sci USA* **86**: 792-796.

Righetti, P.G., Gianazza, E., Gelfi, C., and Chairi, M. (1990) In *Gel electrophoresis of proteins: a practical approach.* Vol. 2nd Ed. Hames, B.D. and Rickwood, D. (eds.). Oxford: Oxford University Press, pp. 149-214.

Rodgers, K.R. (1999) Heme-based sensors in biological systems. *Curr Opin Chem Biol* **3**: 158-67.

Roehl, J.C.G., Warren, M., and Hunt, D. (1988) *Purple Secret: Genes, 'Madness' and the Royal Houses of Europe.* Bantam Press, p. 297.

Sambrook, J., Fritsch, E.F., and Maniatis, T. (1989) Molecular cloning: a laboratory manual, 2nd ed. Cold Spring Harbor Laboratory Press, Cold Spring Harbor, New York.

Sanger, F., Nicklen, S., and Coulson, A.R. (1977) DNA sequencing with chainterminating inhibitors. *Biotechnology* **24**: 104-108.

Sarkany, R.P. (1999) Porphyria. From Sir Walter Raleigh to molecular biology. *Adv Exp Med Biol* **455**: 235-41.

Sasarmann, A., Surdeanu, M., Szegli, G., Horodniceanu, T., Greceanu, V., and Dumitrescu, A. (1968) Hemin-deficient mutants of *Escherichia coli* K-12. *J Bacteriol* **96 (2)**: 570-2.

Sasarman, A., Chartrand, P., Lavoie, M., Tardif, D., Proschek, R., and Lapointe, C. (1979) Mapping of a new *hem* gene in *Escherichia coli* K12. *J Gen Microbiol* **113**: 297-303.

Sasarman, A., Letowski, J., Czaika, G., Ramirez, V., Nead, M.A., Jacobs, J.M., and Morais, R. (1993) Nucleotide sequence of the *hemG* gene involved in the protoporphyrinogen oxidase activity of *Escherichia coli* K12. *Can J Microbiol* **39**: 1155-61.

Sassa, S. (2006) Modern diagnosis and management of the porphyrias. *Br J Haematol* **135 (3)**: 281-92.

Schade, A.L., and Caroline, L. (1946) An Iron.binding Component in Human Bllod Plasma. *Science* **104**: 340-341.

Schmidt, A., Sivaraman, J., Li, Y., Larocque, R., Barbosa, J.A., Smith, C., Matte, A., Schrag, J.D., and Cygler, M. (2001) Three-dimensional structure of 2-amino-3-ketobutyrate CoA ligase from *Escherichia coli* complexed with a PLP-substrate intermediate: inferred reaction mechanism. *Biochemistry* **40**: 5151-5160.

Schneider, G., Kack, H., and Lindqvist, Y. (2000) The manifold of vitamin B6 dependent enzymes. *Struct Fold Des* **8**: R1–R6.

Schulze, J.O., Schubert, W.-D., Moser, J., Jahn, D., and Heinz, D.W. (2006) Evolutionary Relationship between Initial Enzymes of Tetrapyrrole Biosynthesis. *J Mol Biol* **358**: 1212-1220.

Seehra, J.S., Jordan, P.M., and Akhtar, M. (1983) Anaerobic and aerobic coproporphyrinogen III oxidases of *Rhodopseudomonas spheroides*. Mechanism and stereochemistry of vinyl group formation. *Biochem J* **209 (3)**: 709-18.

Senior, N.M., Brocklehurst, K., Cooper, J.B., Wood, S.P., Erskine, P., Shoolingin-Jordan, P.M., Thomas, P.G., and Warren, M.J. (1996) Comparative studies on the 5-aminolaevulinic acid dehydratases from *Pisum sativum*, *Escherichia coli* and *Saccharomyces cerevisiae*. *Biochem J* **320 (Pt 2)**: 401-12.

Senior, N.M., Siligardi, G., Drake, A., Thomas, P.G., and Warren, M.J. (1997) Structural studies on 5-aminolaevulinic acid dehydratase from *Saccharomyces cerevisiae* (yeast). *Biochem Soc Trans* **25 (1)**: 78S.

Shemin, D., and Russel, C.S. (1953) Delta-aminolevulinic acid, its role in the biosynthesis of porphyrins and purins. *J Am Chem Soc* **75**: 4873-4875.

Shepherd, M., Dailey, T.A., and Dailey, H.A. (2006) A new class of [2Fe-2S]-cluster-containing protoporphyrin (IX) ferrochelatases. *Biochem J* **397 (1)**: 47-52.

Shoolingin-Jordan, P.M. (1995) Porphobilinogen deaminase and uroporphyrinogen III synthase: structure, molecular biology, and mechanism. *J Bioenerg Biomembr* **27 (2)**: 181-95.

Shoolingin-Jordan, P.M., LeLean, J.E., and Lloyd, A.J. (1997) Continuous Coupled Assay for 5-Aminolevulinate Synthase. *Methods Enzymol* **281**: 309-16.

Shoolingin-Jordan, P.M., and Cheung, K.M. (1999) Comprehensive natural products chemistry. In *Biosynthesis of heme*. Vol. 4. Barton, D.e.K., J.W., ed.) (ed). Amsterdam, NL: Elservier Science Ltd., pp. 61-103.

Shoolingin-Jordan, P.M., Spencer, P., Sarwar, M., Erskine, P.E., Cheung, K.M., Cooper, J.B., and Norton, E.B. (2002) 5-Aminolaevulinic acid dehydratase: metals, mutants and mechanism. *Biochem Soc Trans* **30 (4)**: 584-90.

Shoolingin-Jordan, P.M., Al-Daihan, S., Alexeev, D., Baxter, R.L., Bottomley, S.S., Kahari, I.D., Roy, I., Sarwar, M., Sawyer, L., and Wang, S.F. (2003) 5-Aminolevulinic acid synthase: mechanism, mutations and medicine. *Biochim Biophys Acta* **1647 (1-2)**: 361-6.

Silva, P.J., and Ramos, M.J. (2008) Comparative density functional study of models for the reaction mechanism of uroporphyrinogen III synthase. *J Phys Chem B* **112**: 3144–3148.

Silva, P.J., Schulz, C., Jahn, D., Jahn, M., and Ramos, M.J. (2010) A Tale of Two Acids: When Arginine Is a More Appropriate Acid than H_3O^+. *J Phys Chem B* **114 (27)**: 8994-9001.

Smith, A.G. (1988) Subcellular localization of two porphyrin-synthesis enzymes in *Pisum sativum* (pea) and *Arum* (cuckoo-pint) species. *Biochem J* **249**: 423-428.

Smith, A.G., Marsh, O., and Elder, G.H. (1993) Investigation of the subcellular location of the tetrapyrrole-biosynthesis enzyme coproporphyrinogen oxidase in higher plants. *Biochem J* **292 (Pt 2)**: 503-8.

Spano, A.J., and Timko, M.P. (1991) Isolation, characterization, and partial amino acid sequence of a chloroplast localized porphobilinogen deaminase from pea (*Pisum sativum* L.). *Biochim Biophys Acta* **1076**: 29-36.

Spencer, M.E., Darlison, M.G., Stephens, P.E., Duckenfield, I.K., and Guest, J.R. (1984) Nucleotide sequence of the sucB gene encoding the dihydrolipoamide succinyltransferase of Escherichia coli K12 and homology with the corresponding acetyltransferase. *Eur J Biochem* **141**: 361-74.

Spencer, J.B., Stolowich, N.J., Roessner, C.A., and Scott, A.I. (1993) The *Escherichia coli cysG* gene encodes the multifunctional protein, siroheme synthetase. *FEBS Lett* **335**: 57-60.

Srivasata, G., Borthwick, I.A., Maguire, D.J., Elferink, C.J., Bawden, M.J., Mercer, J.F.B., and May, B.K. (1988) Regulation of 5-Aminolevulinate Synthetase mRNA in Different Rat Tissues. *J Biol Chem* **263 (11)**: 5202-5209.

Stahl, D.A., Key, R., Flesher, B., and Smit, J. (1992) The Phylogeny of Marine and Freshwater Caulobacters Reflects Their Habitat. *J Bacteriol* **174**: 2193-2198.

Stark, W.M., Hart, G.J., and Battersby, A.R. (1986) Synthetic studies on the proposed spiro intermediate for biosynthesis of the natural porphyrins: inhibition of cosynthetase. *J Chem Soc, Chem Commun:* 465-467.

Tan, D., and Ferreira, G.C. (1996) Active Site of 5-Aminolevulinate Synthase Resides at the Subunit Interface. Evidence from *in* Vivo Heterodimer Formation. *Biochemistry* **35**: 8934-8941.

Tan, D., Harrison, T., Hunter, G.A., and Ferreira, G.C. (1998) Role of arginine 439 in substrate binding of 5-aminolevulinate synthetase. *Biochemistry* **37**: 1478–1484.

Thauer, R.K., and Bonacker, L.G. (1994) Biosynthesis of Coenzyme F430, a nickel porphinoid involved in methanogenesis. *Ciba Found Symp* **180**: 210-22; discussion 222-7.

Toney, M.D. (2005) Reaction specificity in pyridoxal phosphate enzymes. *Arch Biochem Biophys* **433 (1)**: 279-87.

Turbeville, T.D., Zhang, J., Hunter, G.A., and Ferreira, G.C. (2007) Histidine-282 in 5-Aminolevulinate Synthetase Affects Substrate Binding and Catalysis. *Biochemistry* **46 (20)**: 5972-5981.

Vavilin, D.V., and Vermaas, W.F. (2002) Regulation of the tetrapyrrole biosynthetic pathway leading to heme and chlorophyll in plants and cyanobacteria. *Physiol Plant* **115 (1)**: 9-24.

von Eiff, C., McNamara, P., Becker, K., Bates, D., Lei, X.H., Ziman, M., Bochner, B.R., Peters, G. and Proctor, R.A. (2006) Phenotype microarray profiling of *Staphylococcus aureus menD* and *hemB* mutants with the small-colony-variant phenotype. *J Bacteriol* **188 (2)**: 687-93.

Waldrop, G.L., Rayment, I., and Holden, H.M. (1994) Three-dimensional structure of the biotin carboxylase subunit of acetyl-CoA carboxylase. *Biochem* **33**: 10249-10256.

Wang, T., Jurasek, L., and Bridger, W.A. (1972) Succinyl Coenzyme A synthetase of Escherichia coli. Sequence of a peptide containing the active-site phosphohistidine residue. *Biochem* **11***:* 2067-2070.

Wang, K.F., Dailey, T.A., and Dailey, H.A. (2001) Expression and characterization of the terminal heme synthetic enzymes from the hyperthermophilic *Aquifex aeolicus. FEMS Microbiol Lett* **202 (1)**: 115-9.

Warren, M.J., and Jordan, P.M. (1988) Investigation into the nature of substrate binding to the dipyrromethane cofactor of *Escherichia coli* porphobilinogen deaminase. *Biochemistry* **27:** 9020-30.

Warren, M.J., and Smith, A.G. (2008) *Tetrapyrroles: Birth, Life and Death.* New York, USA: Landes Bioscience, Springer Science and Business Media.

Weinstein, J.D., and Beale, S.I. (1983) Separate physiological roles and subcellular compartments for two tetrapyrrole biosynthetic pathways in *Euglena gracilis*. *J Biol Chem* **258:** 6799-807.

Whatley, S.D., Ducamp, S., Gouya, L., Grandchamp, B., Beaumont, C., Badminton, M.N., Elder, G.H., Holme, S.A., Anstey, A.V., Parker, M., Corrigall, A.V., Meissner, P.N., Hift, R.J., Marsden, J.T., Ma, Y., Mieli-Vergani, G., Deybach, J.C., and Puy, H. (2008) C-terminal deletions in the ALAS2 gene lead to gain of function and cause X-linked dominant protoporphyria without anaemia or iron overload. *Am J Hunt Genet* 83 (3)*:* 408-14.

Wolodko, W.T., James, M.N.G., and Bridger, W.A. (1984) Crystallization of Succinyl-CoA Synthetase from *Escherichia coli*. *J Biol Chem* **259 (8)**: 5316-5320.

Wolodko, W.T., Kay, C.M., and Bridger, W.A. (1986) Active enzyme sedimentation, sedimentation velocity, and sedimentation equilibrium studies of succinyl-CoA synthetases of porcine heart and *Escherichia coli*. *Biochem* **25**: 5420-5425.

Wolodko, W.T., Fraser, M.E., James, M.N.G., and Bridger, W.A. (1994) The Crystal Structure of Succinyl-CoA Synthetase from *Escherichia coli* at 2.5 Å Resolution. *J Biol Chem* **269 (8)**: 10883-10890.

Woodcock, S.C., and Jordan, P.M. (1994) Evidence for participation of aspartate-84 as a catalytic group at the active site of porphobilinogen deaminase obtained by site-directed mutagenesis of the *hemC* gene from *Escherichia coli*. *Biochemistry* **33 (9)**: 2688-95.

Word, J.M., Lovell, S.C., Richardson, J.S., and Richardson, D.C. (1999) Asparagine and Glutamine: Using Hydrogen Atom Contacts in the Choice of Side-chain Amide Orientation. *J Mol Biol* **285**: 1735-1747.

Wu, C.K., Dailey, H.A., Rose, J.P., Burden, A., Sellers, V.M., and Wang, B.C. (2001) The 2.0 Å structure of human ferrochelatase, the terminal enzyme of heme biosynthesis. *Nat Struct Biol* **8 (2)**: 156-60.

Yamaguchi, H., Kato, H., Hata, Y., Nishioka, T., Kimura, A., Oda, J., and Katsube, Y. (1993) Three-dimensional structure of the glutathione synthetase from *Escherichia coli* B at 2.0 Å resolution. *J Mol Biol* **229**: 1083-1100.

Yamauchi, K., Hayashi, N., and Kikuchi, G. (1980) Translocation of δ-Aminolevulinate Synthetase from the Cytosol to the Mitochondria and Its Regulation by Hemin in the Rat Liver. *J Biol Chem* **255 (4)**: 1746-1751.

Yamamoto, M., Kure, S., Engel, J.D., and Hiraga, K. (1988) Structure, Turnover, and Heme-mediated Suppression of the Level of mRNA Encoding Rat Liver δ-Aminolevulinate Synthetase. *J Biol Chem* **263 (31)**: 15973-15979.

Zappa, S., Li, K., and Bauer, C.E. (2010) The Tetrapyrrole Biosynthetic Pathway and Its Regulation in *Rhodobacter capsulatus*. *Adv Exp Med Biol* **675:** 229-50.

Zeilstra-Ryalls, J.H., and Kaplan, S. (1996) Control of *hemA* expression in *Rhodobacter sphaeroides* 2.4.1: regulation through alterations in the cellular redox state. *J Bacteriol* **178 (4):** 985-93.

Zhang, J., and Ferreira, G.C. (2002) Transient state kinetic investigation of 5-aminolevulinate synthetase reaction mechanism. *J Biol Chem* **277**: 44660-44669.

7 DANKSAGUNG

Mein besonderer Dank gilt Prof. Dr. Dieter Jahn, der er es mir überhaupt erst ermöglicht hat, diese Arbeit in den letzten Jahren in seiner Arbeitsgruppe anzufertigen. Ich danke ihm für die stets kreativen und motivierenden Diskussionen und auch für die Möglichkeit immer wieder Neues zu erlernen und anzuwenden – so auch für die Auslandserfahrung, die ich in Florida, Tampa sammeln durfte.

Dr. Gunhild Layer danke ich für ihr Interesse an meiner Arbeit und ihre Bereitschaft das Zweitgutachten dieser Dissertation zu übernehmen.

Prof. Dr. Ralf Mendel danke ich für die Übernahme des Vorsitzes der Prüfungskommission.

Herausragender Dank gilt Dr. Martina Jahn für die ausgezeichnete Zusammenarbeit und Betreuung während meiner Doktorarbeit. Sie stand mir immer mit Rat und Tat zur Seite. Danke dafür, Martina!

Großer Dank gilt auch Prof. Dr. Gloria C. Ferreira, ihrem Mann Bill und Greg Hunter, die mich herzlich in Tampa, Florida aufgenommen und mich tatkräftig in meiner Arbeit unterstützt haben. Sie waren mir stets eine große Hilfe, nicht nur in forschungsbedingten Aufgabenstellungen, vielen Dank.

Weiterhin bedanke ich mich auch bei Neil McIntyre, Thomas Lendrihas, Mallory Gillam, Jerome Clayton, Diana Latour und Karla Schramm, die mich ebenfalls herzlich in Tampa, Florida aufgenommen und mir den Aufenthalt dort mehr als angenehm gemacht haben. Danke!

Herzlicher Dank gilt auch Vanessa Hering, die mich stets tatkräftig unterstützt und motiviert hat.

Simone Huhn, Lars Remus, Ilka Heinemann, Nina Diekmann, Claudia Schulz, Melanie Burghartz und Dagmar Zwerschke aus Labor 212 möchte ich für ihre Zusammenarbeit, die hilfreichen Diskussionen und die schönen Stunden bei unseren Laborgrillausflügen bei unserer Chefin danken. Danke Mädels – und Lars!

Weiterer Dank gilt auch Hannes Walther, der immer ein offenes Ohr für mich hatte und mir bei Problemen stets weiterhalf. Danke Hannes!

Den gesamten Arbeitsgruppen der Mikrobiologie der TU Braunschweig danke ich für ihre Mitarbeit, ihr Verständnis bei größeren Proteinproduktionen und für ihre hilfreichen Diskussionen.

Meinen Freunden, insbesondere Alice Wycislo, und Jonas Degener danke ich für ihr tolle Freundschaft, ihre Aufmunterungen und ihr Verständnis.

Ebenfalls danken möchte ich meinem Vater, der immer an mich geglaubt und unterstützt hat.

Meiner Mutter, Thomas und meinen Schwestern danke ich für ihr Vertrauen in mich und ihr Interesse an meiner Arbeit sowie für ihre stets motivierenden Worte.

Weiterer Dank gilt dem Rest meiner Familie, die immer für mich da war und mich nie aufgegeben hat. Vielen vielen Dank dafür.

Mein ganz besonderer Dank gilt meinem Verlobten Torben, der es nicht immer leicht mit mir hatte in dieser Zeit. Ich danke ihm für seine liebevolle Unterstützung, seine motivierenden Worte, sein offenes Ohr und überhaupt dafür, dass er da ist. Torben, ich liebe dich!